DETECTION OF CONTINUOUS PHASE FREQUENCY SHIFT KEYED SIGNALS

JOHN PRIYANTHA FONSEKA

DETECTION OF CONTINUOUS PHASE FREQUENCY SHIFT KEYED SIGNALS

by

© Fonseka John Priyantha, B. Sc.(Eng.) Hons.

A thesis submitted to the School of Graduate Studies
in partial fulfillment of the
requirements for the degree of
Master of Engineering

Faculty of Engineering and Applied Science
Memorial University of Newfoundland
May 1985

St. John's Newfoundland Canada

DEDICATION

To My Family

ABSTRACT

In this thesis, the performance of Limiter Discriminator (LD) receiver, Differentially Coherent (DC) receiver and Coherent Detection-Differential Decoding (CD-DD) receiver is analyzed for the detection of M-ary CPFSK signals under various signal impairments.

The analysis is first carried out for the detection of M-ary CPFSK with modulation index $\frac{1}{M}$ in wideband channels. The effect of symbol timing errors and baseband symbol pulse shaping is considered. It is shown that CD-DD detection has better performance and less sensitivity to timing errors than LD detection and DC detection whereas LD detection and DC detection yield approximately the same performance both in the presence and in the absence of symbol timing errors.

The bandlimiting effect of the front-end filter of the three receivers is then considered. An effective methodology is developed to take into account the effect of Intersymbol Interference (ISI). As in wideband channels, it is shown that even in bandlimited channels, CD-DD detection yields better performance and has less sensitivity to ISI than LD detection and DC detection whereas the latter two detection schemes have almost identical performance and sensitivities.

The performance evaluation of LD detection of M-ary CPFSK with arbitrary modulation index, in both wideband and bandlimited channels, is also considered in order to determine the optimum modulation index which minimizes the error probability. It is shown that the performance of LD detection can be improved by increasing the modulation index above $\frac{1}{M}$. A variable delay differential detection technique which employs a delay interval dependent on the modulation index is analyzed for the detection of binary CPFSK signals with arbitrary modulation index in bandlimited channels. The performance of the variable delay differential detector is shown to be comparable with the performance of LD detector.

Finally, the numerical results obtained for the detection of quaternary CPFSK and octonary CPFSK in bandlimited channels are verified by digital computer simulation.

ACKNOWLEDGEMENTS

I wish to express my deep gratitude to Dr. N. Ekanayake for providing me the privilege of working on this research under his valuable supervision and guidence. Thanks are also extended to Dr. M. O. Toll for initially accepting me to the Graduate program at this University.

I am grateful to Dr. R. Peters, Dean of Engineering, Dr. F. A. Aldrich, Dean of Graduate Studies and Dr. T. R. Chari, Associate Dean of Engineering for providing me with all the necessary facilities, including financial assistance, in carrying out this research.

I thank all my colleagues who helped me in numerous ways during the process of finalizing this thesis.

I also thank Levinia Vatcher for her patience in typing this thesis.

I am indebted to Loyola College, Negombo, Sri Lanka for providing me with a good educational background which helped me throughout my career.

Last but not least, I thank all my family members for the sacrifices they had to undergo as a result of encouraging me for higher studies.

CONTENTS

LIST OF TABLES

LIST OF FIGURES

LIST OF ABBREVIATIONS

A	amplitude of CPFSK signal
A_p	pth Fourier coefficient of sin $\phi(t)$
AM	Amplitude Modulation
ASK	Amplitude Shift Keying
AWGN	Additive White Gaussian Noise
a_k	symbol sequence
a_n	nth data symbol
a(t)	time dependent filtered signal amplitude
B	bandwidth of the filter
B_p	pth fourier coefficient of cos $\phi(t)$
BT	time bandwidth product of the filter
CD-DD	Coherent Detection Differential Decoding
CPFSK	Continuous Phase Frequency Shift Keying
CPSK	Coherent Phase Shift Keying
D	normalized time shift
DC	Differentially Coherent
DPSK	Differential Phase Shift Keying
d(t)	baseband data signal
E_b	bit energy
E_s	symbol energy
$\frac{E_b}{N_0}$	bit signal to noise ratio
$\frac{E_s}{N_0}$	symbol signal to noise ratio

$\frac{E_s'}{N_0}$	signal to noise ratio with correction for filtered noise
$F_1(\alpha)$	cumulative p.d.f. of phase difference
$F_2(\eta)$	cumulative p.d.f. of absolute phase angle
FM	Frequency Modulation
FSK	Frequency Shift Keying
f_0	fundamental frequency
H(f)	Fourier transform of h(t)
H'(t)	pulse response of the filter
h	modulation index
h(t)	lowpass equivalent of H'(t)
$h_{opt.}$	optimum modulation index
I & D	Integrate and Dump
$I_e(k,x)$	Rice function
IF	Intermediate Frequency
ISI	Intersymbol Interference
L	length of the sequence used for simulation
LD	Limiter Discriminator
M	order of signalling
MSK	Minimum Shift Keying
MLSD	Maximum Likelihood Sequence Detection
N	number of clicks
$\bar{N}$	mean value of N
N_+	number of positive clicks

N_-	number of negative clicks
N	number of Fourier coefficients
$\frac{N_0}{2}$	two sided power spectral density of noise
N_p	number of basic patterns
$n(t)$	noise in the channel
$n_c(t)$	inphase component of noise
$n_0(t)$	filtered noise
$n_s(t)$	quadrature component of noise
P_{clicks}	error probability of Limiter Discriminator due to the continuous random variable
$P_{cont.}$	error probability of Limiter Discriminator due to the discrete random variable
P_e	symbol error probability
P_r	probability
P_{eb}	bit error probability
P_{es}	symbol error probability
$P_k(M)$	probability of making an incorrect decision in M-ary CPSK
PAM	Pulse Amplitude Modulation
PM	Phase Modulation
PSK	Phase Shift Keying
$p(t)$	baseband pulse
p.d.f.	probability density function
$R(t)$	envelope of the signal
$r(t)$	received signal
$r(\tau)$	auto-correlation of filtered noise

$r_0(t)$	filtered signal
SNR	signal to noise ratio
T	signalling interval
T_b	bit interval
T_s	symbol interval
t	time
X_n =	constant phase angle in the nth interval
$x(t)$	transmitted CPFSK signal
α	noise in phase angle difference
$\beta_{a_n, a_{n+1}}$	error in the phase angle due to a_{n+1} on a_n
δ'	time shift between received and filtered signals
τ	symbol timing error
ρ	signal to noise ratio
$\rho_{a_n, a_{n+1}}$	SNR at the detection of a_n with a_{n+1}
σ_n^2	noise variance
ω_c	carrier frequency
ω_d	frequency deviation from the carrier
$\theta(t)$	filtered phase variation of the signal
$\phi(t)$	phase variation of the transmitted CPFSK signal
$\Psi(t)$	phase variation of the filtered signal in presence of noise
$\eta(t)$	phase noise component at the output of the filter
$\Delta\Phi$	decision variable of LD detection
$\Delta\phi$	transmitted phase difference
*	convolution

CHAPTER 1

INTRODUCTION

1.1 Digital Signalling Techniques

With the rapid advances in digital technology in recent years, digital signalling techniques have become more attractive over their counterpart, analog signalling techniques. Digital transmission of information has the following advantages over analog transmission:

(i) Ruggedness to transmission noise and interference.

(ii) Efficient regeneration of the coded signal along the transmission path.

(iii) Possibility of a uniform format for different types of baseband signals.

These advantages are however gained at the cost of increased bandwidth.

Digital equivalents of the analog carrier modulation techniques such as Amplitude Modulation (AM), Phase Modulation (PM) and Frequency Modulation (FM) are Amplitude Shift Keying (ASK), Phase Shift Keying (PSK) and Frequency Shift Keying (FSK) respectively.

In ASK signalling, information is encoded in discrete amplitude levels of the carrier signal. ASK has the advantage of having good bandwidth efficiency, however, its

performance is affected severely under high amplitude fading conditions.

In PSK signalling the phase angle of the carrier signal is varied discretely in relation with the information symbols that need to be transmitted. This is a constant amplitude signalling scheme and it also has good bandwidth efficiency. The bandwidth occupancy of PSK signals depends only on the signalling rate and not on the number of discrete phase angles used for signalling. Therefore, PSK is being commonly used in communication systems where high data rates are involved such as digital radio. Because of its constant amplitude, it is also suitable for transmission of data through channels exhibiting amplitude nonlinearity such as satellite channels.

In FSK signalling, carrier frequency is varied from symbol interval to symbol interval depending on the discrete data that need to be transmitted. This is also a constant amplitude signalling scheme. The switching from one frequency to another can be carried out while maintaining the continuity of the phase variation of the signalling waveform and this version of FSK is known as Continuous Phase FSK (CPFSK). On the other hand, switching of frequencies can be done abruptly without paying any attention to the continuity of the phase angle of the carrier signal. In this case, FSK is referred to as noncontinuous phase FSK. The latter

version of FSK results discrete components in the power spectrum which is not desirable in most situations. The spectrum of CPFSK signals depends on the data rate as well as on the number of frequencies that is being used for signalling. In general, the spectrum of CPFSK signals is smooth and discrete components result only if the frequency difference or the frequency deviation is an integer multiple of the signalling rate. We shall discuss the behaviour of spectra of CPFSK signals on the data rate later on in this chapter. In this thesis we are interested only in the continuous phase FSK signals because of their superior spectral characteristics compared to noncontinuous phase FSK. CPFSK is generally preferred in mobile communications and in communication systems operating under frequency selective fading conditions.

1.2 M-ary CPFSK Signals

In general M-ary signalling schemes use an M element symbol set $\{\pm 1, \pm 3, \ldots \pm(M-1)\}$ and one symbol is selected in every signalling interval for transmission.

The discrete symbol sequence $\{a_k\}$ is combined with a baseband pulse $p(t)$ to form the baseband data signal $d(t)$ as,

$$d(t) = \sum_k a_k \, p(t-kT) \qquad (1.1)$$

This data signal is then used for carrier modulation to generate the corresponding CPFSK signal as,

$$x(t) = A \cos(\omega_c t + \omega_d \int_{-\infty}^{t} d(\tau)d\tau) \qquad (1.2a)$$

$$= A \cos(\omega_c t + \phi(t)) \qquad (1.2b)$$

where A and ω_c are the amplitude and frequency of the carrier respectively, while ω_d is the frequency deviation from the carrier.

For a rectangular baseband pulse

$$p(t) = \begin{cases} 1 & , \quad 0<t<T \\ 0 & , \quad \text{elsewhere} \end{cases}$$

the signal x(t) in the nth symbol interval can be represented as,

$$x(t) = A \cos(\omega_c t + a_n \omega_d t + X_n) \quad ; \quad nT<t<(n+1)T \qquad (1.2c)$$

where X_n is a phase angle which is constant over the nth symbol interval and its value is determined by the phase continuity requirement at the symbol transition t=nT. The modulation index h is obtained by normalizing the frequency separation between two adjacent discrete frequencies with respect to the signalling rate $\frac{1}{T}$ as,

$$h = \frac{2\omega_d}{2\pi/T} = \frac{T\omega_d}{\pi} \qquad (1.3)$$

M-ary CPFSK with modulation index 0.5, i.e., the minimum value of h required for the signal set to be orthogonal [19],

is referred to as M-ary Minimum Shift Keying (M-ary MSK). For the binary case this is simply termed as Minimum Shift Keying (MSK).

Fig. (1.1b) shows the phase variation for arbitrary h when the pulse shape p(t) is rectangular [4]. It can be observed from the phase trellis that the phase change occuring during any symbol interval is $\pi a_n h$. The phase angle $\phi(t)$ at symbol transition instants obeys the following recursive equation,

$$\phi((n+1)T) - \phi(nT) = \pi a_n h \qquad (1.4)$$

As we shall discuss later in this chapter, the case $h = \frac{1}{M}$ is of special interest because this value of modulation index yields superior spectral properties. The phase trellis for $h = \frac{1}{M}$ is shown in Fig. (1.2) [13]. For this case the recursive relation (1.4) reduces to,

$$\phi((n+1)T) - \phi(nT) = \frac{\pi a_n}{M} \qquad (1.5)$$

The transmitted signal x(t) given by Eqns. (1.2a) and (1.2b) will be corrupted during transmission by Additive White Gaussian Noise (AWGN), n(t), in the channel. Therefore, the received signal r(t) given by,

$$r(t) = x(t) + n(t)$$

is used for the detection of the signal. In the following section we shall describe the operation of three detection

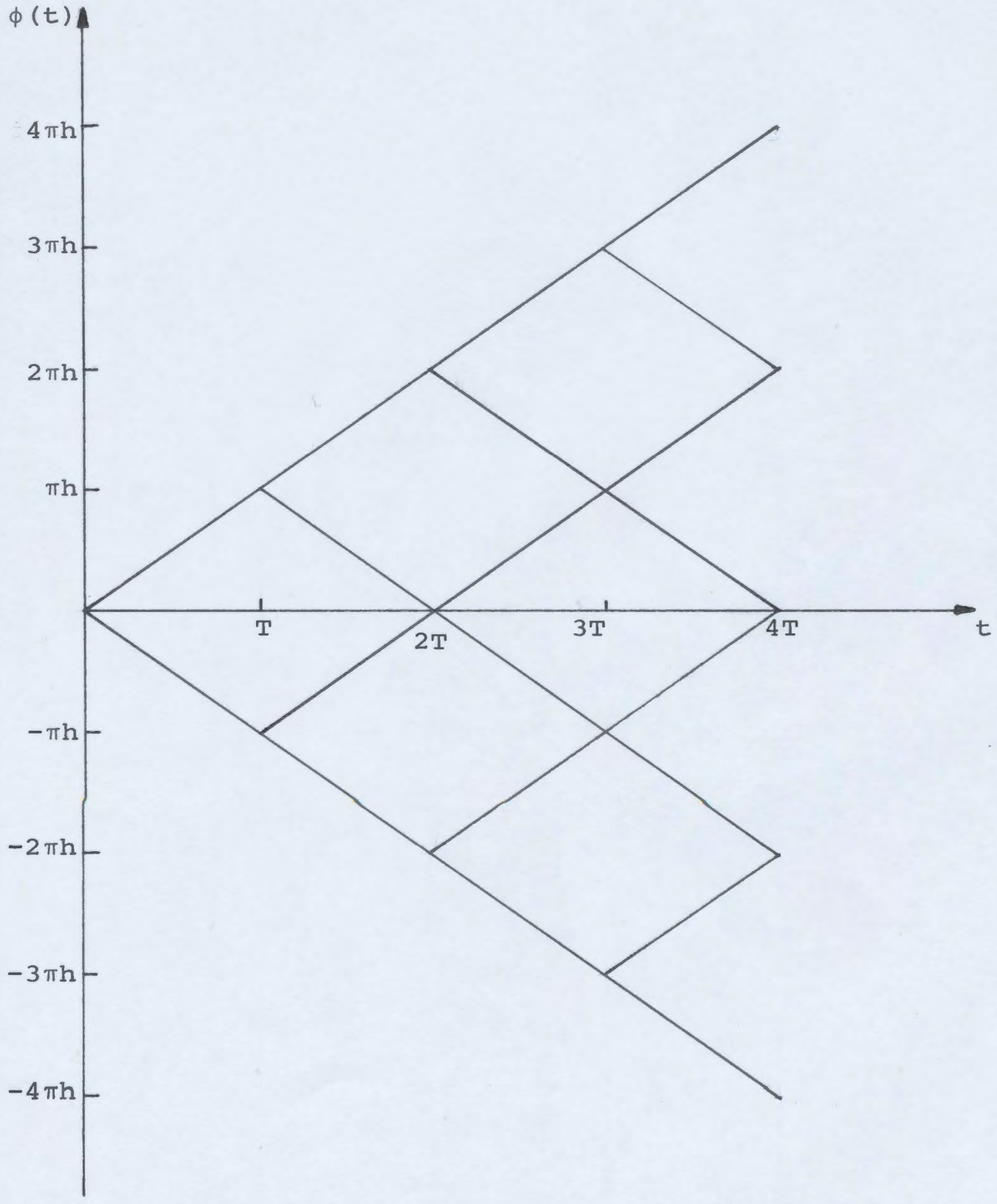

Fig. 1.1 Phase Trellis of Binary CPFSK Signals

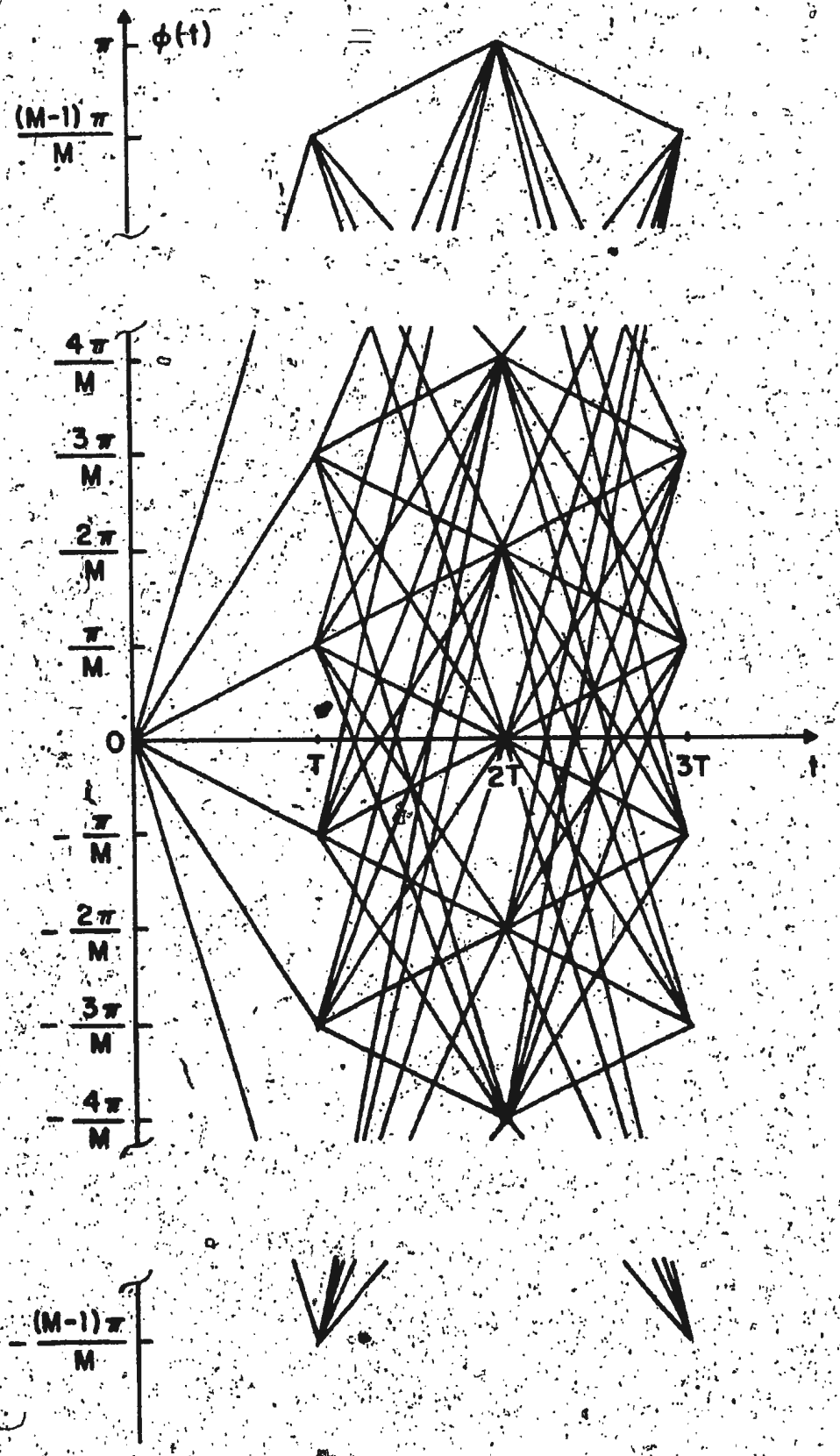

Fig. 1.2 Phase Trellis of M-ary CPFSK signals, Modulation Index $\frac{1}{M}$

schemes which are based on the recursive relations (1.4) and (1.5).

1.3 Detection Schemes

CPFSK signals can be detected either by Maximum Likelihood Sequence Detection (MLSD) techniques or by symbol by symbol detection techniques. In this thesis we consider three symbol by symbol detection techniques for the detection of CPFSK signals, namely, Limiter Discriminator (LD) detection, Differentially Coherent (DC) detection, and Coherent Detection-Differential Decoding (CD-DD) detection.

In all of the above three detection schemes the received signal is first passed through an intermediate frequency (IF) filter in order to remove out of band noise from the received signal. We denote the phase angle of the filtered signal as $\Psi(t)$ which is used to detect the received symbol. The filtered phase variation $\Psi(t)$ can be considered to be an addition of two components as,

$$\Psi(t) = \theta(t) + \eta(t)$$

where $\theta(t)$ is the phase variation which contains the information, i.e. $\theta(t)$ is the filtered phase variation corresponding to the received phase variation $\phi(t)$, and $\eta(t)$ is the phase noise component at the output of the filter.

1.3.1 Limiter Discriminator (LD) Detection

Fig. (1.3a) shows the basic structure of the limiter discriminator detection receiver. This structure however can be simplified for analytical purpose by approximating the post-detection filter and the synchronous sampler by an integrate and dump (I&D) circuit. This yields the receiver structure shown in Fig. (1.3b) which is more appropriate for our analysis.

The function of the limiter is to suppress the amplitude fluctuations of the received signal and it is followed by a frequency discriminator which differentiates the phase of the received signal $\Psi(t)$. The differentiated phase angle $\Psi(t)$ is then integrated over a symbol interval by the integrate and dump circuit to obtain the phase difference that occurs during a symbol interval. The output of the I&D filter $\Delta\Phi$ is decoded to obtain the symbol transmitted during the nth symbol interval.

The decision variable $\Delta\Phi$ in the nth symbol interval can therefore be written as,

$$\Delta\Phi = \int_{nT}^{(n+1)T} \Psi(t)\, dt \qquad (1.6a)$$

Since the phase noise component $\eta(t)$ of $\Psi(t)$ has an ambiguity of a multiple of 2π and also since $\Delta\Phi$, which is the output voltage of the integrator, lies in the interval $(-\infty, \infty)$, the decision variable $\Delta\Phi$ can be written as,

Fig. 1.3a Limiter Discriminator Detection of M-ary CPFSK Signals

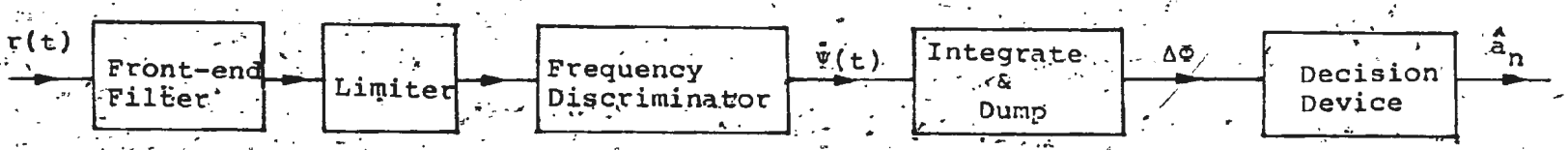

Fig. 1.3b Limiter Discriminator Detection of M-ary CPFSK Signals

$$\Delta\Phi = \Psi((n+1)T) - \Psi(nT) + 2\pi N(nT,(n+1)T) \quad (1.6b)$$

where $\Psi(nT)$ and $\Psi((n+1)T)$ are the phase angles of the filtered signal at $t=nT$ and $t=(n+1)T$ respectively. Also, in Eqn. (1.6b), N denotes the number of encirclements of $\eta(t)$ and is referred to as the number of clicks generated in the interval $(nT,(n+1)T)$. The counter-clockwise encirclements result in positive clicks whereas clockwise encirclements result in negative clicks.

We can outline the following important points that need to be considered in evaluating the performance of LD detection:

(1) Intersymbol Interference caused by the receiver front-end filter.

(2) Non Gaussian statistics of the decision variable.

(3) Generation of clicks during the process of differentiation and integration.

It is to be noted that the points (1) and (2) are common to all three detection techniques being considered.

1.3.2 Differentially Coherent (DC) Detection

Differentially coherent detection of CPFSK signals is similar to the differential detection technique used for the detection of PSK signals [18] and is shown in Fig. (1.4). The phase angle of the filtered signal $\Psi(t)$ is computed at the end of every symbol interval from inphase and quadrature

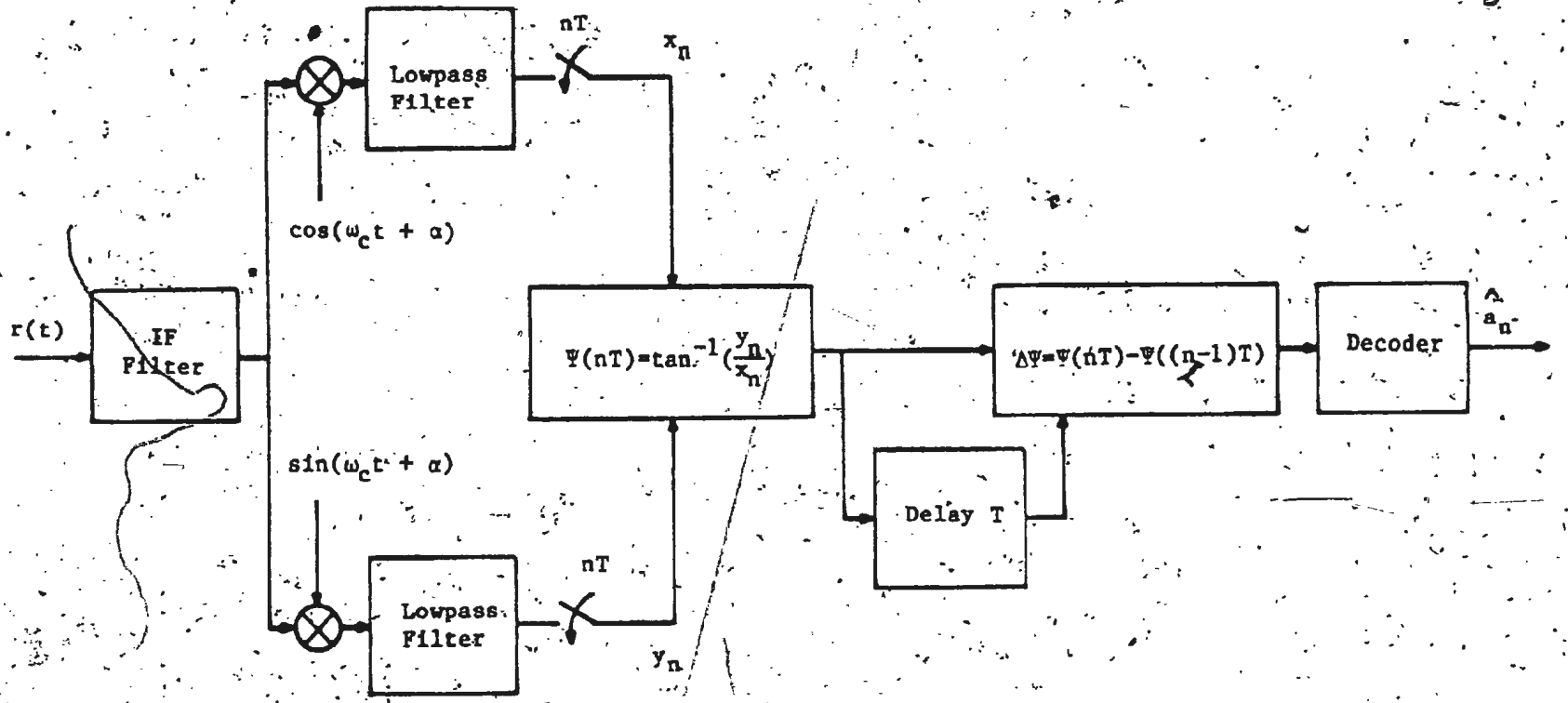

Fig. 1.4 Differentially Coherent Detection of M-ary CPFSK Signals

samples after demodulation, using two noncoherent carriers in quadrature. Differential detection is employed to obtain the phase difference by eliminating the unknown phase angle α. The successive phase angle differences are then decoded as one of the values in the set $\{\pm\frac{\pi}{M}, \pm\frac{3\pi}{M}, \ldots \pm(M-1)\frac{\pi}{M}\}$ to decide the transmitted symbols.

Therefore, the input to the phase detector for any symbol a_n can be written as,

$$\Delta\Psi = \Psi((n+1)T) - \Psi(nT) \qquad (1.7)$$

1.3.3 Coherent Detection - Differential Decoding (CD-DD) Detection

Coherent detection - differential decoding of CPFSK signals is similar to the differential decoding of coherent PSK signals [18] and is shown in Fig. (1.5). The phase angle of the received signal is computed at the end of every symbol interval from the inphase and quadrature phase samples after coherent demodulation, using two coherent carriers in quadrature, which are in exact phase reference with the received signal. Then the phase angle $\phi(nT)$ is estimated from the observed phase angle $\Psi(nT)$ and declared as one of the values in the set $S_1 = \{\pm\frac{\pi}{M}, \pm\frac{3\pi}{M}, \ldots, \pm\frac{(M-1)\pi}{M}\}$ for n odd and one of the values in the set $S_2 = \{0, \pm\frac{2\pi}{M}, \pm\frac{4\pi}{M}, \ldots, \pi\}$ for n even. The phase difference $\phi((n+1)T) - \phi(nT)$ is then decoded to yield the data symbol a_n.

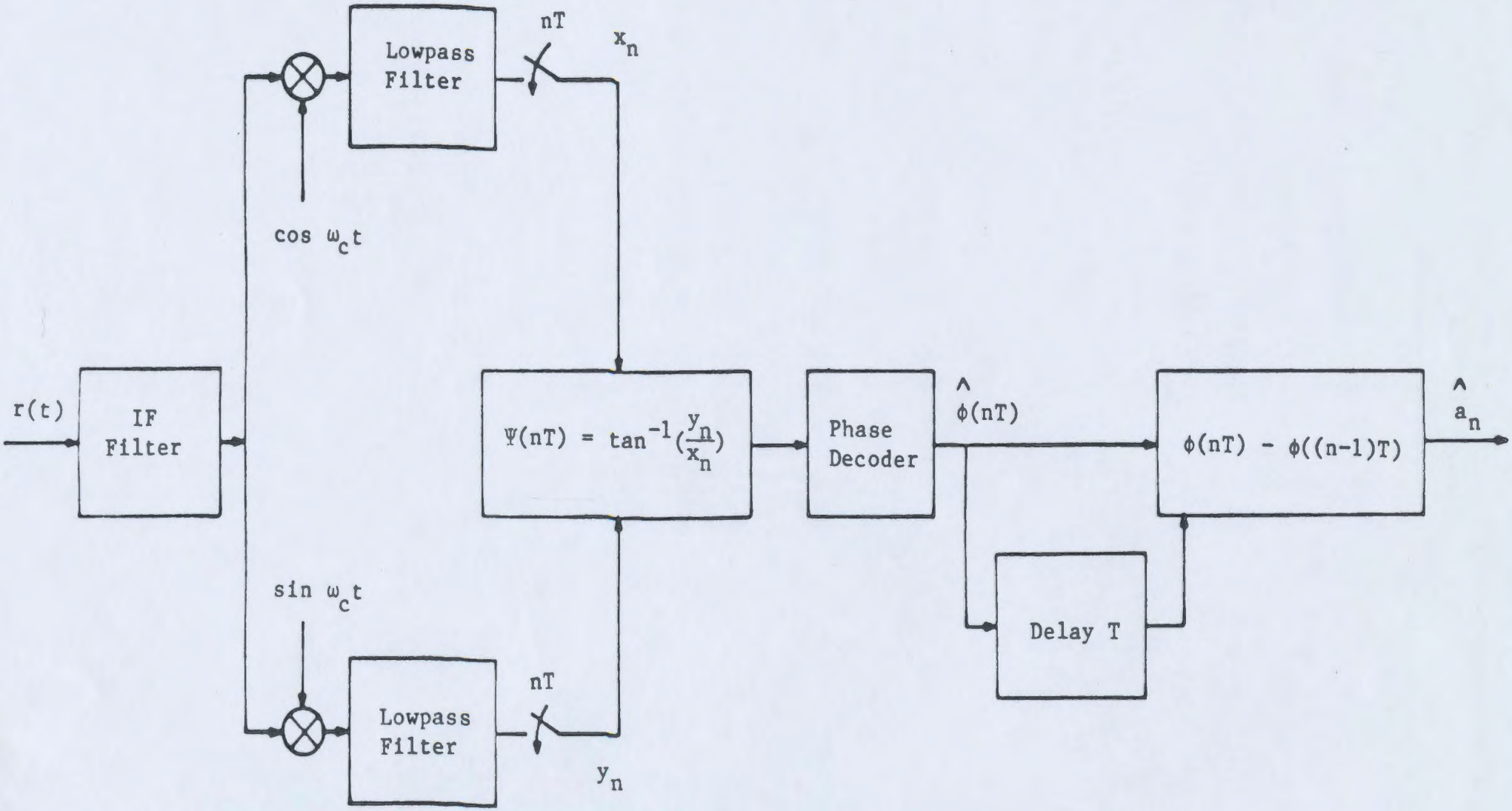

Fig. 1.5 Coherent Detection and Differential Decoding of M-ary CPFSK Signals

1.4 Literature Review

In the past literature [3-7, 13, 27, 36] a considerable body of work can be found on the evaluation of spectra of FSK signals. Although some of these studies include the evaluation of spectra of FSK signals that employ baseband pulse shaping, it is sufficient for us to restrict our attention to spectra of CPFSK signals that employ rectangular symbol pulses. In Figs. (1.6a) to (1.6c), the spectra of binary FSK, quaternary FSK, and octonary FSK are shown for various values of modulation index [19]. These figures indicate the dependency of power spectra on the number of levels as well as on the modulation index h. For small values of h the spectrum is relatively narrow but as h increases, the spectrum spreads out occupying a larger frequency band. The value of modulation index $h = \frac{1}{M}$ is of particular interest and the spectrum of CPFSK for M=4 and 8 for this modulation index is shown in Fig (1.7) with the spectrum of PSK signals [13]. It can be seen that CPFSK with this modulation index yields a narrower spectrum compared to PSK.

Reviewing the literature on the detection of CPFSK signals, the symbol by symbol detection techniques currently available are the synchronous detection, the noncoherent detection (which are similar to those in detection of ASK signals) and the limiter discriminator detection. The error

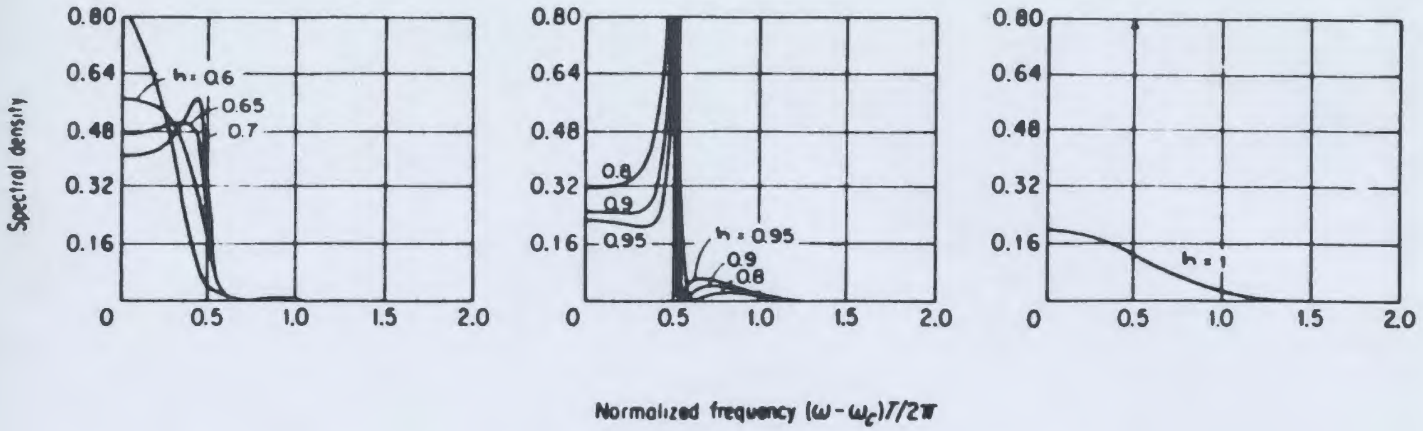

Fig. 1.6a Spectra of Binary CPFSK Signals

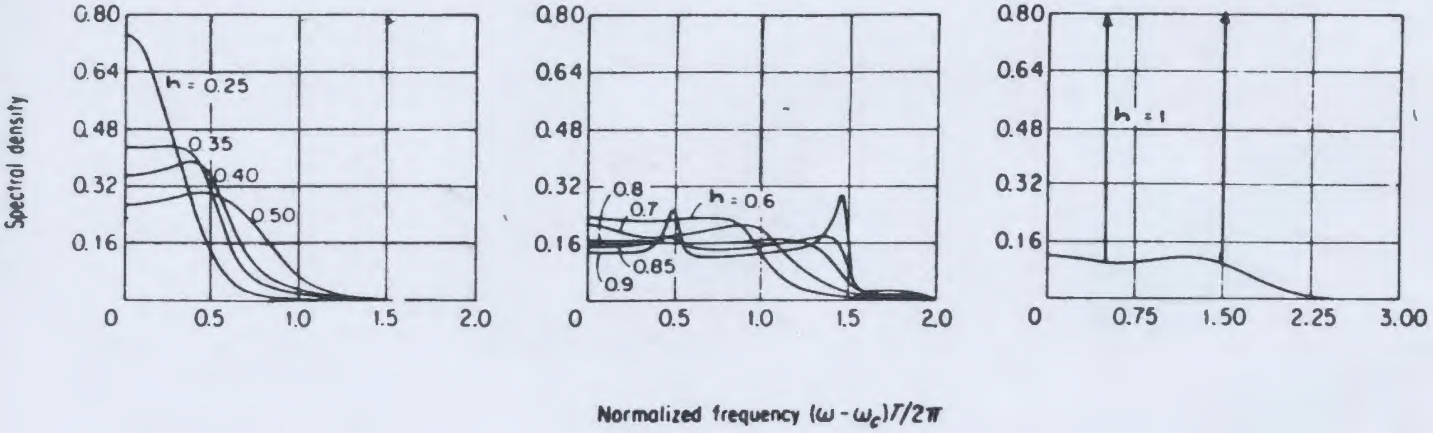

Fig. 1.6b Spectra of Quaternary CPFSK Signals

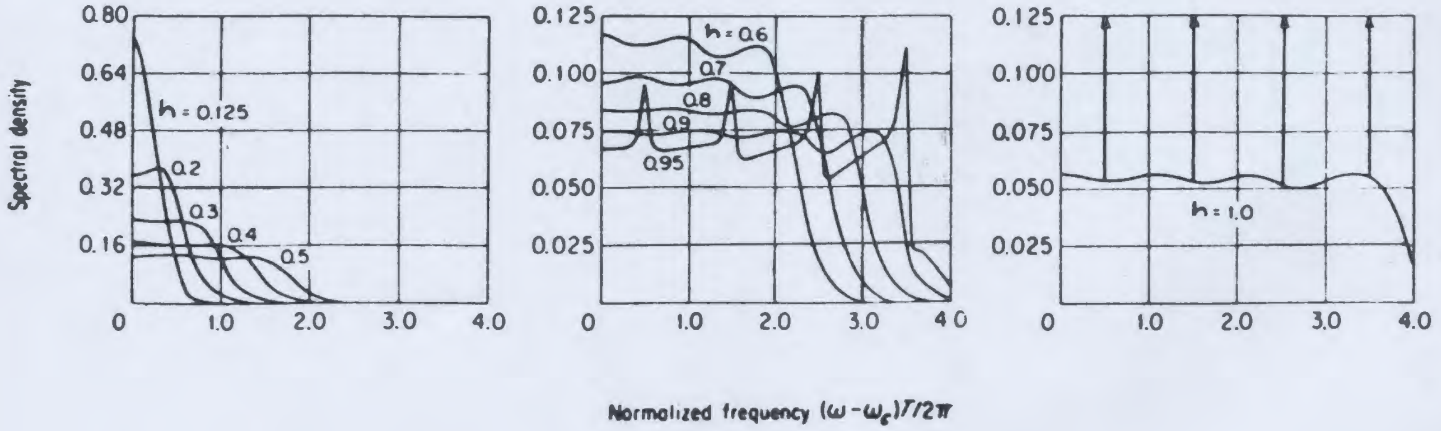

Fig. 1.6c Spectra of Octonary CPFSK Signals

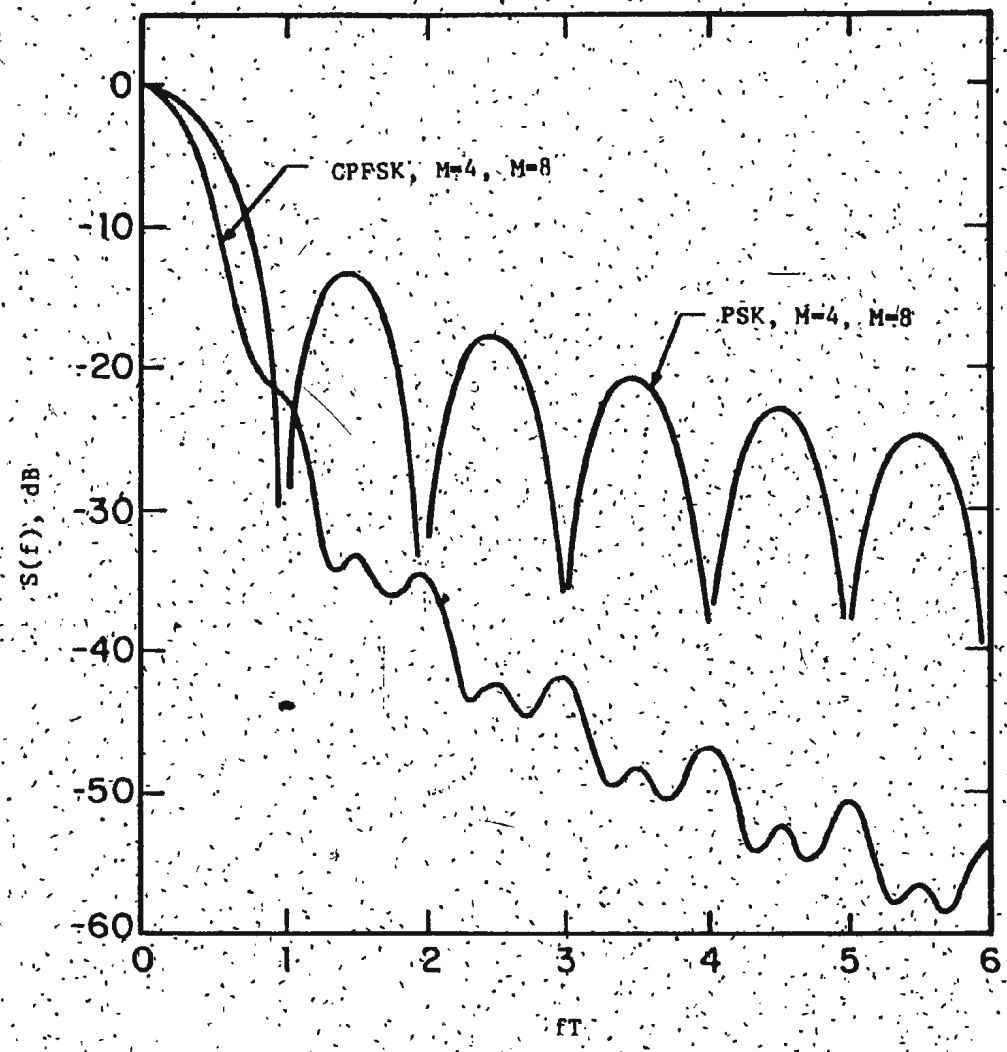

Fig. 1.7 Spectra of CPFSK Signals (Modulation Index $\frac{1}{M}$) and PSK Signals

performance of these detection techniques are almost 3 dB inferior to that of coherent PSK signalling. However, M-ary orthogonal FSK signalling yields better performance than PSK signalling for M>2 [19] but orthogonal FSK occupies a wider spectrum compared to PSK signals. In 1972, deBuda [12] has shown that coherent detection of binary CPFSK with modulation index $\frac{1}{2}$, i.e. MSK signalling, using a two-bit observation interval yields the same error performance as in coherent binary PSK (CPSK) signalling. With this discovery, CPFSK signalling with modulation index $\frac{1}{M}$ has gained considerable attention [1,13,16,20,21,37].

Memory imposed upon the CPFSK signals by continuous phase transitions has enabled the development of sequence detection techniques [15,24,28,34] which use a sequence of symbols to make decisions. Maximum Likelihood Sequence Detection (MLSD) of CPFSK signals yields better performance than coherent PSK signalling [24,28,34], but realization of this receiver is rather complex.

Among currently known symbol by symbol detection techniques for CPFSK signals, the limiter discriminator detector is considered as a conventional method. The performance of limiter discriminator detection of narrowband CPFSK signals in wideband Additive White Gaussian Noise (AWGN) channel has received considerable attention [8-11,17,22-26,32-35,38-41]. Salz [32] has analyzed the

performance of the limiter discriminator detection technique for the detection of CPFSK signals with modulation index $\frac{1}{M}$ over bandlimited channels. His analysis has been carried out omitting the effect of clicks. However, later on, Pawula [25] has pointed out that the effect of clicks cannot be neglected even at high SNR and hence the above results of Salz [32] is no longer considered to be valid. Tjhung [40] has analyzed this detection technique for the detection of narrowband binary CPFSK signals for arbitrary value of modulation index. The method used by Tjhung involves Fourier series expansions of long bit patterns, numerical convolutions and multipattern averaging. This method has been simplified to some extent by Cartier [9], considering only adjacent symbol interferences. A new approach to this problem has been suggested by Pawula [25], also considering adjacent symbol interferences. The advantage of Pawula's method is that it does not require Fourier series expansions of long bit patterns or numerical convolutions.

Recently, two symbol by symbol detection methods for the detection of M-ary CPFSK signals with modulation index $\frac{1}{M}$, namely, Differentially Coherent (DC) detection and Coherent Detection-Differential Decoding (CD-DD) detection, have been suggested by Ekanayake [13]. DC detection has been first introduced by Anderson et. al. [2] for the detection of

binary CPFSK signals. Simon et. al. [38] have compared the performance of LD detection with that of DC detection of narrowband binary CPFSK signals for arbitrary value of modulation index. Their results indicate that LD detection yields smaller error probabilities than DC detection except for the modulation index h = 0.5. However, it has been pointed out by Ekanayake [14] that in order to achieve optimum performance using DC detection for arbitrary value of h, its delay time has to be adjusted accordingly.

In this thesis we consider the performance evaluation of LD detection, DC detection and CD-DD detection of M-ary CPFSK signals. In our analysis we generalize the method developed by Pawula [25] for the binary CPFSK to include the M-ary CPFSK signals.

1.5 Scope of the Thesis

As mentioned in the previous section, CPFSK signals with modulation index $\frac{1}{M}$ have better bandwidth efficiency than PSK signals. However, the utilization of CPFSK as a bandwidth efficient signalling technique depends on the availability of easily realizable detection techniques. Therefore, it is of significant importance to determine the relative performance among various detection schemes in order to select a suitable detection scheme for a given situation. In this thesis we address this problem and do a comparative

performance evaluation of LD detection, DC detection and CD-DD detection under various signal impairment conditions. The organization of the remainder of the thesis is as follows.

In Chapter 2, the performance comparison is first carried out for a wideband channel under ideal conditions. The modulation index of the M-ary CPFSK signals is assumed to be $\frac{1}{M}$. Secondly, we extend the analysis to include the effect of symbol timing errors on the performance of the three detection schemes. Finally, the effectiveness of the baseband symbol pulse shaping in reducing timing errors is considered.

It is also important to determine the relative performance of the three detection schemes when bandlimiting effect of the channel is taken into consideration. Therefore, in Chapter 3, we analyze the performance of the three detection methods in a bandlimited channel. Again, the modulation index of CPFSK signals is assumed to be $\frac{1}{M}$. It is also assumed that the bandlimiting effect causes only adjacent intersymbol interference. We shall develop an analytical technique to take into account the effect of adjacent intersymbol interference which can be considered as a generalization of the recent results of Pawula [25], which has been published for binary CPFSK signalling.

In Chapter 4, the performance evaluation of LD detection of M-ary CPFSK signals for arbitrary value of modulation index is considered. The optimum value of the modulation index which yields minimum error probability of LD detection for the detection of M-ary CPFSK signals in wideband and bandlimited channels, is determined. It is shown that, by increasing h above $\frac{1}{M}$, the performance of LD detection can be considerably improved specially for multilevel CPFSK schemes. In Chapter 4, we also analyze the performance of variable delay DC detection which utilizes a delay time dependent on the modulation index, for the detection of binary CPFSK signals with arbitrary modulation index, in bandlimited channels.

In order to verify the analytical results obtained in Chapters 3 and 4, a digital computer simulation of the systems is performed. The simulation technique and the results are presented in Chapter 5.

Finally in Chapter 6, we summarize the conclusions and outline some of the possible future research areas.

CHAPTER 2

PERFORMANCE ANALYSIS OF CPFSK SIGNALS IN WIDEBAND CHANNELS

2.1 Introduction

In this chapter we compare the performance of the CD-DD detection, DC detection and LD detection of CPFSK signals for the modulation index 1/M. The channel is assumed to be wideband. It is also assumed that the front-end IF filter of the three recievers does not cause signal distortion. In the present analysis, the sole purpose of IF filtering is to reject the out of band noise.

First, the analysis is done assuming the availability of perfect symbol synchronization information at the receivers. Secondly, the analysis is extended to include the effect of symbol synchronization errors. Finally, the effectiveness of baseband pulse shaping in reducing the effect of symbol timing errors is analyzed. The numerical results for the symbol error probability of the three detection schemes are computed for each of the above three cases for M = 2,4 and 8.

2.2 Mathematical Model

Recalling Eqn. (1.2c), a CPFSK signal with modulation index h, during the nth symbol interval can be

written as,

$$x(t) = \sqrt{\frac{2E_s}{T}} \cos\left(\omega_c t + \frac{\pi a_n h}{T} \int_{nT}^{t} p(t-nT)dt + X_n\right);$$

$$nT < t < (n+1)T \qquad (2.1a)$$

$$= \sqrt{\frac{2E_s}{T}} \cos\left(\omega_c t + \phi(t)\right) \qquad (2.1b)$$

where E_s is the signal energy, a_n is the symbol transmitted and $p(t)$ is the baseband pulse which is non-zero only in the interval $0 < t < T$. The phase angle X_n given as,

$$X_n = \pi h \sum_{k=0}^{(n-1)} a_k$$

results from the phase continuity requirement and is constant during the nth symbol interval.

For a rectangular baseband pulse of the form,

$$p(t) = \begin{cases} 1^{\circ}, & 0 < t < T \\ 0, & \text{elsewhere} \end{cases} \qquad (2.2)$$

$\phi(t)$ reduces to,

$$\phi(t) = \frac{\pi a_n t}{MT} + X_n - n\pi a_n h \qquad \text{for } h = \frac{1}{M} \qquad (2.3)$$

The received signal in the presence of additive Gaussian noise can be expressed as,

$$r(t) = \sqrt{\frac{2E_s}{T}} \cos\left(\omega_c t + \phi(t)\right) + n_c(t) \cos\left(\omega_c t + \phi(t)\right) - n_s(t) \sin\left(\omega_c t + \phi(t)\right)$$

$$= R(t) \cos\left(\omega_c t + \phi(t) + \eta(t)\right) \qquad (2.4a)$$

$$= R(t) \cos(\omega_c t + \Psi(t)) \qquad (2.4b)$$

where $n_c(t)$ and $n_s(t)$ are the inphase and quadrature components of narrowband Gaussian noise.

In (2.4a), $\eta(t) = \tan^{-1}\left[\frac{n_s(t)}{\sqrt{\frac{2E_s}{T}} + n_c(t)}\right]$ is the phase noise component and $R(t)$ is the envelope of the signal which is not relevant to the three detection methods.

2.3 Performance in Absence of Timing Errors

2.3.1 CD-DD Detection

In this detection scheme $\phi(nT)$ is decoded from the observed phase angle $\Psi(nT)$ and declared as one of the values in the set $S_1 = \{\pm \frac{\pi}{M}, \pm \frac{3\pi}{M}, \ldots, \pm(M-1)\frac{\pi}{M}\}$ for n odd and one of the values in the set $S_2 = \{0, \pm \frac{2\pi}{M}, \pm \frac{4\pi}{M}, \ldots, \pi\}$ for n even. Similarly $\phi((n+1)T)$ is decoded from $\Psi((n+1)T)$. Then the phase difference $\phi((n+1)T) - \phi(nT)$ is decoded according to the Eqn. (1.5) to obtain the data symbol a_n.

The symbol a_n is detected correctly not only when both the estimates $\phi(nT)$ and $\phi((n+1)T)$ are correct but also when both are in error by the same amount.

The symbol error probability, P_e, of this receiver is evaluated in terms of the error probabilities of M-ary

Coherent PSK (CPSK) receiver [18] as,

$$P_e = 1-\left[\Pr\left[-\frac{\pi}{M} < \eta(nT) < \frac{\pi}{M}\right] \Pr\left[-\frac{\pi}{M} < \eta((n+1)T) < \frac{\pi}{M}\right]\right.$$

$$\left. + \sum_{k=1}^{(M-1)} \Pr\left[(2k-1)\frac{\pi}{M} < \eta(nT) < (2k+1)\frac{\pi}{M}\right]\right.$$

$$\left. \cdot \Pr\left[(2k-1)\frac{\pi}{M} < \eta((n+1)T) < (2k+1)\frac{\pi}{M}\right]\right\}$$

$$= 1 - (1 - P_e(M))^2 - \sum_{k=1}^{(M-1)} P_k^2(M)$$

$$\simeq 2 P_e(M) \qquad \text{at high SNR} \qquad (2.5)$$

where $P_e(M)$ is the symbol error probability in M-ary CPSK and $P_k(M)$ is the probability of making an incorrect decision in M-ary CPSK such that the decoded phase is in error by a value $\frac{2k\pi}{M}$ in the set $\{\pm\frac{2\pi}{M}, \pm\frac{4\pi}{M}, \ldots, \pi\}$.

Both $P_e(M)$ and $P_k(M)$ in Eqn. (2.5) can be readily calculated in terms of the cumulative p.d.f. of the absolute phase angle $F_2(\eta)$ [26] given in Appendix A as,

$$P_e(M) = 1 - \Pr\left[-\frac{\pi}{M} < \eta < \frac{\pi}{M}\right]$$

$$= F_2\left(-\frac{\pi}{M}\right) - F_2\left(\frac{\pi}{M}\right)$$

$$= 2 F_2\left(-\frac{\pi}{M}\right) \qquad (2.6a)$$

and

$$P_k(M) = \Pr\left[(2k-1)\frac{\pi}{M} < \eta < (2k+1)\frac{\pi}{M}\right]$$

$$= F_2\left((2k+1)\frac{\pi}{M}\right) - F_2\left((2k-1)\frac{\pi}{M}\right);$$

$$k = 1, 2, \ldots (M-1) \qquad (2.6b)$$

where

$$F_2(\eta) = \frac{-\,\mathrm{Sgn}(\eta)}{2\pi} \int_0^{\frac{\pi}{2}-|\eta|} e^{-\rho \sin^2 \eta \sec^2 \theta}\, d\theta$$

$\rho = \frac{E_s}{\sigma_n^2}$ is the signal to noise ratio.

2.3.2 DC Detection

In this detection scheme, the phase difference, $\Psi((n+1)T) - \Psi(nT)$ is decoded as one of the values in the set $\{\pm \frac{\pi}{M}, \pm \frac{3\pi}{M}, \ldots \pm (M-1)\frac{\pi}{M}\}$ and then the symbol a_n is decoded from this phase difference according to the relation (1.5).

The symbol error probability of this detection scheme is exactly identical to the error probability of Differential PSK (DPSK) detection, [26], which can be expressed as,

$$P_{DP}(M) = 1 - \Pr\left[(a_n - 1)\frac{\pi}{M} < \{\Psi((n+1)T) - \Psi(nT)\}\big|_{a_n} < (a_n + 1)\frac{\pi}{M}\right]$$

$$= 1 - \Pr\left[-\frac{\pi}{M} < \eta((n+1)T) - \eta(nT) < \frac{\pi}{M}\right]$$

$$= \frac{\sin(\frac{\pi}{M})}{2\pi} \int_{-\frac{\pi}{2}}^{\frac{\pi}{2}} \frac{e^{-\rho[1-\cos(\frac{\pi}{M})\cos t]}}{[1 - \cos(\frac{\pi}{M})\cos t]}\, dt \qquad (2.7a)$$

$P_{DP}(M)$ can also be calculated using the cumulative p.d.f. of the phase difference, $F_1(\alpha)$ as,

$$P_{DP}(M) = 1 - Pr[-\frac{\pi}{M} < \eta((n+1)T) - \eta(nT) < \frac{\pi}{M}]$$

$$= 1 - Pr[-\frac{\pi}{M} < \alpha < \frac{\pi}{M}]$$

$$= F_1(-\frac{\pi}{M}) - F_1(\frac{\pi}{M})$$

$$= 2\, F_1(-\frac{\pi}{M}) \qquad (2.7b)$$

where

$$F_1(\alpha) = -\frac{Sgn(\alpha)}{2\pi} \int_0^{\frac{\pi}{2}} e^{-\rho \frac{\sin^2 \alpha}{1 + \cos \alpha \cos \theta}} d\theta$$

and $\alpha = \eta((n+1)T) - \eta(nT) \bmod 2\pi$, is the noise component of the phase difference, $\Delta\phi = \phi((n+1)T) - \phi(nT)$.

2.3.3. LD Detection

Recalling Eqns. (1.6a), (2.4a) and (2.4b), the decision variable of the LD detection can be written as,

$$\Delta\Phi = \int_{nT}^{(n+1)T} \Psi(t)\, dt$$

$$= \phi((n+1)T) - \phi(nT) + \eta((n+1)T) - \eta(nT) + 2\pi N$$

$$= \frac{\pi a_n}{M} + \alpha + 2\pi N \qquad (2.8)$$

where $\alpha = \eta((n+1)T) - \eta(nT) \bmod 2\pi$ and N denotes the number of clicks in the interval nT to (n+1)T. Strictly, the number of clicks N is composed of a positive clicks component, N_+, and a negative clicks component, N_-, [30] as,

$$N = N_+ + N_-$$

However it has been pointed out in [30] that only negative clicks are significant for positive symbols, i.e. $N_- >> N_+$, when a_n is positive, and vice-versa. It is well known that [30] N is a Poisson random variable with mean $\bar{N}$, so that,

$$Pr(N=n) = \frac{e^{-\bar{N}}\,\bar{N}^n}{n!} \qquad (2.9a)$$

and

$$\bar{N} = \frac{1}{2\pi}\left|\int_{nT}^{(n+1)T} e^{-p(\tau)}\,\dot{\phi}(\tau)\,d\tau\right| \qquad (2.9b)$$

The modulo 2π representation of α is valid at high SNR. The slicing levels of the receiver are $0, \pm\frac{2\pi}{M}, \pm\frac{4\pi}{M}, \ldots \pm\frac{(M-2)\pi}{M}$. An error occurs when $\alpha + 2\pi N$ exceeds in magnitude the distance from the transmitted level to the nearest decision threshold by $\frac{\pi}{M}$. The two outside levels $\pm(M-1)$ can only be in error in one direction each. The error rate calculations in this case is somewhat similar to that in Pulse Amplitude Modulated (PAM) systems. Making use of the symmetry of the signal set, and considering the positive symbols, the probability of error can be evaluated by

evaluating the conditional error probability as,

$$P_{e,LD}\Big|_{a_n} = \begin{cases} 1-\Pr[(a_n-1)\frac{\pi}{M} < \Delta\Phi \Big|_{a_n} < (a_n+1)\frac{\pi}{M}], & a_n \neq (M-1) \\ \\ 1-\Pr[(M-2)\frac{\pi}{M} < \Delta\Phi \Big|_{a_n} < \infty], & a_n = (M-1) \end{cases}$$

$$= \begin{cases} 1-\Pr[-\frac{\pi}{M} < \alpha < \frac{\pi}{M}] \Pr(N=0\Big|_{a_n}), & a_n \neq (M-1) \\ \\ 1-\Pr[-\frac{\pi}{M} < \alpha < \pi] \Pr(N=0\Big|_{a_n}), & a_n = (M-1) \end{cases}$$

and then averaging over a_n one obtains,

$$P_{e,LD} = 1 - \frac{2}{M} \sum_{|a_n| \neq (M-1)} \{\Pr(N=0\Big|_{a_n}) \Pr(-\frac{\pi}{M} < \alpha < \frac{\pi}{M})\}$$

$$- \frac{2}{M} \Pr(N=0\Big|_{a_n=(M-1)}) \Pr(-\frac{\pi}{M} < \alpha < \pi) \qquad (2.10)$$

The probabilities $\Pr(-\frac{\pi}{M} < \alpha < \frac{\pi}{M})$ and $\Pr(-\frac{\pi}{M} < \alpha < \pi)$ can be readily evaluated using the cumulative p.d.f. $F_1(\alpha)$ as,

$$\Pr(-\frac{\pi}{M} < \alpha < \frac{\pi}{M}) = 1 - 2\,F_1(-\frac{\pi}{M}) \qquad (2.11a)$$

and

$$\Pr(-\frac{\pi}{M} < \alpha < \pi) = 1 - F_1(-\frac{\pi}{M}) \qquad (2.11b)$$

$\Pr(N=0\Big|_{a_n})$ is the probability of getting zero clicks in the interval nT to (n+1)T, when a_n is transmitted. It follows

from Eqns. (2.9a) and (2.9b), that

$$\Pr(N=0|a_n) \doteq e^{-\bar{N}}$$

$$\simeq 1 - \bar{N} \qquad \text{for } \rho \gg 1$$

and

$$\bar{N} = |a_n| \frac{e^{-\rho}}{2M} \tag{2.12}$$

Combining Eqns. (2.10), (2.11a), (2.11b) and (2.12) the error probability of the LD detection can be written as,

$$P_{e,LD}(M) = \frac{2}{M} \sum_{a_n \neq (M-1)} (1 - \frac{a_n}{2M} e^{-\rho})(1 - 2F_1(-\frac{\pi}{M}))$$

$$+ \frac{2}{M} (1 - \frac{(M-1)}{2M} e^{-\rho})(1-F_1(-\frac{\pi}{M}))$$

$$= \frac{2(M-1)}{M} F_1(-\frac{\pi}{M}) + \frac{1}{M^2} e^{-\rho}(1+3 \ldots +(M-1));$$

$$= \frac{2(M-1)}{M} F_1(-\frac{\pi}{M}) + \frac{1}{4} e^{-\rho}, \quad \rho \gg 1$$

(2.13)

Combining Eqns. (2.7b) and (2.13), the error probabilities of LD detection and DC detection can be related as,

$$P_{e,LD}(M) = P_{DP}(M) - \frac{P_{DP}(M)}{M} + \frac{e^{-\rho}}{4}, \quad \rho \gg 1$$

(2.14)

It is of interest to note that for the binary CPFSK (i.e. MSK), $P_{e,LD}(2) = P_{DP}(2) = \frac{1}{2} e^{-\rho}$. Thus, LD detection

and DC detection yield the same error performance at high SNR. For M>2, one can observe from Eqn. (2.14) that LD detection yields slightly better performance than the DC detection, but the difference is rather insignificant to be of practical importance.

2.4 Effect of Symbol Timing Error

In this section we consider the effect of symbol timing errors on the error rate performance of the three detection methods. In all three cases it is assumed that the timing error $\tau>0$ and it can be shown that the results are valid for $\tau<0$.

2.4.1 CD-DD Detection

Referring to Fig. (2.1) and with the aid of Eqns. (2.4a) and (2.4b), the phase angle at $t = nT + \tau$ is obtained as,

$$\Psi(nT+\tau) = \phi(nT) + \frac{\pi\tau}{MT} a_n + \eta(nT+\tau) \qquad (2.15a)$$

and the phase angle at $t=(n+1)T + \tau$ is obtained as,

$$\Psi((n+1)T+\tau) = \phi((n+1)T) + \frac{\pi\tau}{MT} a_{n+1} + \eta((n+1)T+\tau) \qquad (2.15b)$$

Since $\phi(nT)$ is independent of a_n and $\phi((n+1)T)$ is independent of a_{n+1}, the expression (2.5) with the following definitions

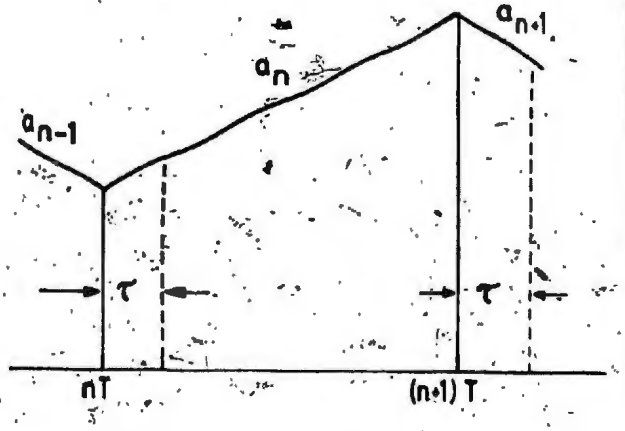

Fig. 2.1 Effect of Symbol Timing Error

for $P_e(M)$ and $P_k(M)$ can be used for computing the error probabilities:

$$P_e(M,\tau) = 1 - \frac{2}{M} \sum_{i=1}^{M/2} \Pr\left[-\frac{\pi}{M} < \eta + (2i-1)\beta < \frac{\pi}{M}\right]$$

$$= \sum_{i=1}^{M/2} \left[F_2\left(-\frac{\pi}{M} - (2i-1)\beta\right) - F_2\left(\frac{\pi}{M} - (2i-1)\beta\right)\right] \tag{2.16a}$$

$$P_k(M,\tau) = \frac{1}{M} \sum_{i=1}^{M/2} \left\{\Pr\left[(2k-1)\frac{\pi}{M} < \eta + (2i-1)\beta < (2k+1)\frac{\pi}{M}\right]\right.$$

$$\left. + \Pr\left[(2k-1)\frac{\pi}{M} < \eta - (2i-1)\beta < (2k+1)\frac{\pi}{M}\right]\right\}$$

$$= \frac{1}{M} \sum_{i=1}^{M/2} \left\{\left[F_2\left((2k+1)\frac{\pi}{M} - (2i-1)\beta\right)\right.\right.$$

$$\left. - F_2\left((2k-1)\frac{\pi}{M} - (2i-1)\beta\right)\right]$$

$$+ \left[F_2\left((2k+1)\frac{\pi}{M} + (2i-1)\beta\right)\right.$$

$$\left.\left. - F_2\left((2k-1)\frac{\pi}{M} + (2i-1)\beta\right)\right]\right\},$$

$$k = 1, 2 \ldots (M-1) \tag{2.16b}$$

where $\beta = \frac{\pi\tau}{MT}$ and η is defined in (2.4a). The cumulative p.d.f. $F_2(\alpha)$ is given in Appendix A. At high SNR, one can use the approximation for the error probability,

$$P_e \approx 2P_e(M,\tau)$$

2.4.2 DC Detection

In presence of a symbol timing error τ, the phase detector input can be written as [c.f. Eqns. (1.7), (2.15a), (2.15b)],

$$\Delta\Psi = \frac{\pi a_n}{M} + \frac{\pi\tau}{MT}(a_{n+1} - a_n) + \alpha \qquad (2.17)$$

where $\alpha = \eta((n+1)T+\tau) - \eta(nT+\tau)$. Making use of the symmetry of the signal set and considering only the positive symbols, the error probability can be evaluated straightforwardly by evaluating the conditional error probability as,

$$P_e\Big|_{a_n, a_{n+1}} = 1 - \Pr[-\tfrac{\pi}{M} < \alpha + \tfrac{\pi\tau}{MT}(a_{n+1}-a_n) < \tfrac{\pi}{M}]$$

and then averaging over a_n and a_{n+1} one obtains,

$$P_e(\tau) = 1 - \frac{1}{M^2}\sum_{i=0}^{(M-1)} \varepsilon_i (M-i) \Pr[-\tfrac{\pi}{M} < \alpha + 2i\beta < \tfrac{\pi}{M}]$$

$$= \frac{1}{M^2}\sum_{i=0}^{(M-1)} \varepsilon_i (M-i)[F_1(-\tfrac{\pi}{M} - 2i\beta) - F_1(\tfrac{\pi}{M} - 2i\beta)] \qquad (2.18)$$

where

$$\varepsilon_i = \begin{cases} 1 & \text{for } i = 1 \\ 2 & \text{for } i > 1 \end{cases}$$

and the cumulative p.d.f. $F_1(\alpha)$ is given in Appendix A.

2.4.3 LD Detection

The decision variable for the nth symbol in presence of a symbol timing error can be written [c.f. Eqns. (2.8), (2.15a), (2.15b)] as,

$$\Delta\Phi = \frac{\pi a_n}{M} + \frac{\pi\tau}{MT}(a_{n+1} - a_n) + \alpha + 2\pi N$$

$$= \Lambda + 2\pi N \qquad (2.19)$$

where N is the average number of clicks in the interval $nT+\tau$ to $(n+1)T+\tau$. As the two intervals $[nT+\tau,(n+1)T]$ and $[(n+1)T, (n+1)T + \tau]$ lie in two different signalling intervals, the clicks in these two intervals have to be evaluated separately. When a_n and a_{n+1} are of the same sign, the clicks in the two intervals are in the same direction whereas when a_n and a_{n+1} are of opposite signs, the clicks are in the opposite direction. Assuming $\tau>0$ and considering only positive a_n because of the symmetry of the signal set, the probability of making an error conditioned on a_n and a_{n+1} can be written as,

$$P(e|\tau,a_n,a_{n+1}>0) = \begin{cases} 1-Pr[(a_n-1)\frac{\pi}{M}<\Lambda<(a_n+1)\frac{\pi}{M}]Pr(N_1=N_2=0), \\ \qquad\qquad a_n\neq(M-1) \\ 1-Pr[(a_n-1)\frac{\pi}{M} < \Lambda < \infty]Pr(N_1=N_2=0), \\ \qquad\qquad a_n=(M-1) \end{cases} \qquad (2.20a)$$

$$P(e|\tau,a_n,a_{n+1}<0)=\begin{cases}1-Pr[(a_n-1)\frac{\pi}{M}<\Lambda<(a_n+1)\frac{\pi}{M}]Pr(N_1=N_2), & a_n\neq(M-1)\\ 1-[Pr[(a_n-1)\frac{\pi}{M}<\Lambda<\infty]Pr(N_1=N_2)+Pr(N_2>N_1)], & a_n=(M-1)\end{cases} \tag{2.20b}$$

The average number of clicks $\bar{N}_1$ in the interval $(nT+\tau)$ to $(n+1)T$ is given by,

$$\bar{N}_1 = \frac{e^{-\rho}}{2M}\left(1-\frac{\tau}{T}\right)|a_n| \tag{2.21a}$$

and the average number of clicks $\bar{N}_2$ in the interval $(n+1)T$ to $(n+1)T+\tau$ is given by,

$$\bar{N}_2 = \frac{e^{-\rho}}{2M}\frac{\tau}{T}|a_{n+1}| \tag{2.21b}$$

also,

$$Pr(N_1=N_2=0) = e^{-(\bar{N}_1+\bar{N}_2)} \simeq 1-(\bar{N}_1+\bar{N}_2) \tag{2.22a}$$

$$Pr(N_1=N_2) = \sum_{K=0}^{\infty}\frac{e^{-(\bar{N}_1+\bar{N}_2)}(\bar{N}_1\bar{N}_2)^k}{(k!)^2} \tag{2.22b}$$

$$Pr(N_2>N_1) = \sum_{k_1=0}^{\infty}\sum_{k_2=k_1}^{\infty} e^{-(\bar{N}_1+\bar{N}_2)}\frac{(\bar{N}_1)^{k_1}}{k_1!}\frac{(\bar{N}_2)^{k_2}}{k_2!}$$

$$<< Pr(N_1=N_2) \tag{2.22c}$$

As before using the symmetry of the signal set, one could simplify the expressions (2.20a) and (2.20b) to yield,

$$P_{e|_\tau} = 1 - \frac{2}{M^2} \sum_{i=1}^{(\frac{M}{2}-1)} \sum_{j=1}^{M} \{1 - \frac{a_i e^{-\rho}}{2M} - \frac{\tau}{2MT} (|a_j|-a_i)e^{-\rho}\}$$

$$\cdot [Pr(-\frac{\pi}{M} < \alpha + \frac{\pi\tau}{MT}(a_j-a_i) < \frac{\pi}{M})]$$

$$- \frac{2}{M^2} \sum_{j=1}^{M} \{1 - \frac{e^{-\rho}(M-1)}{2M} + \frac{\tau}{2MT}(|a_j|-(M-1))e^{-\rho}\}$$

$$\cdot [Pr(-\frac{\pi}{M} < \alpha + \frac{\pi\tau}{MT}(a_j - (M-1)) < \pi)]$$

$$= 1 - \frac{2}{M^2} \sum_{i=1}^{(\frac{M}{2}-1)} \sum_{j=1}^{M} \{1 - \frac{a_i e^{-\rho}}{2M} - \frac{\tau}{2MT}(|a_j|-a_i)e^{-\rho}\}$$

$$\cdot [1-F_1(-\frac{\pi}{M} - \frac{\pi\tau}{MT}(a_j-a_i))+F_1(\frac{\pi}{M} - \frac{\pi\tau}{MT}(a_j-a_i))]$$

$$- \frac{2}{M^2} \sum_{j=1}^{M} \{1 - \frac{e^{-\rho}(M-1)}{2M} + \frac{\tau}{2MT}(|a_j|-(M-1))e^{-\rho}\}$$

$$\cdot [1 - F_1(-\frac{\pi}{M} - \frac{\pi\tau}{MT}(a_j - a_i))] \qquad (2.23)$$

The cumulative p.d.f. $F_1(\alpha)$ is given in Appendix A. As before $P_{e|_\tau}$ could be approximated at high SNR as,

$$P_{e|\tau} = \frac{2}{M^2} \sum_{i=1}^{\frac{M}{2}} \sum_{j=1}^{M} \left\{ \frac{a_i \bar{e}^{\rho}}{2M} + \frac{\tau}{2MT} (|a_j| - a_i) \bar{e}^{\rho} \right\}$$

$$+ \frac{2}{M^2} \sum_{i=1}^{(\frac{M}{2}-1)} \sum_{j=1}^{M} \left[F_1\left(-\frac{\pi}{M} - \frac{\pi\tau}{MT}(a_j - a_i)\right) \right.$$

$$\left. - F_1\left(\frac{\pi}{M} - \frac{\pi\tau}{MT}(a_j - a_i)\right) \right]$$

$$+ \frac{2}{M^2} \sum_{j=1}^{M} F_1\left(-\frac{\pi}{M} - \frac{\pi\tau}{MT}(a_j - a_i)\right), \quad \rho >> 1 \tag{2.24}$$

2.5 Effect of Pulse Shaping on Symbol Timing Error

In order to reduce the effect of symbol timing errors, it is desirable to have smooth phase transitions at the symbol transition instants. In recent literature [4], the symbol pulse shaping using a raised cosine pulse has been analyzed in the context of spectral shaping. These pulse shaping functions also cause phase trellis to have smooth phase transitions reducing phase variations near symbol transition instants. A raised-cosine pulse suitable for our purpose is,

$$p(t) = \begin{cases} 2 \sin^2 \frac{\pi t}{T} & , \ 0 < t < T \\ 0 & , \text{ elsewhere} \end{cases} \tag{2.25}$$

The phase variation corresponding to this pulse is obtained from Eqns. (2.1a) and (2.1b) as,

$$\phi(t) = \frac{\pi a_n h}{T} \int_{nT}^{t} p(t-n\tau)\,dt + X_n$$

$$= \frac{\pi a_n h}{T}\left[t - \frac{T}{2\pi}\sin\frac{2\pi t}{T}\right] + X_n \quad ,$$

and the corresponding phase trellis is shown in Fig. (2.2), for binary CPFSK signals.

The effect of timing error on the performance of CPFSK when this pulse is used for symbol weighting can be analyzed as in the case of rectangular pulse weighting in section 2.4. The following modifications for Eqns. (2.15a), (2.15b), (2.21a) and (2.21b) are necessary for this case:

$$\Psi(nT+\tau) = \phi(nT)+\left[\frac{\pi t}{MT} - \frac{\sin\left(\frac{2\pi\tau}{T}\right)}{2M}\right] a_n+\eta(nT+\tau) \qquad (2.26a)$$

$$\Psi((n+1)T+\tau) = \phi((n+1)T)+\left[\frac{\pi\tau}{MT} - \frac{\sin\left(\frac{2\pi\tau}{T}\right)}{2M}\right]a_{n+1} + \eta((n+1)T+\tau) \qquad (2.26b)$$

$$\bar{N}_1 = \frac{|a_n|}{2M}\left[\left(1 - \frac{\tau}{T}\right) - \frac{1}{2\pi}\sin 2\pi\left(1 - \frac{\tau}{T}\right)\right] \qquad (2.27)$$

$$\bar{N}_2 = \frac{|a_{n+1}|}{2M}\left[\frac{\tau}{T} - \frac{1}{2\pi}\sin\left(\frac{2\pi\tau}{T}\right)\right] \qquad (2.28)$$

We note that when $\tau=0$, the pulse shaping has no effect on the error rate performance of the three detection methods.

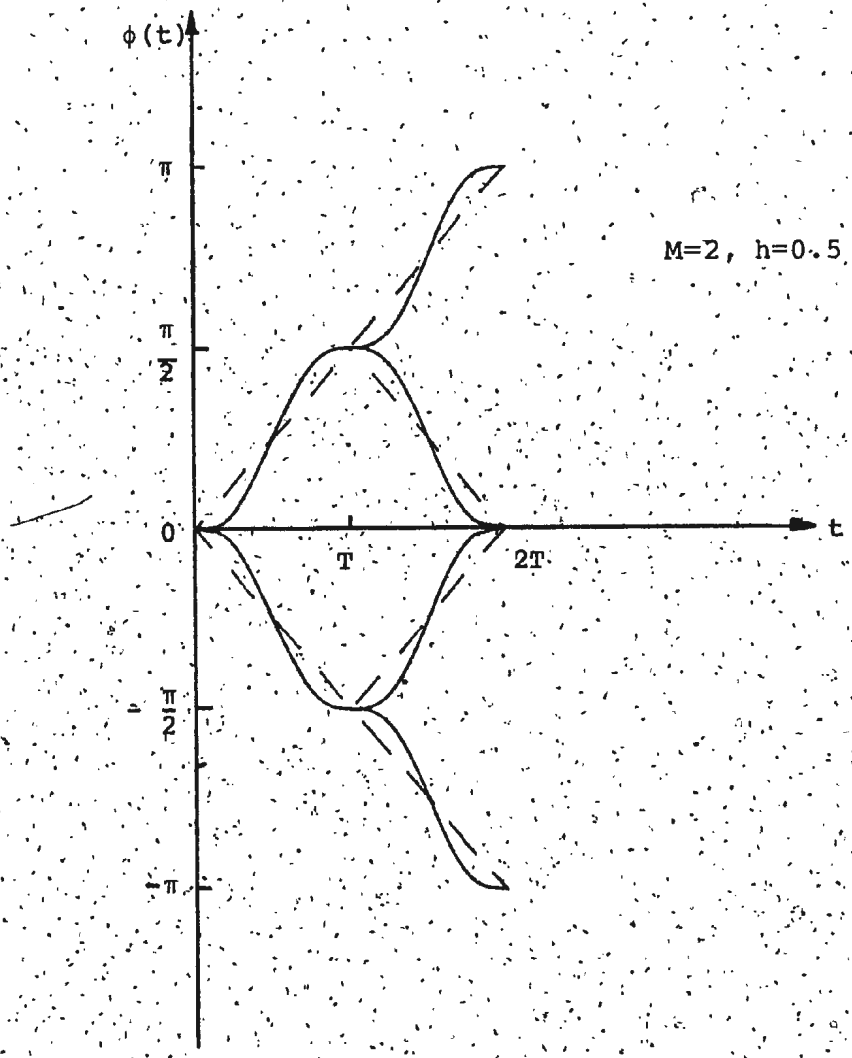

Fig. 2.2 Phase Trellis with Baseband Symbol Pulse Shaping

2.6 Numerical Results and Discussion

The error probabilities of CD-DD detection, DC detection and LD detection are computed in absence of timing errors using the expressions derived in section 2.3 and plotted in Fig. (2.3) for M = 2, 4 & 8. We observe that LD detection results marginally better performance than DC detection when M>4. For the binary case, i.e. M=2, DC detection and LD detection yield the same performance. This is in agreement with the previously published results for the narrowband case [38]. On the other hand, CD-DD scheme is about 1dB better for M=2 and about 2dB better for M=4 and 8, than LD and DC detections. The reason for obtaining superior performance in LD detection in comparison to DC detection is due to the fact that the outside two levels $\pm(M-1)$ are detected with smaller error probability in LD detection because these levels are affected by noise in one direction only. Even though the clicks cause performance degradation, their effect is balanced by the small error probabilities of the outside two levels. The DC detection yields equal error probability for all the symbols. The extra reliability of the outside two symbols $\pm(M-1)$ aids LD detection to yield better performance than DC detection despite the presence of the clicks.

The error probabilities for the three detection techniques in presence of a symbol timing error are shown in

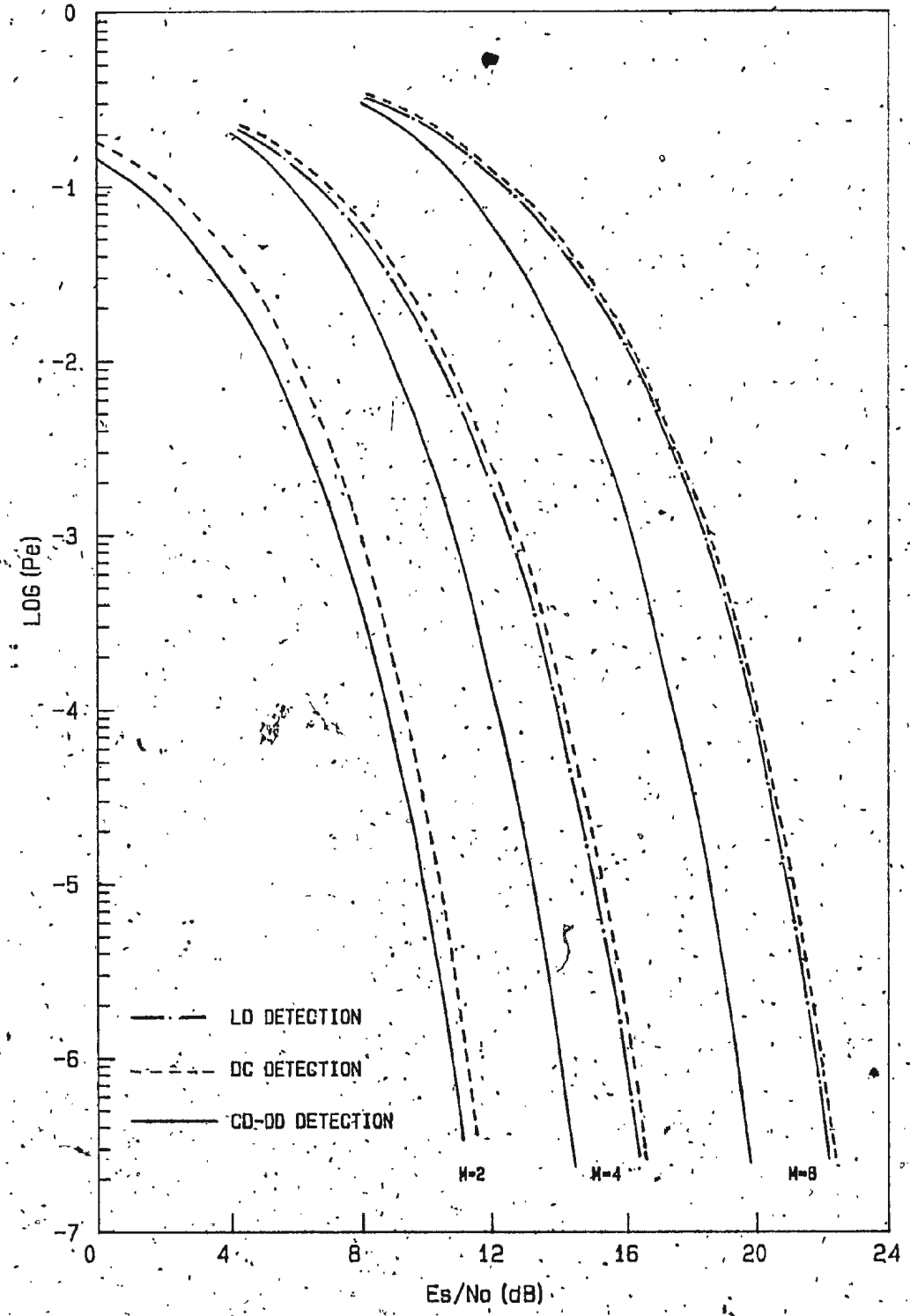

Fig. 2.3 Symbol Error Probability of CPFSK for CD-DD Detection, LD Detection and DC Detection (M=2,4 and 8, Wideband Channel and no Timing Error)

Figs. (2.4) – (2.6). It can be seen that the performance of LD and DC receivers degrades rapidly as the timing error increases. This is because of the piece-wise continuous nature of the phase trellis. The CD-DD detection does not suffer as much as the other two detection techniques by symbol timing errors. Further, there exist upper limits for the symbol timing error for the three detection techniques above which the detectors become useless. Noting that the maximum allowable error in the decision variable is $\frac{\pi}{M}$ for all three detection schemes, these upper limits can be obtained from Eqns. (2.15a), (2.15b), (2.17) and (2.19) as,

$$\tau_{max} = \begin{cases} \frac{T}{2(M-1)} & \text{for LD detection and DC detection} \\ \\ \frac{T}{(M-1)} & \text{for CD-DD detection} \end{cases}$$

We may conclude therefore, that CD-DD detection is less sensitive and more tolerable to symbol timing errors than LD detection and DC detection.

As indicated in the previous sections, the smoothening of the phase trellis at the symbol transition instants reduces the sensitivity and at the same time it improves the tolerance to the timing errors in all three detection techniques. In particular the performance of the LD detection and DC detection degrade less rapidly by timing errors. Upper limits of the timing error with pulse shaping

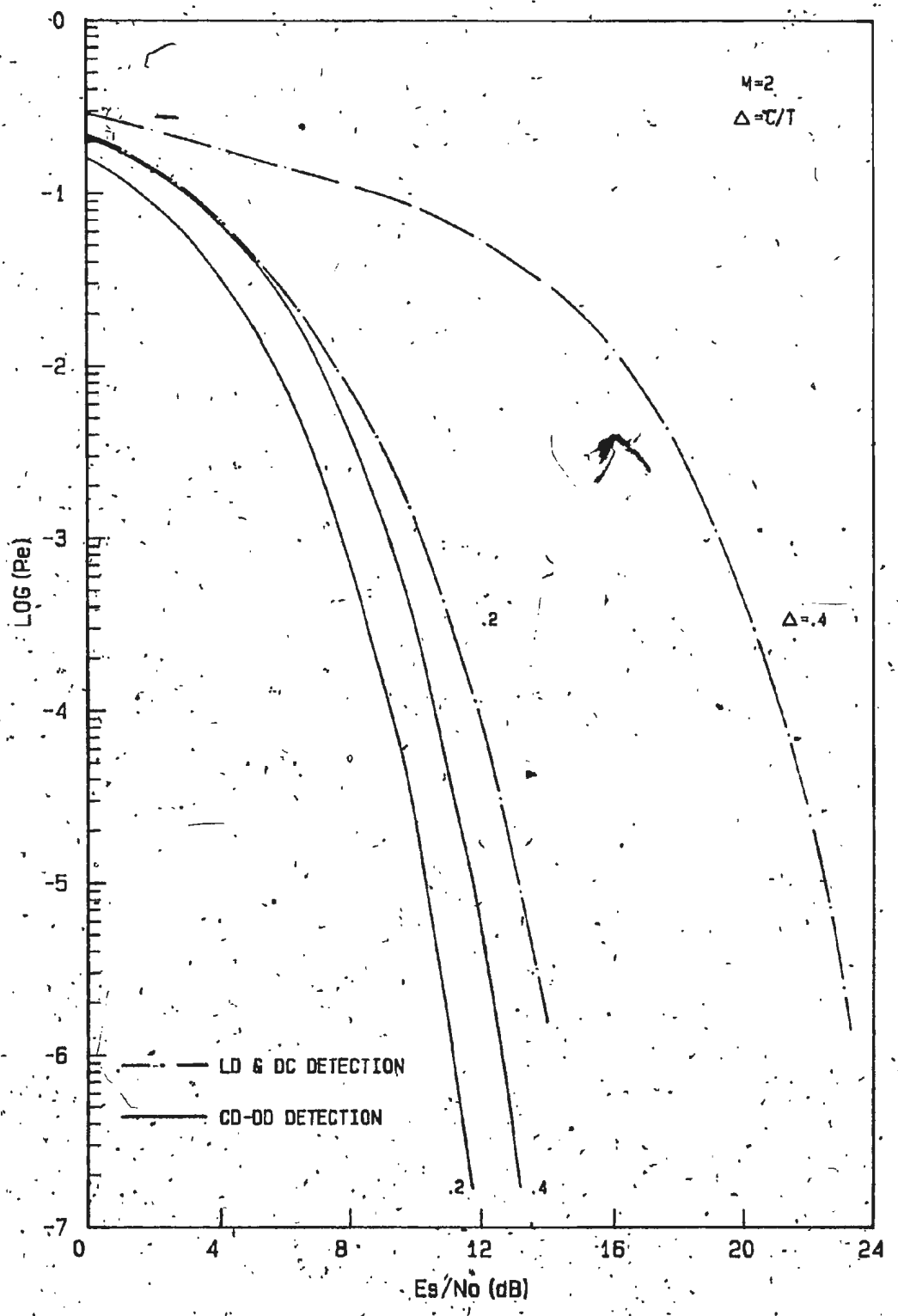

Fig. 2.4 Symbol Error Probability of Binary CPFSK for CD-DD Detection, LD Detection and DC Detection in the Presence of Symbol Timing Error

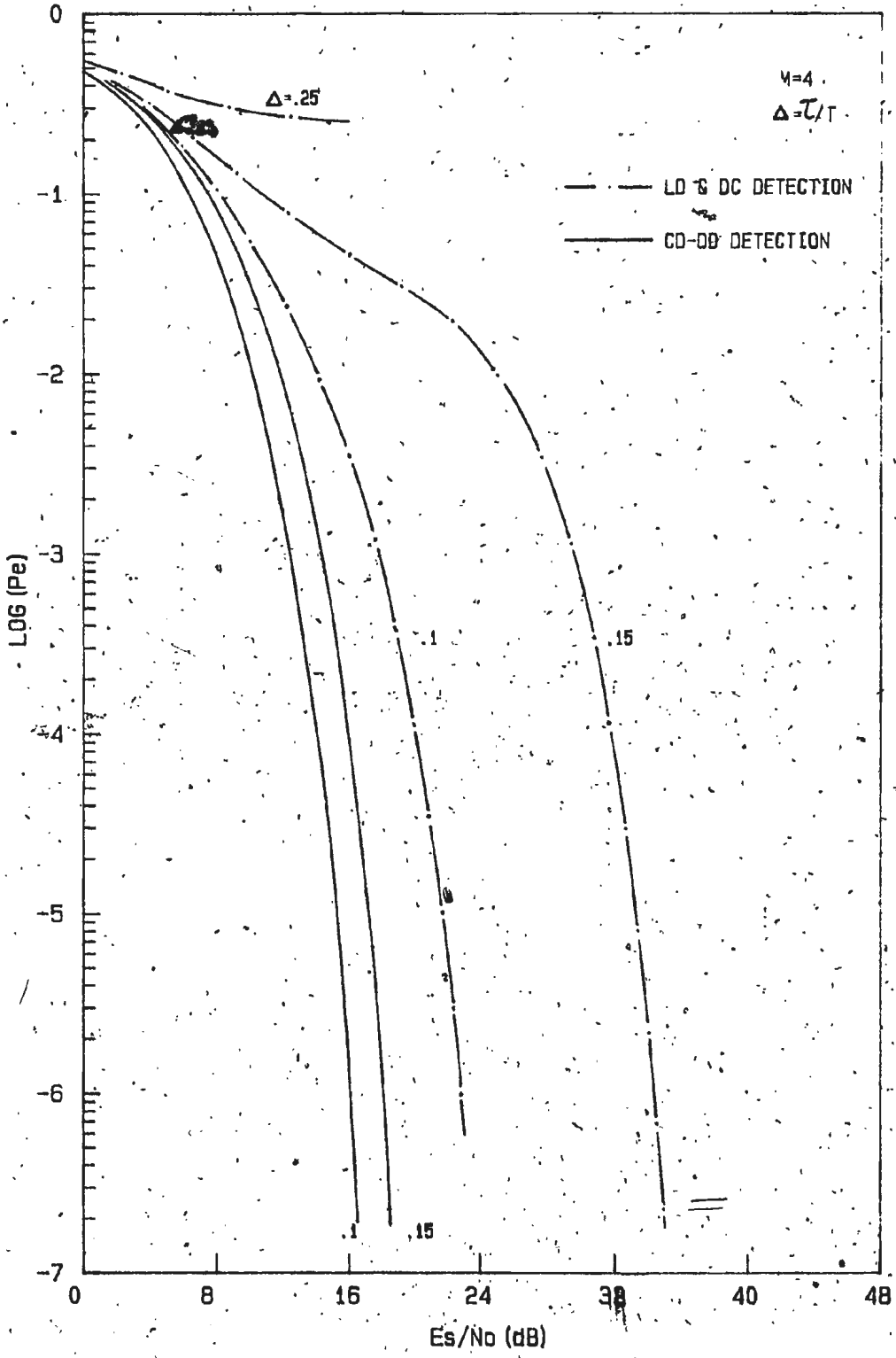

Fig. 2.5 Symbol Error Probability of Quaternary CPFSK for CD-DD Detection, LD Detection and DC Detection in the Presence of Symbol Timing Error

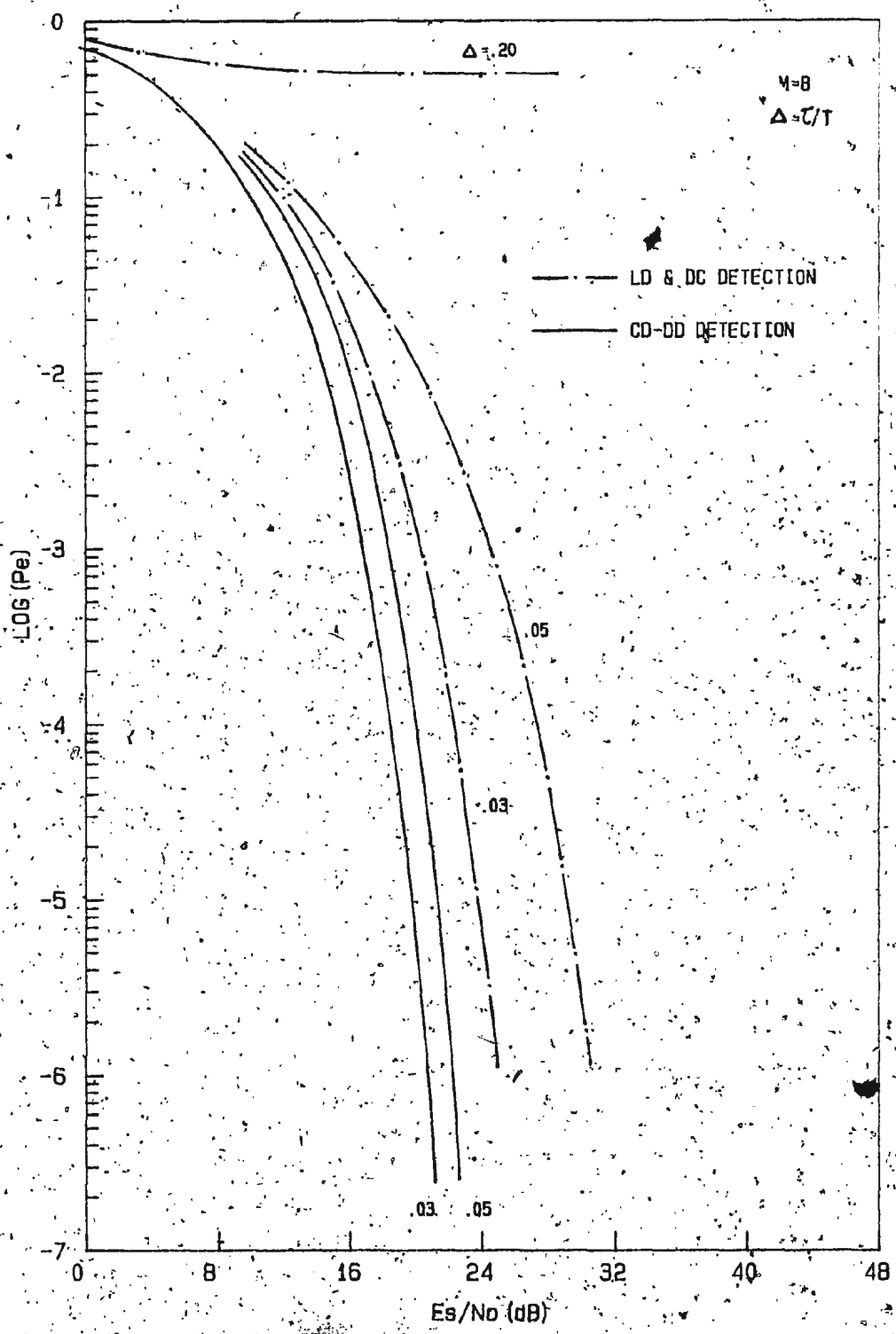

Fig. 2.6 Symbol Error Probability of Octonary CPFSK for CD-DD Detection, LD Detection and DC Detection in the Presence of Symbol Timing Error

follow from Eqns. (2.26a) and (2.26b) and satisfy,

$$\tau_{max} = \frac{T}{2(M-1)} + \frac{T}{2\pi} \sin\left(\frac{2\pi\ \tau_{max}}{T}\right) ;$$

for LD detection and DC detection

and $$\tau_{max} = \frac{T}{(M-1)} + \frac{T}{2\pi} \sin\left(\frac{2\pi\ \tau_{max}}{T}\right) ;$$

for CD-DD detection.

The pulse shaping function we have used in obtaining the numerical results has been suggested in the context of spectral shaping. We observe from Fig. (2.7) that these pulse shapes which improve spectral roll-off [4], also reduce the sensitivity to timing errors in all three receivers.

2.7 Conclusions

In this chapter, we have compared the differentially coherent detection technique and the coherent detection - differential decoding technique with the conventional limiter-discriminator detection technique for M-ary CPFSK with modulation index $\frac{1}{M}$. The effect of symbol timing errors has also been analyzed. From the numerical results, it has been concluded that differentially coherent detection and limiter-discriminator detection yield approximately the same performance. Also these two detection techniques exhibit high sensitivity to symbol timing errors.

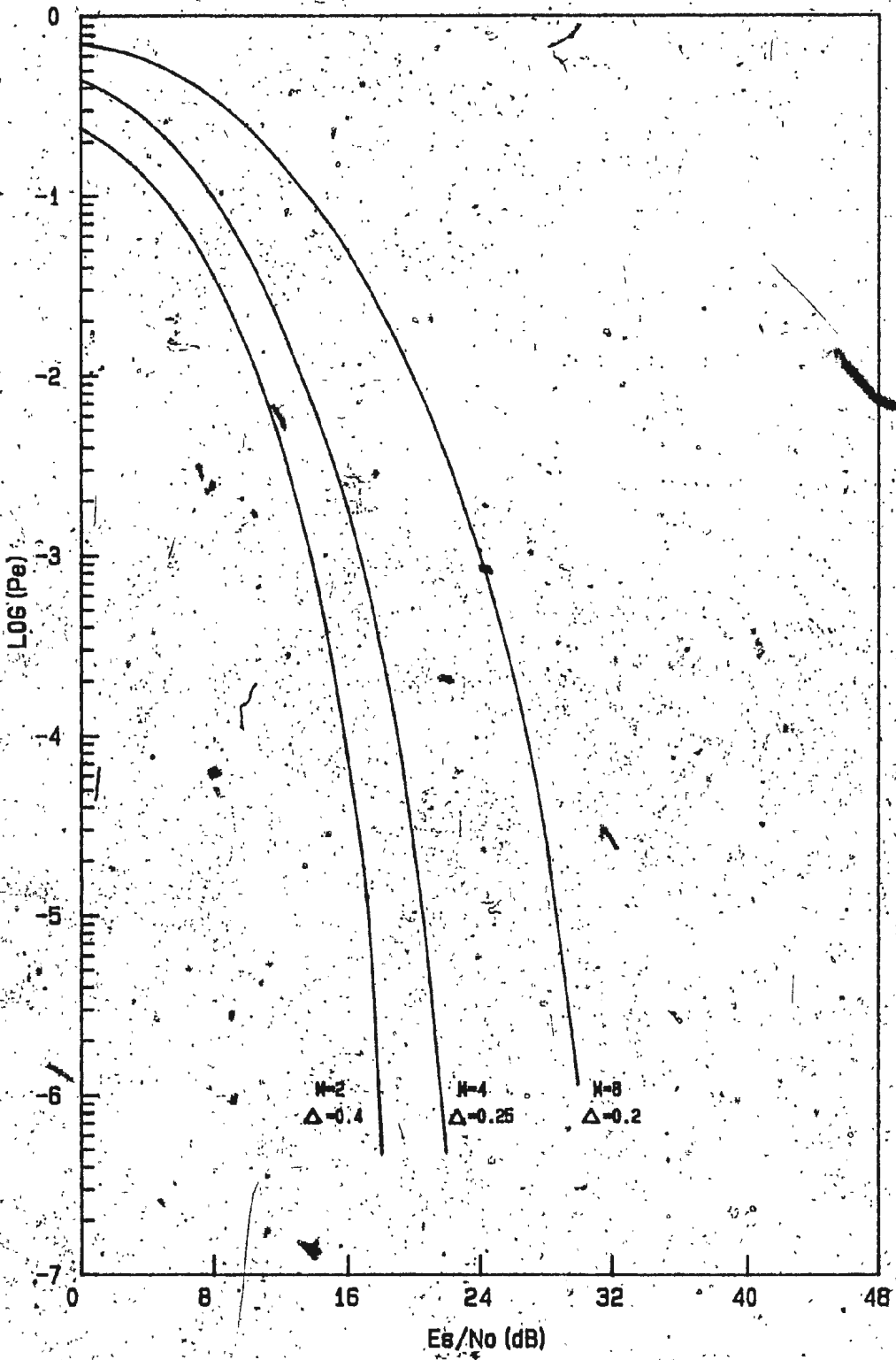

Fig. 2.7 Effect of Pulse Shaping and Symbol Timing Error on the Performance of LD Detection and DC Detection

It has been shown that symbol pulse shaping can be employed for reducing the sensitivity to timing errors. This is an added advantage of symbol pulse shaping which has been previously suggested for spectral shaping of CPFSK signals. The Coherent Detection - Differential Decoding technique has shown to yield better performance than the other two detection methods. However this improvement is gained at the expense of establishing a coherent carrier at the receiver.

CHAPTER 3

PERFORMANCE ANALYSIS OF CPFSK SIGNALS IN BANDLIMITED CHANNELS

3.1 Introduction

In this chapter, we compare the performance of CD-DD detection, DC detection and LD detection when bandlimiting effect of the channel is taken into consideration. The modulation index of CPFSK signals is assumed to be $\frac{1}{M}$. The Intersymbol Interference (ISI) caused by the front-end IF filter in all three detection schemes has been analyzed. The methodology we shall develop in this chapter which takes into account the effect of ISI, can be considered as a generalization of the recent results on binary CPFSK [25].

We first consider the signal distortion caused by IF filtering in detail as this is common to all three detection schemes. Secondly, we develop a methodology to handle ISI. This technique is then employed to analyze the performance of the three detection schemes. Finally, numerical results for the symbol error probabilities are presented for a Gaussian filter and a second order Butterworth filter.

3.2 IF Filtering

In this section, we consider the effect of the

receiver front-end IF filter on CPFSK signals. IF filtering changes the phase variation of the received signal and also spreads the signal corresponding to a particular symbol interval over the other symbol intervals causing Intersymbol Interference (ISI).

We recall from section 2.2 that the received signal in the presence of additive white noise can be represented as,

$$r(t) = \sqrt{\frac{2E_s}{T}} \cos(\omega_c t + \phi(t)) + n(t) \qquad (3.1)$$

Assuming the IF filter to have a frequency response symmetric about its center frequency ω_c, which implies that its impulse response is of the form $H'(t) = 2h(t) \cos \omega_c t$, the filtered signal can be expressed as,

$$r_0(t) = r(t) * H'(t)$$

$$= \sqrt{\frac{2E_s}{T}}\, a(t) \cos(\omega_c t + \theta(t)) + n_0(t) \qquad (3.2)$$

where

$$\theta(t) = \tan^{-1} \frac{h(t) * \sin \phi(t)}{h(t) * \cos \phi(t)} \qquad (3.3)$$

$$a(t) = \left[(h(t) * \sin \phi(t))^2 + (h(t) * \cos \phi(t))^2\right]^{1/2} \qquad (3.4)$$

$$h(t) * \sin \phi(t) = \int_{-\infty}^{\infty} h(\tau) \sin \phi(t-\tau)\, d\tau \qquad (3.5a)$$

$$h(t) * \cos \phi(t) = \int_{-\infty}^{\infty} h(\tau) \cos \phi(t-\tau)\, d\tau \qquad (3.5b)$$

$n_0(t)$ is the filtered noise component and $h(t)$ is the impulse response of the low pass equivalent of the IF filter. Expressing $n_0(t)$ in terms of its inphase and quadrature components $n_c(t)$ and $n_s(t)$, one can obtain,

$$r_0(t) = \sqrt{\frac{2E_s}{T}}\, a(t) \cos(\omega_c t + \theta(t)) + n_c(t) \cos(\omega_c t + \theta(t)) - n_s(t) \sin(\omega_c t + \theta(t))$$

$$= R(t) \cos(\omega_c t + \theta(t) + \eta(t))$$

$$= R(t) \cos(\omega_c t + \Psi(t)) \qquad (3.6)$$

where

$$\eta(t) = \tan^{-1} \frac{n_s(t)}{\sqrt{\frac{2E_s}{T}}\, a(t) + n_c(t)} \qquad (3.7)$$

is the noise component of the filtered phase angle and $R(t)$ is the envelope of the filtered signal which is not relevant to the three detection methods under consideration.

The time dependent SNR at the output of the filter can be written as,

$$\rho(t) = \frac{E_s\, a^2(t)}{E\{n_0^2(t)\}}$$

$$= \frac{E_s}{N_0} \frac{a^2(t)}{T \int_{-\infty}^{\infty} |H(f)|^2 df} \qquad (3.8a)$$

$$= \frac{E_s'}{N_0}\, a^2(t) \qquad (3.8b)$$

where

$$\frac{E_s'}{N_0} = \frac{E_s}{N_0} \frac{1}{T \int_{-\infty}^{\infty} |H(f)|^2 df} \qquad (3,8c)$$

H(f) is the Fourier Transform of h(t) and $\frac{N_0}{2}$ is the two sided power spectral density of n(t).

The filtered signal given by Eqn. (3.6) is common to all three detection schemes since IF filtering is done in all of them. Fig. (3.1) shows the phase variation of the filtered signal for a selected transmitted sequence. The time shift δ', between the filtered phase $\theta(t)$ and the transmitted phase $\phi(t)$ is generally non zero, specifically if the filter has non zero phase response. In deriving the error probability expressions in the following sections, we assume that the filter phase response is zero so that $\delta'=0$. These expressions can however be easily modified to accommodate real filters by simply shifting the filtered phase response by a time period of δ'.

The phase variation $\theta(t)$ and the SNR $\rho(t)$ given by Eqns. (3.3) and (3.8a), during any particular symbol interval are dependent on the neighbouring symbols. In all three detection schemes the decision on the symbol a_n is based on the phase angles $\theta(nT)$ and $\theta((n+1)T)$ taken at time instants $t=nT$ and $t=(n+1)T$ respectively. Since these phase angles are dependent on the values of the neighbouring symbols, the ISI

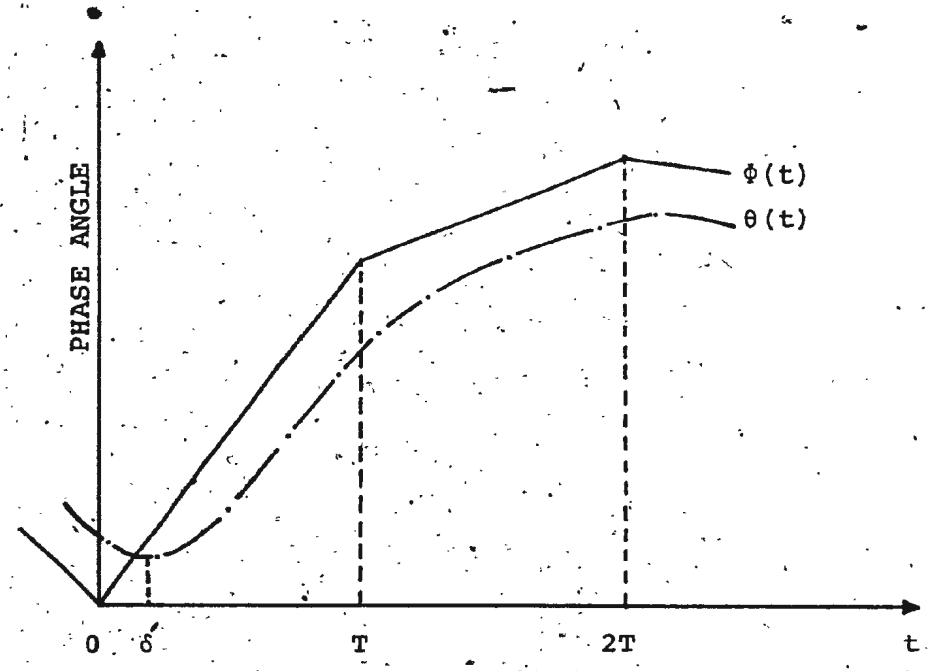

Fig. 3.1 Phase Variation of the Received and Filtered Signals

effect has to be taken into account in evaluating the performance of the detection schemes. The performance evaluation in the presence of ISI can be carried out by, first evaluating the performance conditioned on ISI and then averaging over all possible ISI combinations. However, as we shall show in the next section, the number of symbol patterns that need to be considered can be reduced significantly.

3.3. ISI Consideration

In this section, we develop a technique to analyze the effect of ISI assuming that only the adjacent symbols cause ISI. Although the method is strictly an ensemble averaging process, it requires a much less number of symbol patterns to account for all possible ISI combinations. In ref. [25], this technique has been discussed for the binary CPFSK signals using two basic bit patterns, all ones and alternating ones. We shall observe that this method can be satisfactorily extended to analyze the effect of ISI in multilevel CPFSK by simply increasing the number of symbol patterns that need to be considered.

In addition to the adjacent ISI assumption, which implies the duration of the interference caused by any symbol does not exceed a symbol duration T, it is reasonable to make a stronger assumption that the interference during the first

half of a symbol interval is only due to the previous symbol and that during the second half is only due to the following symbol (see Fig. (3.2)). Therefore any symbol interval T can be treated as being interfered by two independent interferences each having a duration $\frac{T}{2}$. We refer to this half interval interference caused by a single symbol as single symbol interference. In order for this assumption to be valid, the time-bandwidth product (BT) has to be sufficiently large; it shall be verified that when the time-bandwidth product (BT_b) is approximately greater than 1.0, the ISI decays rapidly and does not last more than half a symbol duration. This restriction on BT value does not limit the applicability of our analysis, because the receivers tend to yield poor performance when BT becomes small. Figs. (3.3) to (3.5) show the variation of $\theta(t)$ and $a(t)$ for a Gaussian filter which are computed using a few selected symbol patterns. These variations have been considered for the worst combinations which result in maximum interference. Moreover, the ISI is stronger for large values of h due to the increased rate of phase change. These variations illustrate the validity of the assumption for the selected cases. Therefore it follows that for all cases we consider in our analysis, the single symbol interference assumption is reasonably valid.

By considering the symbol interval in two parts,

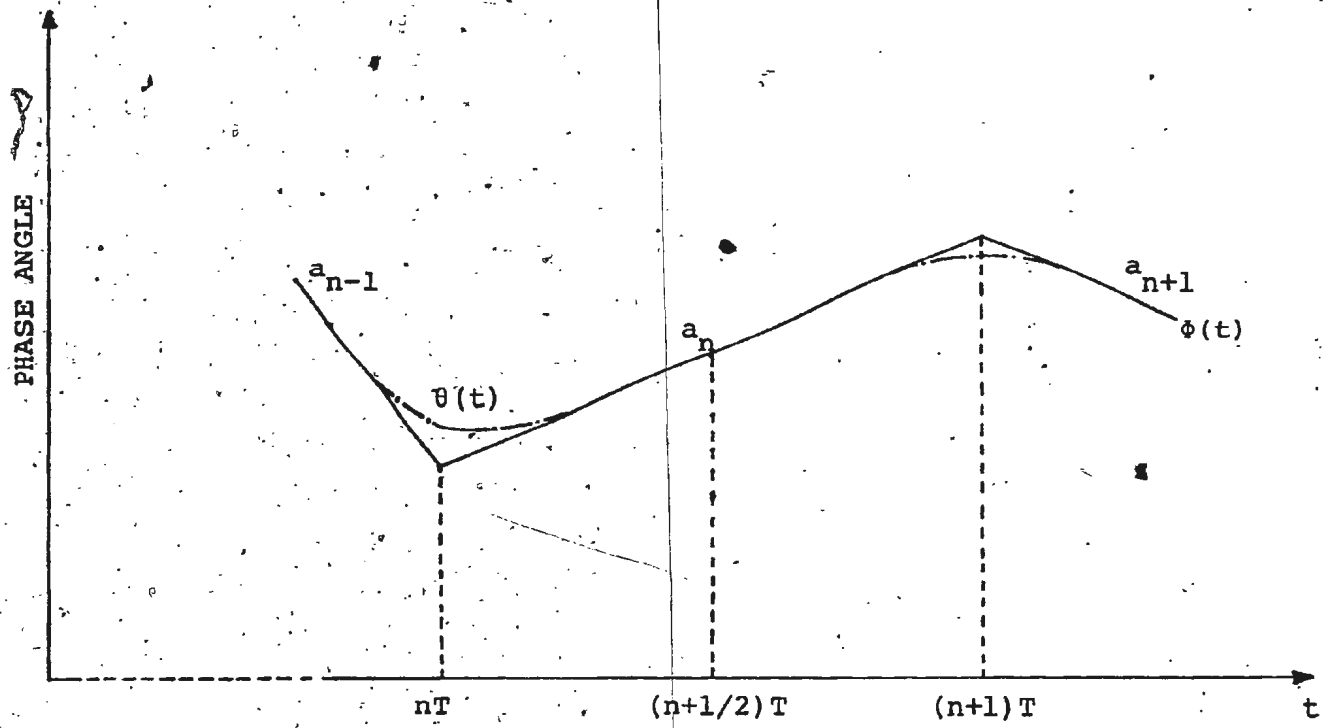

Fig. 3.2 Effect of Single Symbol Interference

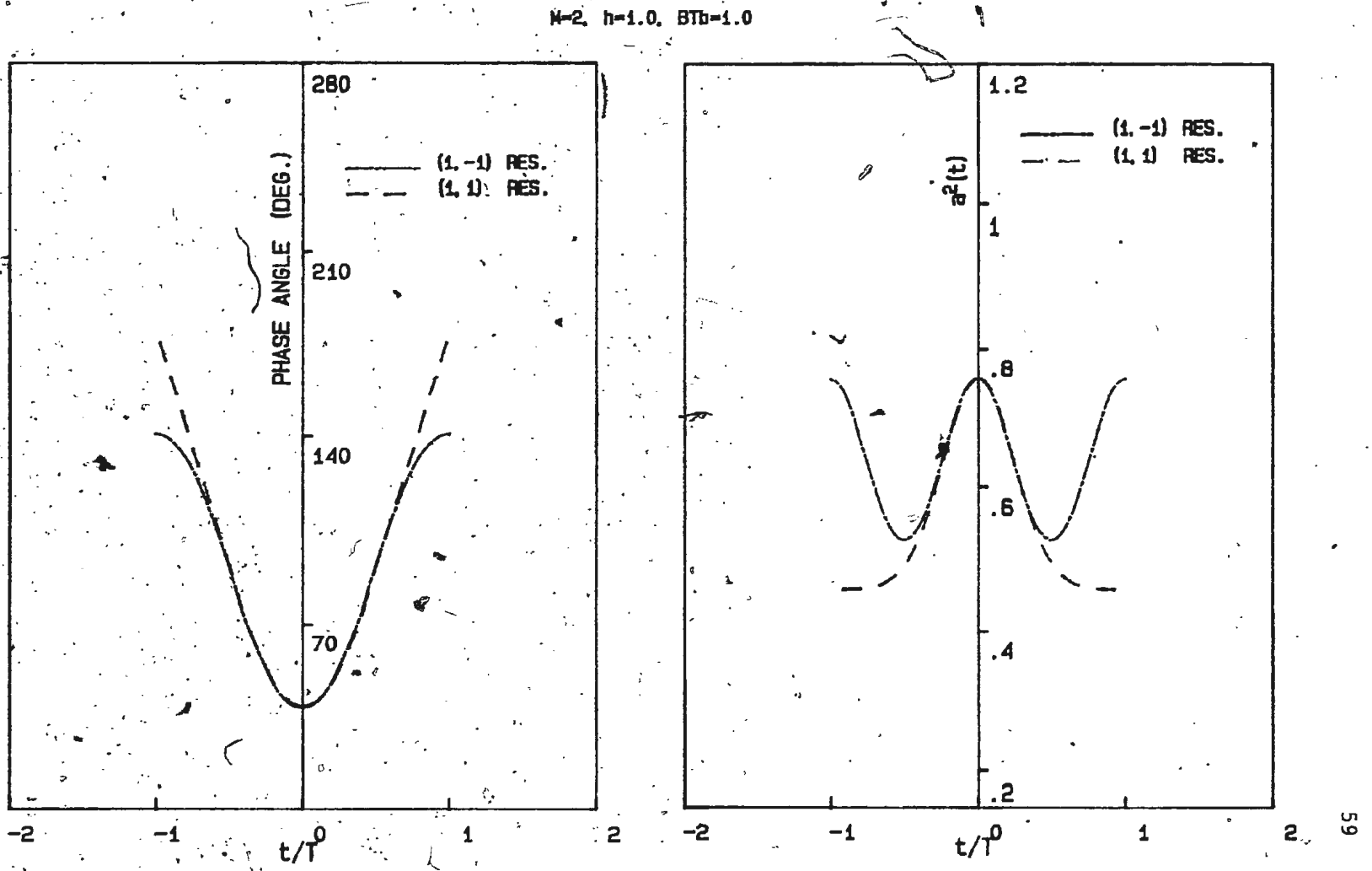

Fig. 3.3 Phase Angle and SNR Variation of the Filtered Signal of Binary CPFSK with a Gaussian Filter ($h=1$, $BT_b=1.0$)

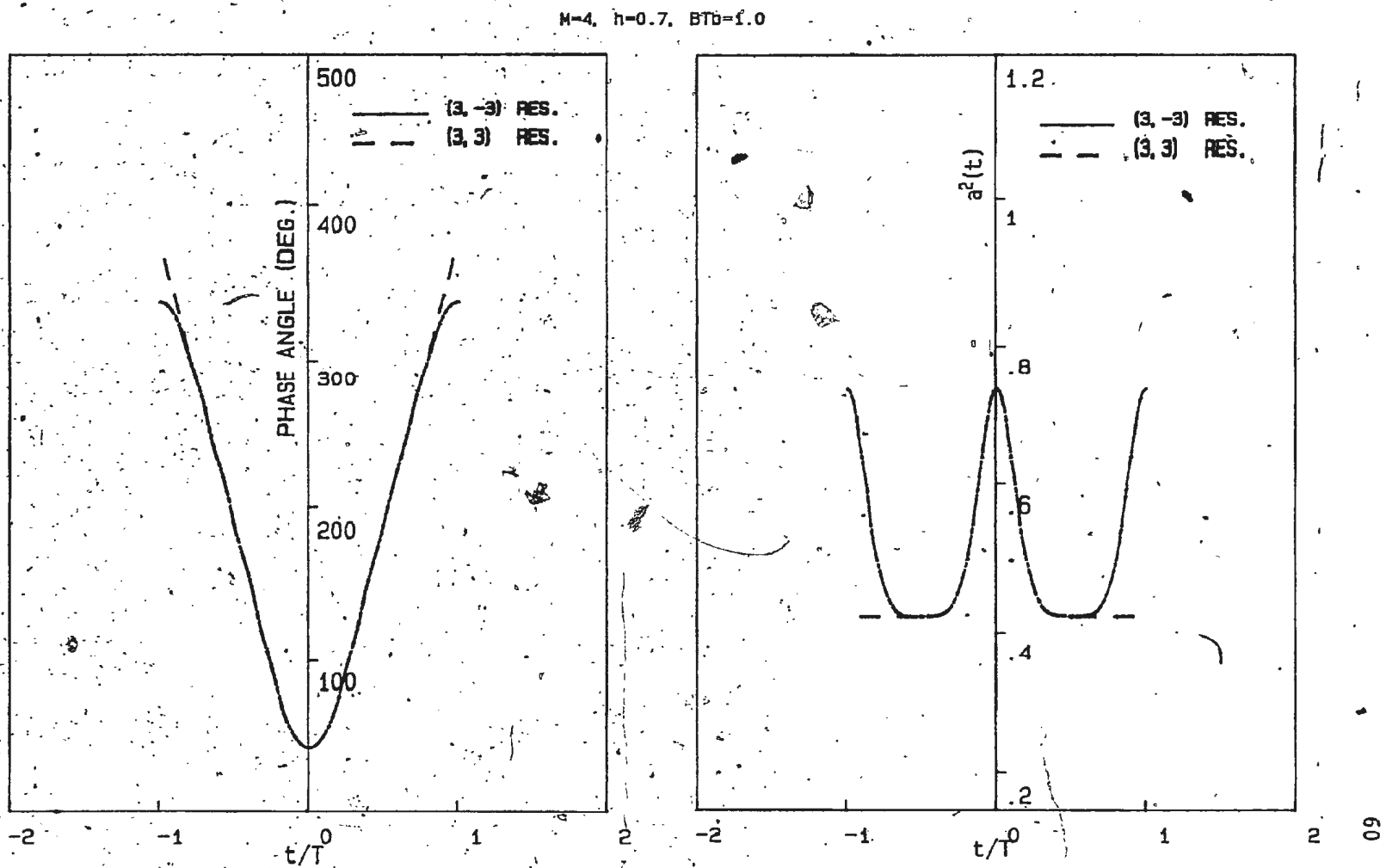

Fig. 3.4 Phase Angle and SNR Variation of the Filtered Signal of Quaternary CPFSK with a Gaussian Filter (h=0.7, BT_b = 1.0)

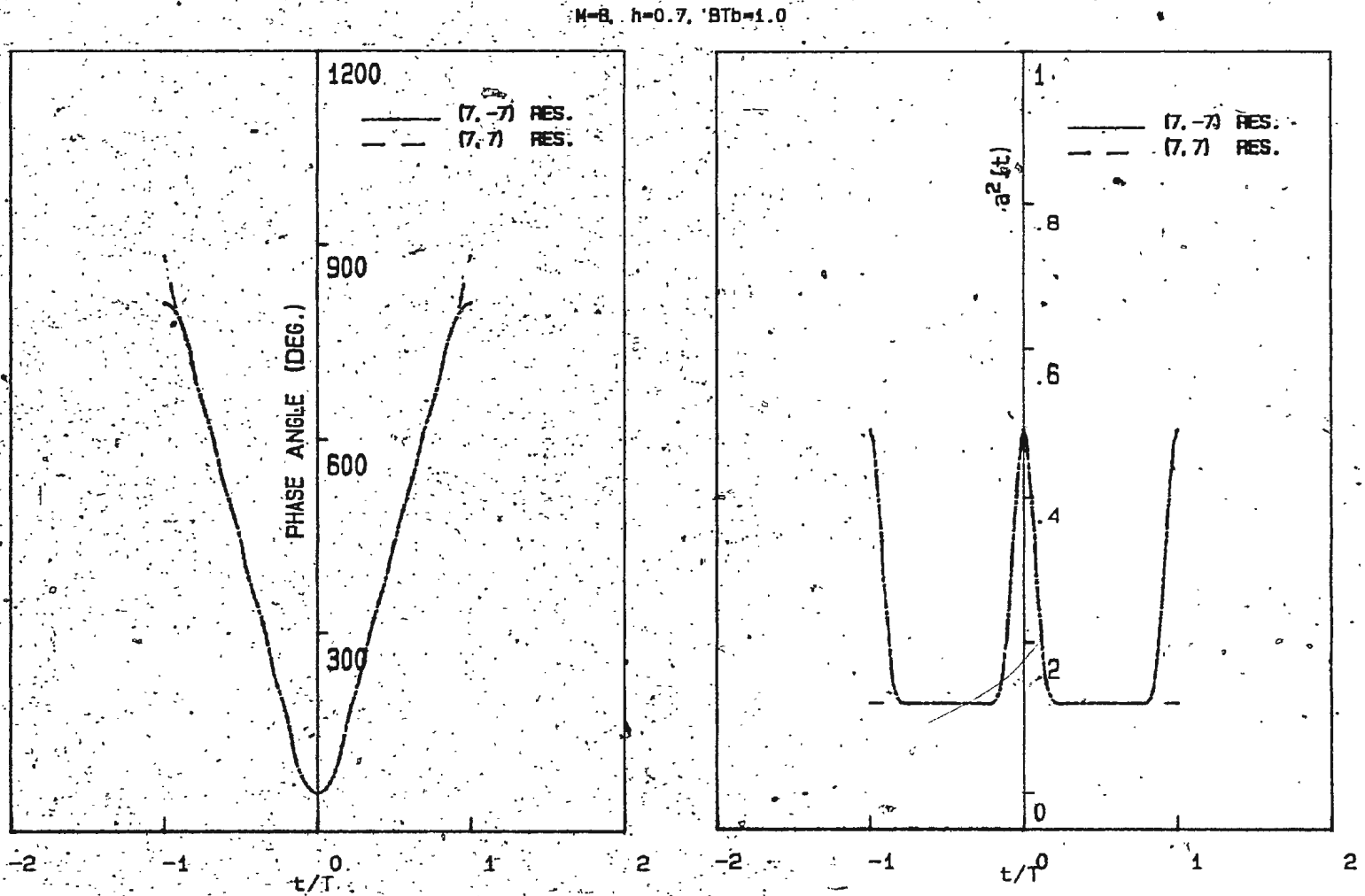

Fig. 3.5 Phase Angle and SNR Variation of the Filtered Signal of Octonary CPFSK with a Gaussian Filter ($h=0.7$, $BT_b=1.0$)

the adjacent ISI caused on any given symbol can be analyzed using only M single symbol interferences. Therefore, due to the symmetry of the signal set, considering only positive symbols as detected symbols, the entire adjacent ISI combinations can be analyzed using $\frac{M^2}{2}$ single symbol interferences.

3.4 Evaluation of Single Symbol Interference

The interference caused by symbol a_{n+1} on symbol a_n can be determined by considering an arbitrary symbol sequence. However, one can judiciously select a suitable symbol pattern which will considerably simplify the analysis [25]. For this purpose, we select a repetitive symbol sequence which results an even symmetric, periodic variation for $\phi(t)$ with a period of $4T_c$ as shown in Fig. (3.6). The symbol pattern which yields the above variation of $\phi(t)$ is $(\ldots, -a_n, a_n, a_{n+1}, -a_{n+1}, -a_n, a_n \ldots)$. We note that this is the symbol pattern which has the minimum period thus reducing the number of Fourier series coefficients required in calculations. The resulting $\phi(t)$ due to the selected sequence over a full period $0<t<4T$ is,

$$\phi(t) = \begin{cases} \dfrac{\pi a_n t}{MT} & , \quad 0 < t < T \\ \dfrac{\pi a_{n+1} t}{MT} + \dfrac{\pi}{M}(a_n - a_{n+1}) & , \quad T<t<2T \\ \phi(4T - t) & , \quad 2T<t<4T \end{cases} \qquad (3.9)$$

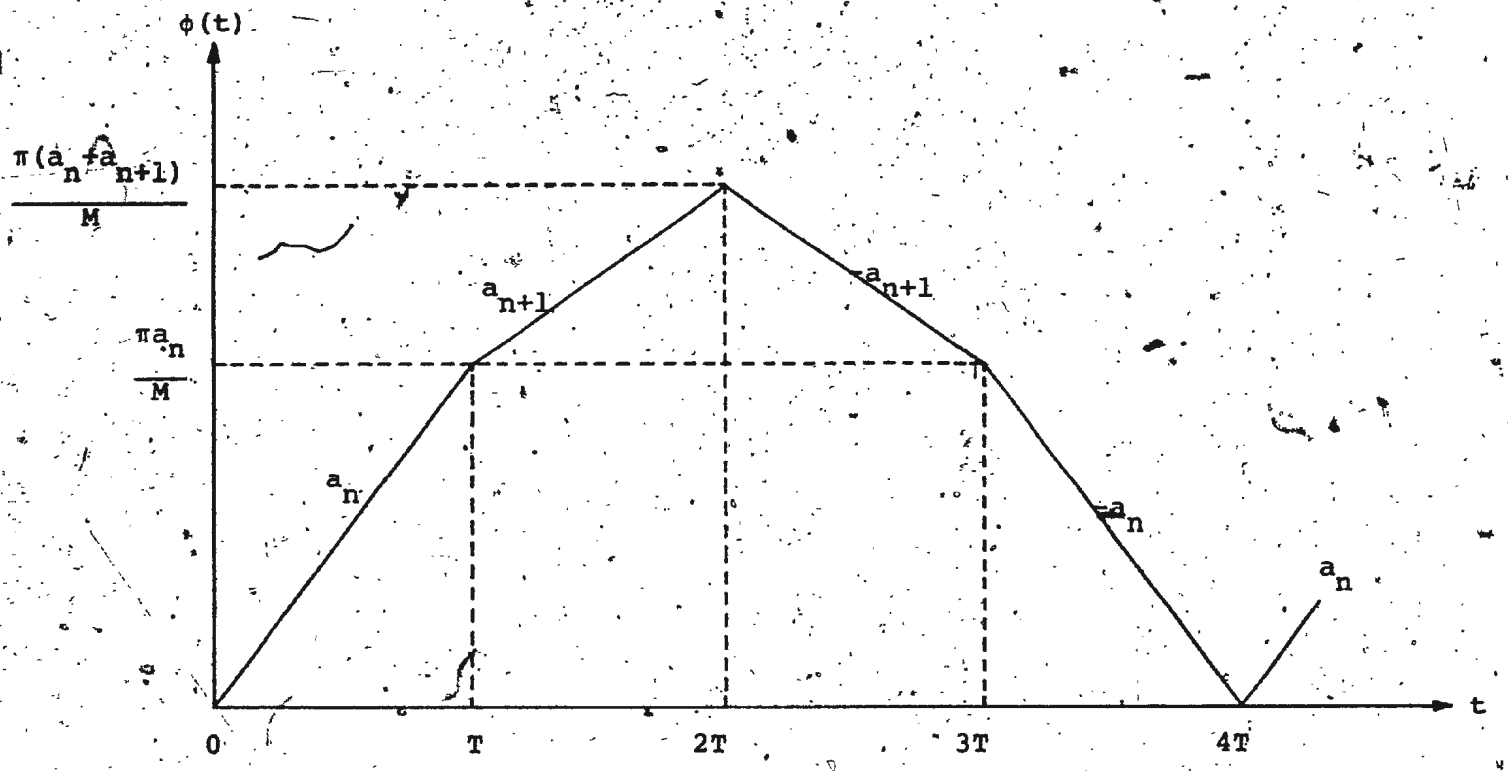

Fig. 3.6 Phase Variation for the Selected Symbol Sequence

Since $\sin \phi(t)$ and $\cos \phi(t)$ are both periodic with period $4T$, they can be expressed in Fourier series expansions as,

$$\sin \phi(t) = \frac{A_0}{2} + \sum_{p=1}^{N'} A_p \cos (2\pi p f_0 t) \qquad (3.10a)$$

and

$$\cos \phi(t) = \frac{B_0}{2} + \sum_{p=1}^{N'} B_p \cos(2\pi p f_0 t) \qquad (3.10b)$$

where $f_0 = \frac{1}{4T}$. The number of coefficients N' has to be sufficiently large to obtain the filtered phase and SNR accurately. The Fourier Coefficients A_p's and B_p's are given in Appendix B.

Using the Fourier expansions (3.10a) and (3.10b), $\theta(t)$ and $a(t)$ can be expressed as,

$$\theta_{a_n, a_{n+1}}(t) = \tan^{-1} \frac{P(t)}{Q(t)} \qquad (3.11)$$

and

$$\rho_{a_n, a_{n+1}}(t) = \frac{[(P(t))^2 + (Q(t))^2]}{T \int_{-\infty}^{\infty} |H(f)|^2 \, df} \qquad (3.12)$$

where

$$P(t) = \frac{A_0}{2} + \sum_{p=1}^{N'} A_p \, |H(pf_0)| \cos (2\pi p f_0 t + \angle H(pf_0)) \qquad (3.13a)$$

and

$$Q(t) = \frac{B_0}{2} + \sum_{p=1}^{N'} B_p |H(pf_0)| \cos (2\pi pf_0 t + \underline{/H(pf_0)}) \tag{3.13b}$$

Noting that in the above selected basic pattern the interference caused by the symbol a_{n+1} on the symbol a_n is totally present during the interval $\frac{T}{2} < t < T$, the Eqns. (3.11) and (3.12) provide the phase variation and SNR corresponding to that particular single symbol interference. We next define for convenience,

$$\beta_{a_n,a_{n+1}} \triangleq \frac{\pi a_n}{M} - \theta_{a_n,a_{n+1}}(T) \tag{3.14}$$

which is the error in the phase angle at $t=(n+1)T$ due to the interference caused by a_{n+1} on a_n

and $$\rho_{a_n,a_{n+1}} \triangleq \rho_{a_n,a_{n+1}}(T) \tag{3.15}$$

which is the SNR at $t=(n+1)T$.

By interchanging a_n and a_{n+1} in the above selected basic pattern, it can be observed that,

$$\beta_{a_{n+1},a_n} = -\beta_{a_n,a_{n+1}} \tag{3.16a}$$

and

$$\rho_{a_{n+1},a_n} = \rho_{a_n,a_{n+1}} \tag{3.16b}$$

For any given symbol a_n, all single symbol interferences are obtained by considering all possible

combinations of (a_n, a_{n+1}). Although M such combinations exist, a reduction by a factor of two is possible for M>2, due to the following reasons:

(1) The interference caused by $a_{n+1} = -a_n$ on a_n is present in all basic patterns in the interval $0 < t \leq \frac{T}{2}$.

(2) The interference caused by $a_{n+1} = a_n$ on a_n can be evaluated [25] as,

$$\theta(t) = \phi(t) \tag{3.17a}$$

and

$$\rho(t) = \frac{E_s}{N_0} \frac{\left|H\left(\frac{\beta_n}{2MT}\right)\right|^2}{T \int_{-\infty}^{\infty} |H(f)|^2 \, df}$$

$$= \frac{E'_s}{N_0} \left|H\left(\frac{a_n}{2MT}\right)\right|^2 \tag{3.17b}$$

during the interval $\frac{T}{2} < t < T$, for $a_{n+1} = a_n$.

Hence for any given symbol a_n, all single symbol interferences are obtained using (M-2) basic patterns. However, for the binary case (i.e. M=2) a single basic pattern of alternating ones [25] has to be considered.

Because of the symmetry of the signal set, we need to consider only one half of the symbol set for a_n, which results in a total number of basic patterns,

$$N_p = \begin{cases} \frac{M}{2}(M-2) & , M>2 \\ 1 & , M=2 \end{cases} \tag{3.18}$$

It is of interest to note that although a total number of $M^3/2$ symbol patterns are involved in causing adjacent ISI, only $\frac{M}{2}(M-2)$ number of basic patterns are actually required to analyze all of them.

3.5 Performance Evaluation

In this section we consider the performance evaluation of the detection schemes. The detection of the symbol a_i with a_ℓ and a_t as adjacent symbols is considered as shown in Fig (3.7). The observed phase angles and SNR values for this pattern of $(\ldots a_\ell, a_i, a_t \ldots)$, at time instants $t = nT$ and $t = (n+1)T$ can be expressed in terms of single symbol interferences as, [c.f. Eqns. (3.6), (3.14), (3.15), (3.16a) and (3.16b)]

$$\Psi(nT) = \phi(nT) + \beta_{a_i,a_\ell} + \eta(nT) \qquad (3.19a)$$

and

$$\Psi((n+1)T) = \phi((n+1)T) - \beta_{a_i,a_t} + \eta((n+1)T) \qquad (3.19b)$$

and

$$\rho(nT) = \rho_{a_i,a_\ell} \qquad (3.20a)$$

$$\rho((n+1)T) = \rho_{a_i,a_t} \qquad (3.20b)$$

The symbol error probability associated with the detection of the symbol a_i is first evaluated by conditioning

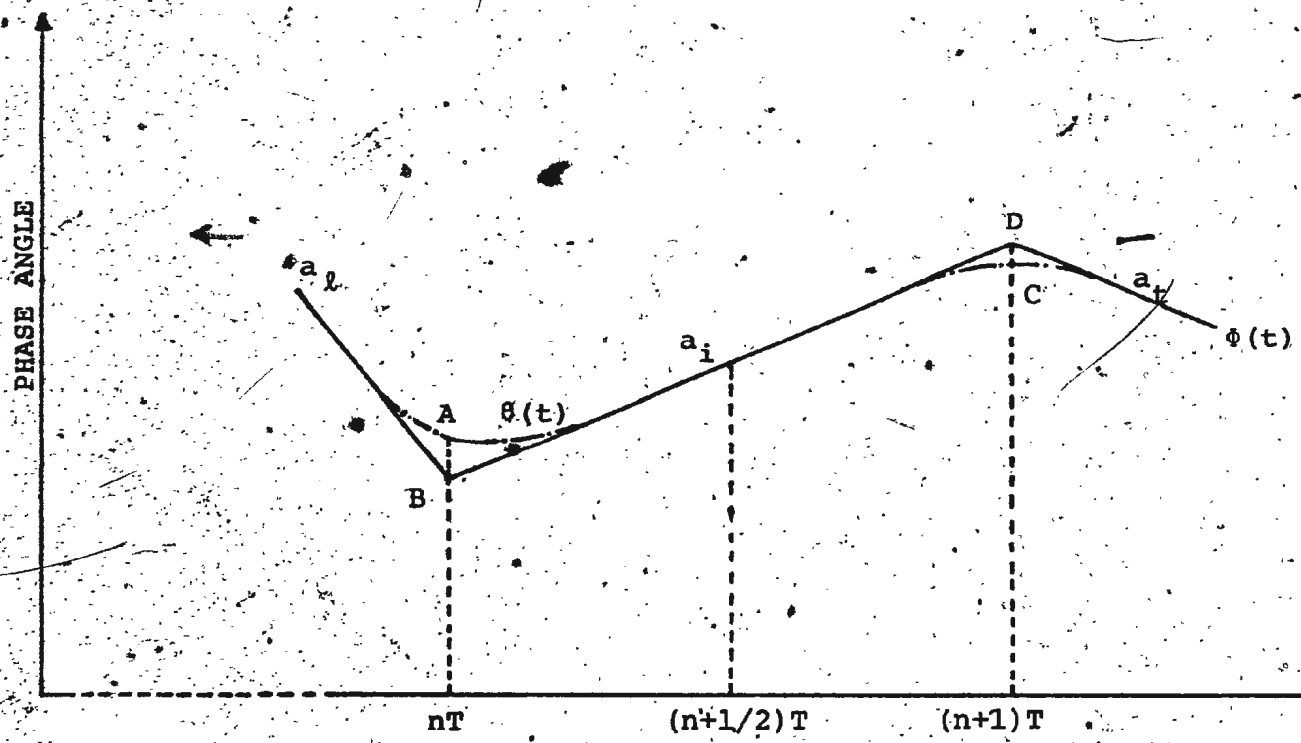

$$AB = |\beta_{a_i,a_\ell}|$$

$$CD = |\beta_{a_i,a_t}|$$

$$\rho(nT) = \rho_{a_i,a_\ell}$$

$$\rho((n+1)T) = \rho_{a_i,a_t}$$

Fig 3.7 Effect of Intersymbol Interference at Sampling Instants

on ISI due to adjacent symbols a_ℓ and a_t. The unconditional error probability is then evaluated by averaging over all possible ISI combinations. Only the positive half of the symbol set is considered for a_i due to the symmetry.

3.5.1 CD-DD Detection

Recalling section 2.3.1, the error probability associated with the symbol a_i in the general pattern $(\ldots a_\ell, a_i, a_t \ldots)$ being considered can be written as,

$$P_{e|a_\ell,a_i,a_t} = 1-\text{pr}[\text{correct decision}|_{a_\ell,a_i,a_t}]$$

$$= 1-\Pr[-\tfrac{\pi}{M} < (\Psi(nT)-\phi(nT))|_{a_\ell,a_i} < \tfrac{\pi}{M}]$$

$$\cdot \Pr[-\tfrac{\pi}{M}<(\Psi((n+1)T)-\phi((n+1)T))|_{a_i,a_t}<\tfrac{\pi}{M}]$$

$$- \sum_{k=1}^{(M-1)} \{\Pr[(2k-1)\tfrac{\pi}{M}<(\Psi(nT)-\phi(nT))|_{a_\ell,a_i}<(2k+1)\tfrac{\pi}{M}]$$

$$\cdot \Pr[(2k-1)\tfrac{\pi}{M}<(\Psi((n+1)T)-\phi((n+1)T))|_{a_i,a_t}<(2k+1)\tfrac{\pi}{M}]\}$$

$$\approx 1-\Pr[-\tfrac{\pi}{M}<(\Psi(nT)-\phi(nT))|_{a_\ell,a_i}<\tfrac{\pi}{M}]$$

$$\cdot \Pr[-\tfrac{\pi}{M} <(\Psi((n+1)T) - \phi((n+1)T))|_{a_i,a_t}<\tfrac{\pi}{M}]$$

$$\approx \{1-\Pr[-\tfrac{\pi}{M} <(\Psi(nT)-\phi(nT))|_{a_\ell,a_i} < \tfrac{\pi}{M}]\}$$

$$+ \{1 - \Pr[-\tfrac{\pi}{M} < (\Psi((n+1)T) - \phi((n+1)T))|_{a_i,a_t} < \tfrac{\pi}{M}]\}$$

$$= 2 - \Pr\left[-\frac{\pi}{M} < \beta_{a_i,a_\ell} + \eta(nT) < \frac{\pi}{M}\right]$$

$$- \Pr\left[-\frac{\pi}{M} < -\beta_{a_i,a_t} + \eta((n+1)T) < \frac{\pi}{M}\right]; \text{at high SNR}$$

(3.21)

The unconditional error probability is then obtained by averaging over all possible combinations of a_ℓ, a_i and a_t as,

$$P_e = E\left[P_e \middle| a_\ell, a_i, a_t\right]$$

$$= 2\left[1 - \frac{2}{M^2}\sum_{i=1}^{M/2}\sum_{\ell=1}^{M} \Pr\left[-\frac{\pi}{M} < \beta_{a_i,a_\ell} + \eta(nT) < \frac{\pi}{M}\right]\right];$$

at high SNR (3.22)

Each of the above probabilities can be numerically evaluated as shown in Appendix C.

3.5.2 DC Detection

The phase detector input for the general symbol pattern $(\ldots a_\ell, a_i, a_t \ldots)$ being considered, can be written as, [c.f. Eqns. (3.19a) and (3.19b)]

$$\Delta\Psi = \Psi((n+1)T) - \Psi(nT)$$

$$= \theta((n+1)T) - \theta(nT) + \eta((n+1)T) - \eta(nT)$$

$$= \phi((n+1)T) - \phi(nT) - (\beta_{a_i,a_\ell} + \beta_{a_i,a_t}) + \alpha$$

$$= \frac{\pi a_i}{M} - (\beta_{a_i,a_\ell} + \beta_{a_i,a_t}) + \alpha \qquad (3.23)$$

where

$$\alpha = \eta((n+1)T) - \eta(nT) \bmod 2\pi.$$

The symbol error probability is found by first evaluating the conditional error probability,

$$P_e|_{a_\ell, a_i, a_t} = 1 - Pr[-\frac{\pi}{M} < (\Delta\Psi - \frac{\pi a_i}{M})|_{a_\ell, a_i, a_t} < \frac{\pi}{M}]$$

$$= 1 - Pr[-\frac{\pi}{M} < -(\beta_{a_i,a_\ell} + \beta_{a_i,a_t}) + \alpha < \frac{\pi}{M}]$$

and then averaging this over a_ℓ, a_i and a_t as,

$$P_e = 1 - \frac{2}{M^3} \sum_{i=1}^{M/2} \sum_{\ell=1}^{M} \sum_{t=1}^{M} Pr[-\frac{\pi}{M} < -(\beta_{a_i,a_\ell} + \beta_{a_i,a_t}) + \alpha < \frac{\pi}{M}] \quad (3.24)$$

Each of the above probabilities can be numerically evaluated as shown in Appendix C.

3.5.3 LD Detection

The decision variable of the LD detector for the symbol pattern (... a_ℓ, a_i, a_t ...) is

$$\Delta\Phi = \Psi((n+1)T) - \Psi(nT) + 2\pi N$$

$$= \theta((n+1)T) - \theta(nT) + \eta((n+1)T) - \eta(nT) + 2\pi N$$

$$= \frac{\pi a_i}{M} - (\beta_{a_i,a_\ell} + \beta_{a_i,a_t}) + \alpha + 2\pi N \quad (3.25)$$

where $\alpha = \eta((n+1)T) - \eta(nT) \bmod 2\pi$ and N denotes the number of clicks in the interval nT to (n+1)T.

The probability of making an error on the symbol a_i

can be written as,

$$P_{e|a_\ell,a_i,a_t} = \begin{cases} 1-\Pr\left[-\frac{\pi}{M} < \left(\Delta\Phi - \frac{\pi a_i}{M}\right)\Big|_{a_\ell,a_i,a_t} < \frac{\pi}{M}\right], & a_i \neq (M-1) \\ 1-\Pr\left[-\frac{\pi}{M} < \left(\Delta\Phi - \frac{\pi a_i}{M}\right)\Big|_{a_\ell,a_i,a_t} < \infty\right], & a_i = (M-1) \end{cases}$$

$$= \begin{cases} 1-\Pr\left[-\frac{\pi}{M} < -\left(\beta_{a_i,a_\ell} + \beta_{a_i,a_t}\right) + \alpha < \frac{\pi}{M}\right]\Pr(N=0), & a_i \neq (M-1) \\ 1-\Pr\left[-\frac{\pi}{M} < -\left(\beta_{a_i,a_\ell} + \beta_{a_i,a_t}\right) + \alpha < \pi\right]\Pr(N=0), & a_i = (M-1) \end{cases}$$

Recalling that $\Pr(N=0) \approx 1-\bar{N}$ at high SNR where $\bar{N} = \int_{nT}^{(n+1)T} e^{-\rho(\tau)}\,\theta(\tau)\,d\tau$, the conditional error probability of the symbol a_i at high SNR is,

$$P_{e|a_\ell,a_i,a_t} = \begin{cases} \left(1-\Pr\left[-\frac{\pi}{M} < -\left(\beta_{a_i,a_\ell} + \beta_{a_i,a_t}\right) + \alpha < \frac{\pi}{M}\right]\right) + \bar{N}, & a_i \neq (M-1) \\ \left(1-\Pr\left[-\frac{\pi}{M} < -\left(\beta_{a_i,a_\ell} + \beta_{a_i,a_t}\right) + \alpha < \pi\right]\right) + \bar{N}, & a_i = (M-1) \end{cases}$$

Next we observe that $P_{e|a_\ell,a_i,a_t}$ can be treated as a sum of two terms as,

$$P_{e|a_\ell,a_i,a_t} = P_{\text{cont.}|a_\ell,a_i,a_t} + P_{\text{clicks}|a_\ell,a_i,a_t}, \quad \rho \gg 1 \qquad (3.26a)$$

where

$$P_{cont.}\Big|_{a_\ell, a_i, a_t} = \begin{cases} 1-Pr\left[-\frac{\pi}{M} < -(\beta_{a_i,a_\ell}+\beta_{a_i,a_t})+\alpha < \frac{\pi}{M}\right], & a_i \neq (M-1) \\ 1-Pr\left[-\frac{\pi}{M} < -(\beta_{a_i,a_\ell}+\beta_{a_i,a_t})+\alpha < \pi\right], & a_i = (M-1) \end{cases} \tag{3.26b}$$

and

$$P_{clicks}\Big|_{a_\ell, a_i, a_t} = \frac{1}{2\pi}\left|\int_{T/2}^{T}\left[e^{-\rho_{a_i,a_\ell}(\tau)}\cdot\dot{\theta}_{a_i,a_\ell}(\tau) + e^{-\rho_{a_i,a_t}(\tau)}\cdot\dot{\theta}_{a_i,a_t}(\tau)\right]d\tau\right| \tag{3.26c}$$

$\dot{\theta}(\tau)$ in Eqn. (3.26c) is the first derivative of $\theta(t)$ with respect to t, which can be obtained from Eqn. (3.11) as,

$$\dot{\theta}_{a_n,a_{n+1}}(t) = \frac{X(t) - Y(t)}{(P(t))^2+(Q(t))^2} \tag{3.27a}$$

where

$$X(t)=2\pi f_0\, P(t) \sum_{p=1}^{N'} p\, B_p |H(pf_0)| \sin(2\pi p f_0 t + \angle H(pf_0)) \tag{3.27b}$$

$$Y(t)=2\pi f_0\, Q(t) \sum_{p=1}^{N'} p\, A_p |H(pf_0)| \sin(2\pi p f_0 t + \angle H(pf_0)) \tag{3.27c}$$

and $\rho(t)$ is given by Eqn. (3.12). (P(t) and Q(t) are given by Eqns. (3.13a) and (3.13b)).

The average error probability which is composed of two components $P_{cont.}$ and P_{clicks}, can be written as,

$$P_e = P_{cont.} + P_{clicks} \quad , \rho >> 1 \tag{3.28a}$$

where

$$P_{cont.} = E\{P_{cont.}\Big|_{a_\ell, a_i, a_t}\}$$

$$= 1 - \frac{2}{M^3}\left\{\sum_{i=1}^{(\frac{M}{2}-1')}\sum_{\ell=1}^{M}\sum_{t=1}^{M} Pr[-\frac{\pi}{M} < -(\beta_{a_i,a_\ell} + \beta_{a_i,a_t}) + \alpha < \frac{\pi}{M}]\right.$$

$$\left. + \sum_{\ell=1}^{M}\sum_{t=1}^{M'} Pr[-\frac{\pi}{M} < -(\beta_{(M-1),a_\ell} + \beta_{(M-1),a_t}) + \alpha < \pi]\right\} \tag{3.28b}$$

and

$$P_{clicks} = \frac{1}{\pi M^3}\sum_{i=1}^{M/2}\sum_{\ell=1}^{M}\sum_{t=1}^{M}\left|\int_{\frac{T}{2}}^{T}\{e^{-\rho_{a_i,a_\ell}(\tau)}\cdot\theta_{a_i,a_\ell}(\tau)\right.$$

$$\left. + e^{-\rho_{a_i,a_t}(\tau)}\cdot\theta_{a_i,a_t}(\tau)\}d\tau\right| \tag{3.28c}$$

Each of the probabilities in $P_{cont.}$ is evaluated as shown in Appendix C.

It is important to note that the performance evaluation of the CD-DD detection and DC detection does not depend on the single symbol interference assumption and is based only on the adjacent ISI assumption. The assumption on

single symbol interference is required only to evaluate P_{clicks} of LD detection which makes use of phase and SNR over the entire symbol interval.

3.6 Numerical Results and Discussion

Numerical results are provided for the following two filters:

(1) Gaussian filter;

$$H(f) = e^{-\pi f^2/2B^2}$$

(2) Second-order Butterworth filter;

$$H(f) = \frac{2}{1 + (1 + j\sqrt{8}\frac{f}{B})^2}$$

H(f) is the transfer function of the low-pass equivalent of the IF filter. The validity of the assumption on single symbol interference has been illustrated in section 3.3 for a Gaussian filter. Similarly, it can be shown that it is valid for a Butterworth filter with the only difference from the Gaussian filter being the time shift δ between the filtered and the received phase variations. This time shift is caused by the non-zero phase response of the Butterworth filter.

The performance of the three detection schemes has been numerically evaluated for M=2,4 and 8 cases for $h = \frac{1}{M}$ as described in section 3.5. The performance degradation with respect to wideband case is calculated at a symbol error rate of 10^{-5} and these results are plotted in Figs. (3.8) and

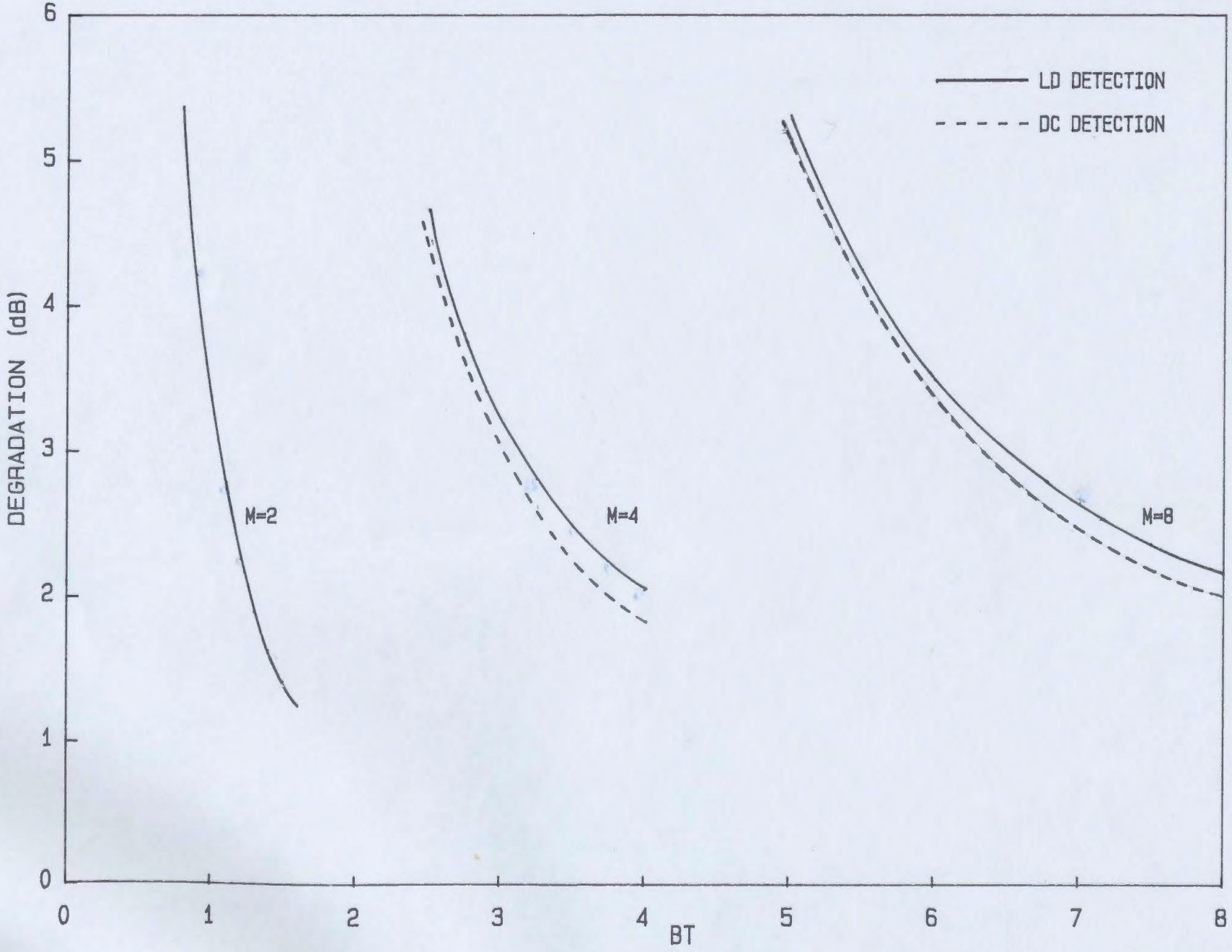

Fig. 3.8a SNR Degradation for LD Detection and DC Detection for a Gaussian Filter (M=2,4 and 8)

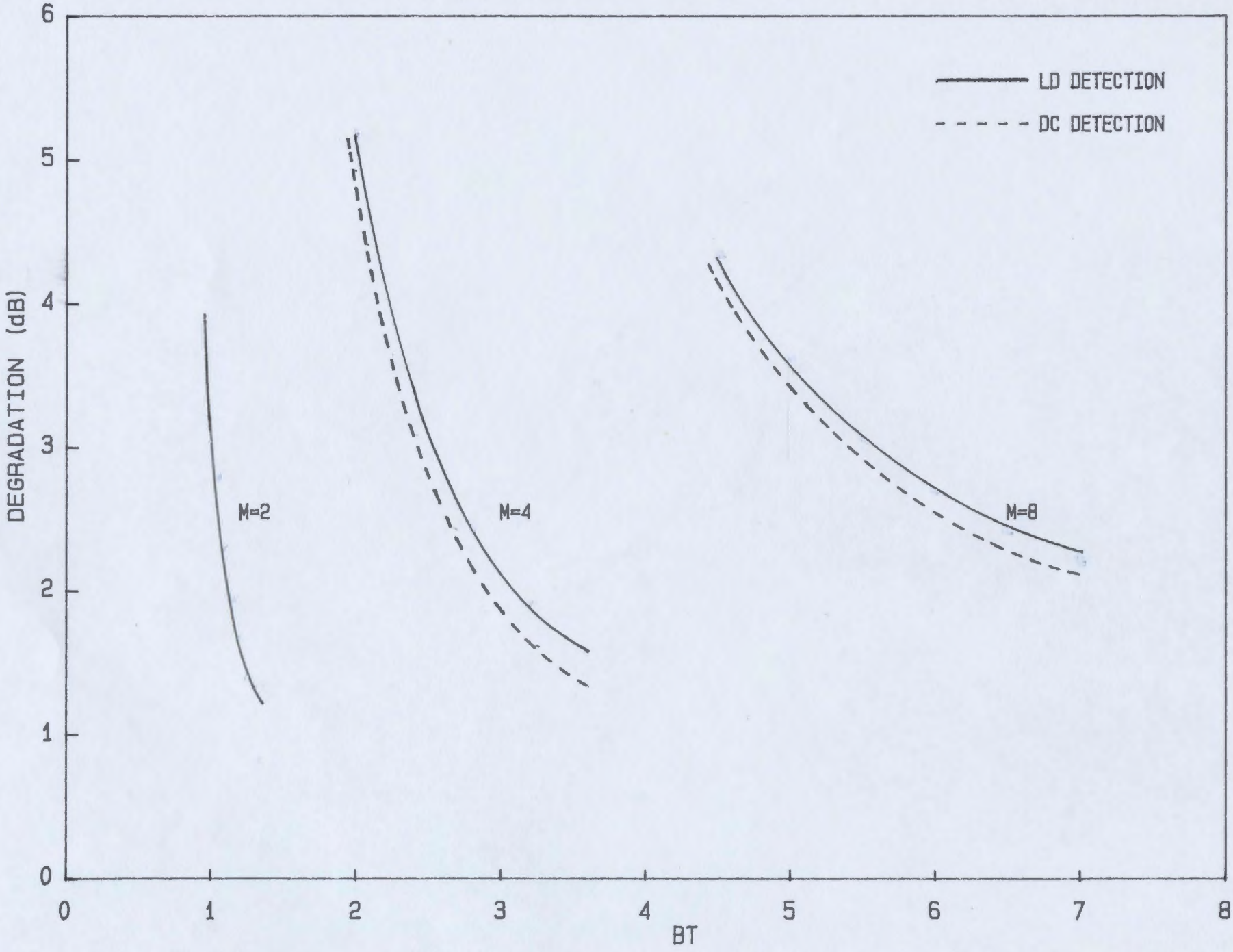

Fig. 3.8b SNR Degradation for LD Detection and DC Detection for a Second Order Butterworth Filter (M=2,4 and 8)

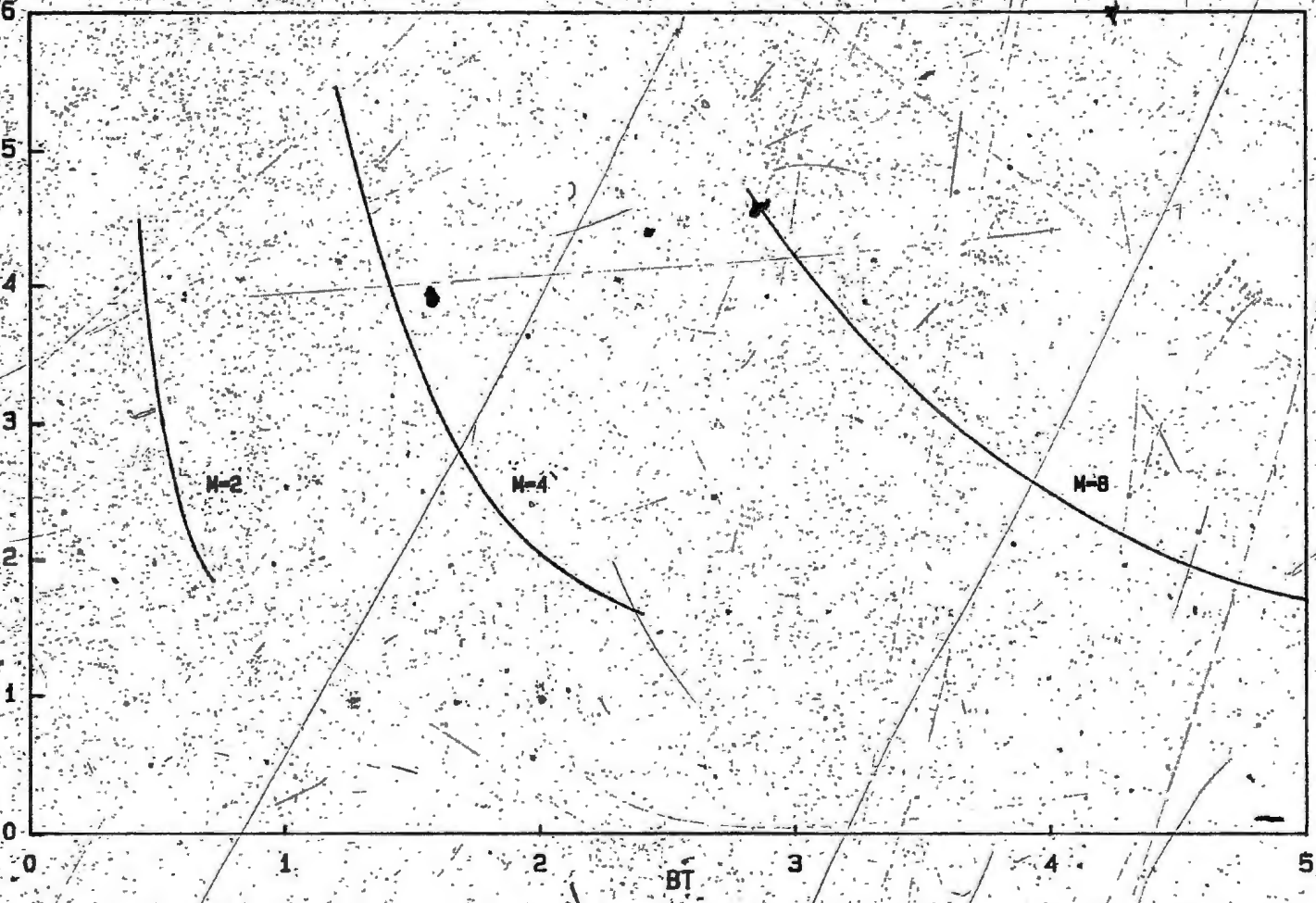

Fig. 3.9a SNR Degradation for CD-DD Detection for a Gaussian Filter (M=2,4 and 8)

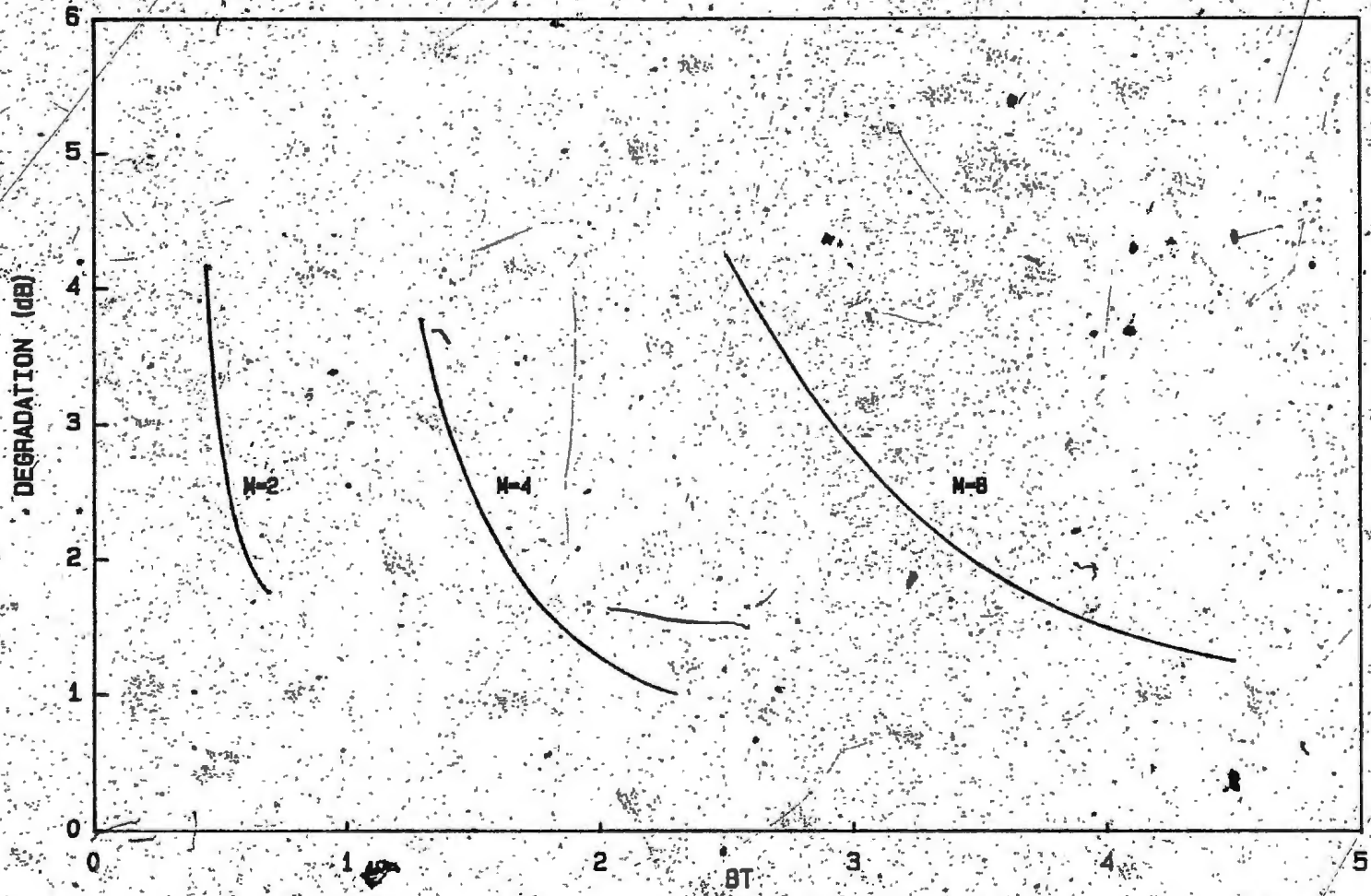

Fig. 3.9b SNR Degradation for CD-DD Detection for a Second Order Butterworth Filter (M=2,4 and 8)

(3.9) against the time bandwidth product BT_b for the two filters. Figs. (3.10) - (3.12) show the symbol error probability variations with E_s'/N_0 for the narrowband case along with the corresponding wideband case results for a selected set of BT values. It can be observed that LD detection and DC detection yield almost the same error performance whereas CD-DD detection yields the best performance of all three detection schemes. This observation was made also when the channel is wideband in the previous chapter. It can be observed that the effect of ISI becomes more significant as M increases. This is mainly because even a small phase error due to ISI causes the signal points to fall in an incorrect region since the regions are smaller and the signal points are closely located, when M is large.

A comparison of the cases M=2,4 and 8 can be carried out by comparing bit error probabilities (P_{eb}), BT_b and E_b/N_0 values for the three cases. T_b is the bit duration and E_b is the bit energy. We recall the followings between the symbol and bit parameters [18, pp. 231],

$$P_{es} \approx P_{eb}(\log_2 M) \quad \text{at high SNR}$$

$$T_s = T_b(\log_2 M) \; ; \; \frac{E_s}{N_0} = \frac{E_b}{N_0}(\log_2 M)$$

Table (3.1) provides the corresponding E_b/N_0 (dB) values for a selected set of BT_b values at a bit error probability of

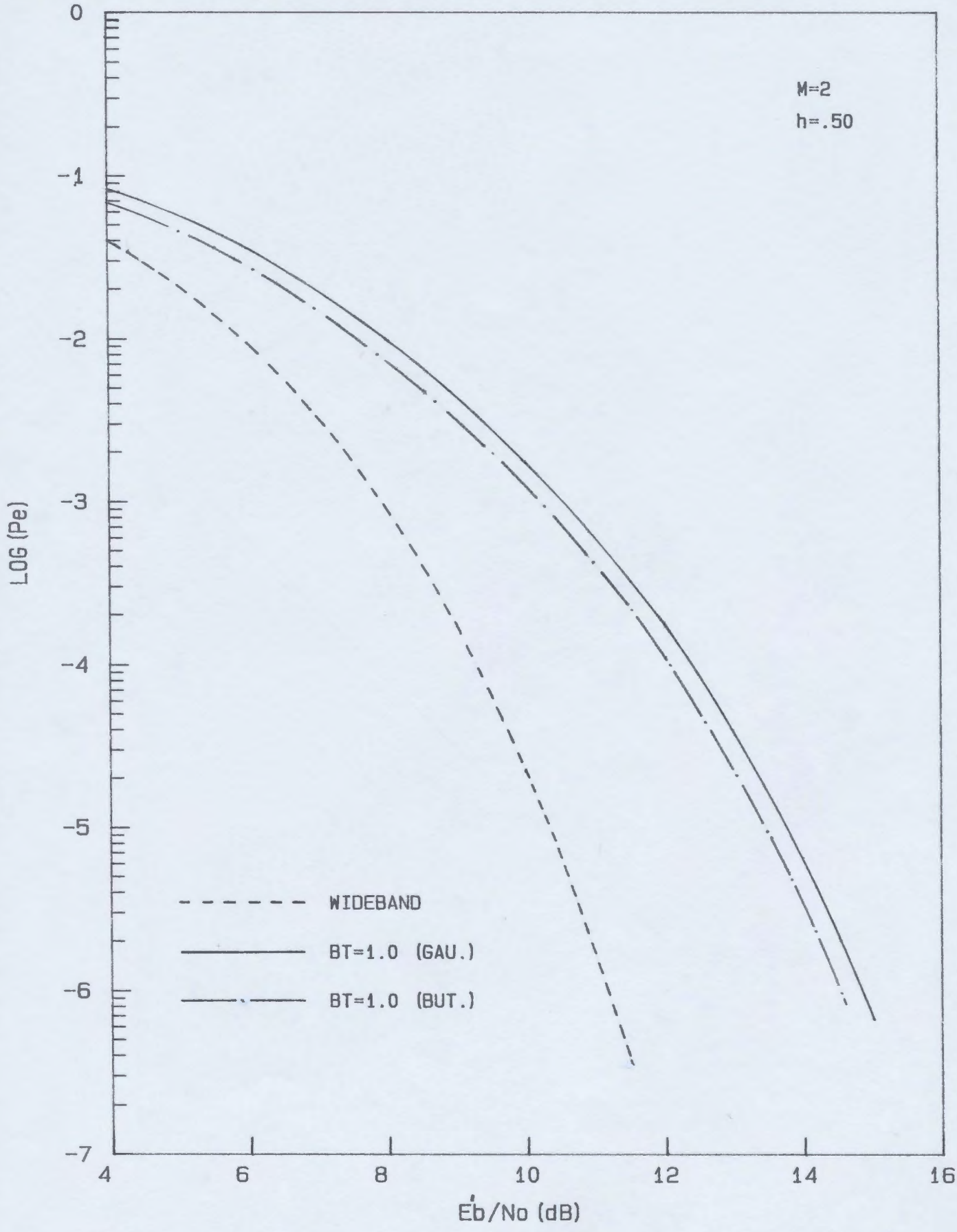

Fig. 3.10a Symbol Error Probability of Binary CPFSK with Modulation Index 0.5, for LD Detection and DC Detection in Wideband and Bandlimited Channels

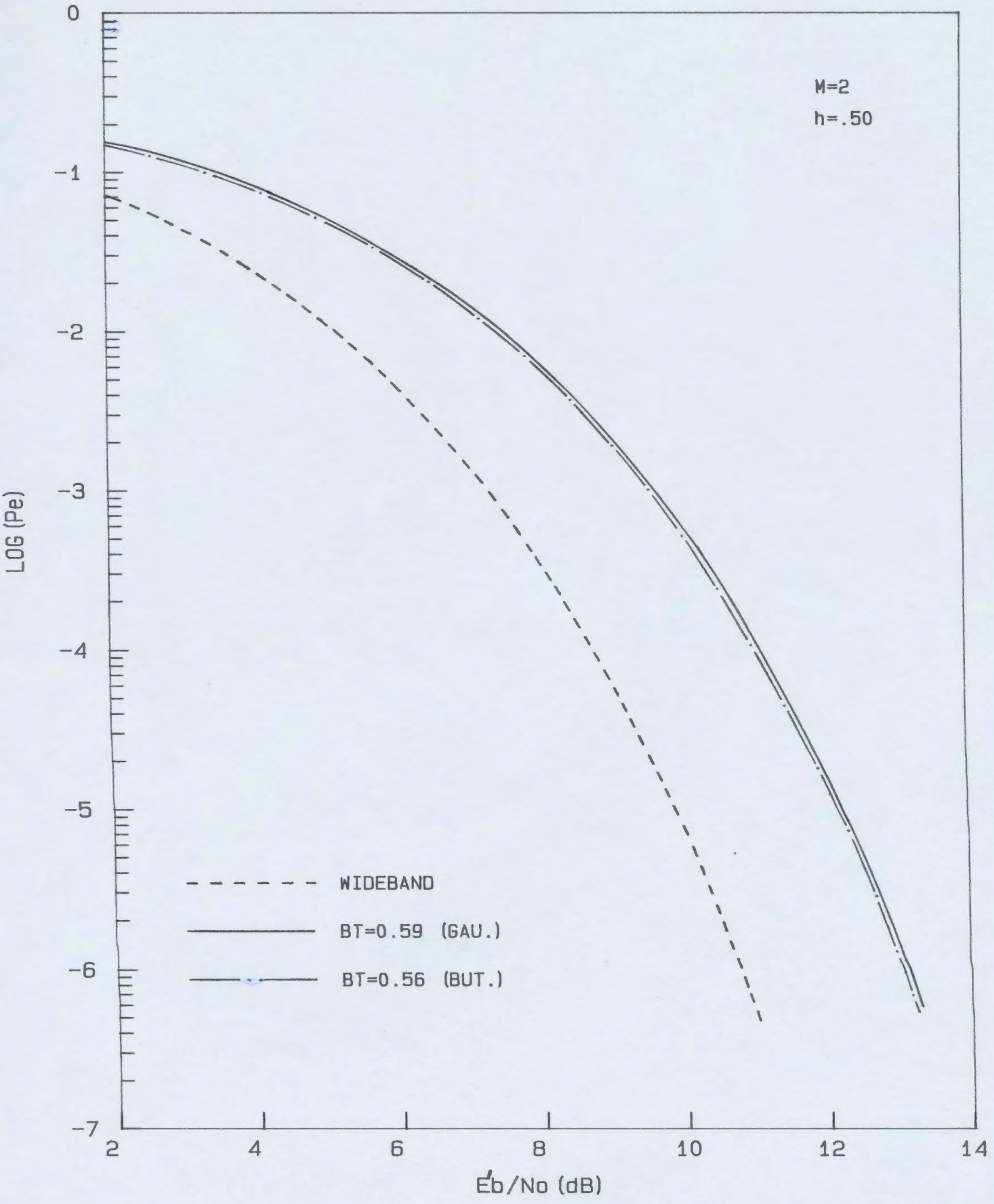

Fig. 3.10b Symbol Error Probability of Binary CPFSK with Modulation Index 0.5, for CD-DD Detection in Wideband and Bandlimited Channels

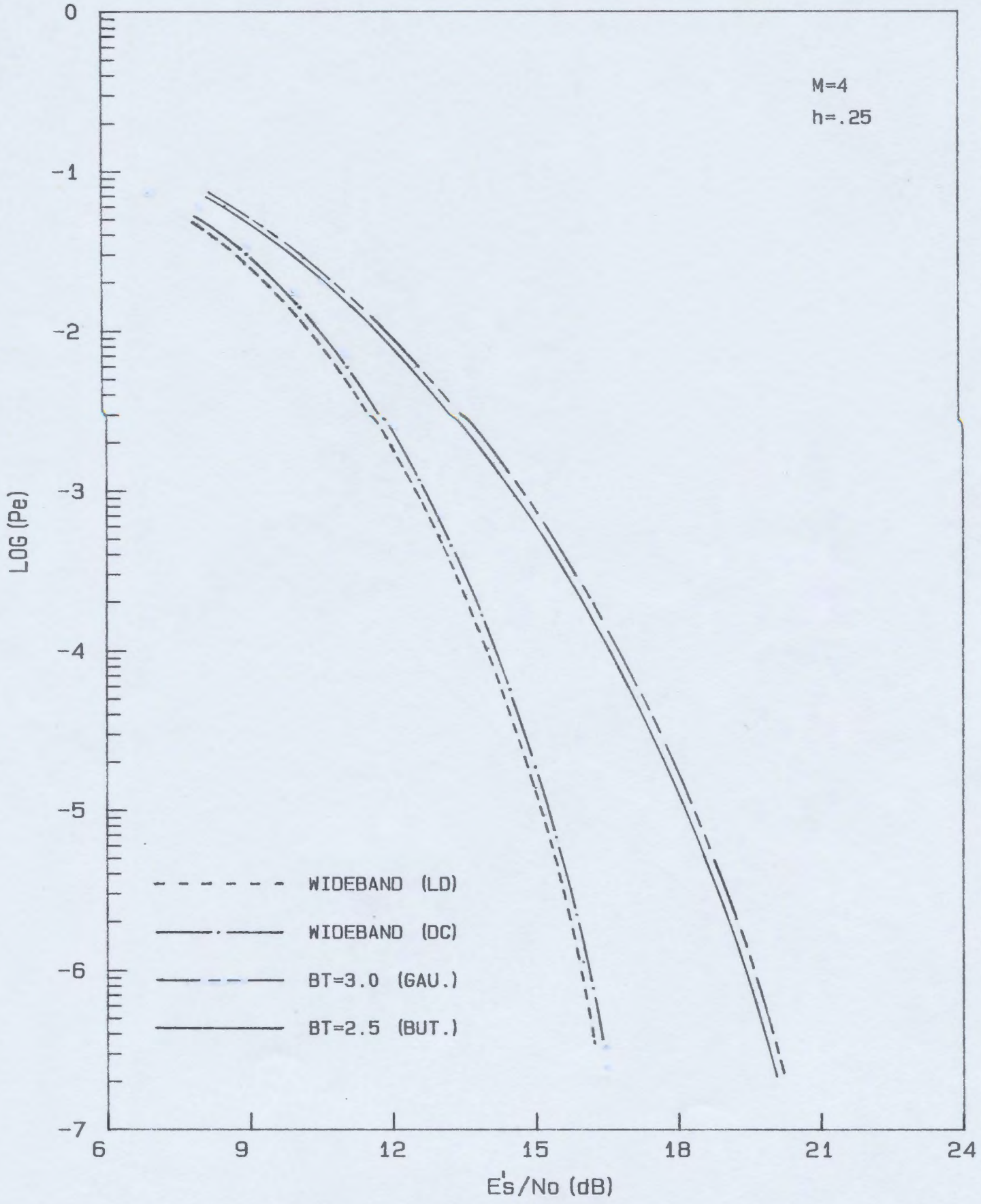

Fig. 3.11a Symbol Error Probability of Quaternary CPFSK with Modulation Index 0.25, for LD Detection and DC Detection in Wideband and Bandlimited Channels

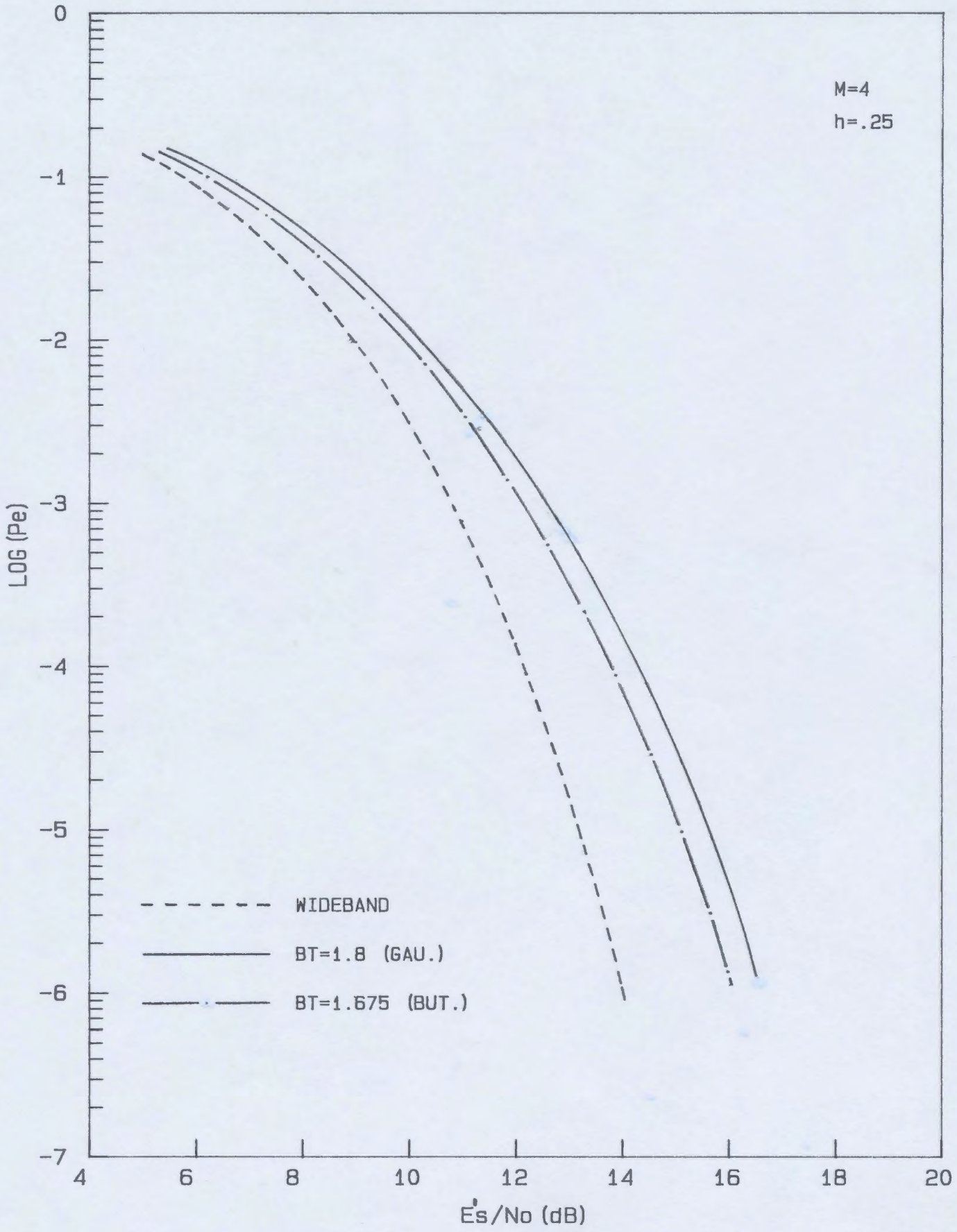

Fig. 3.11b Symbol Error Probability of Quaternary CPFSK With Modulation Index 0.25, for CD-DD Detection in Wideband and Bandlimited Channels

Fig. 3.12a Symbol Error Probability of Octonary CPFSK with Modulation Index 0.125, for LD Detection and DC Detection in Wideband and Bandlimited Channels

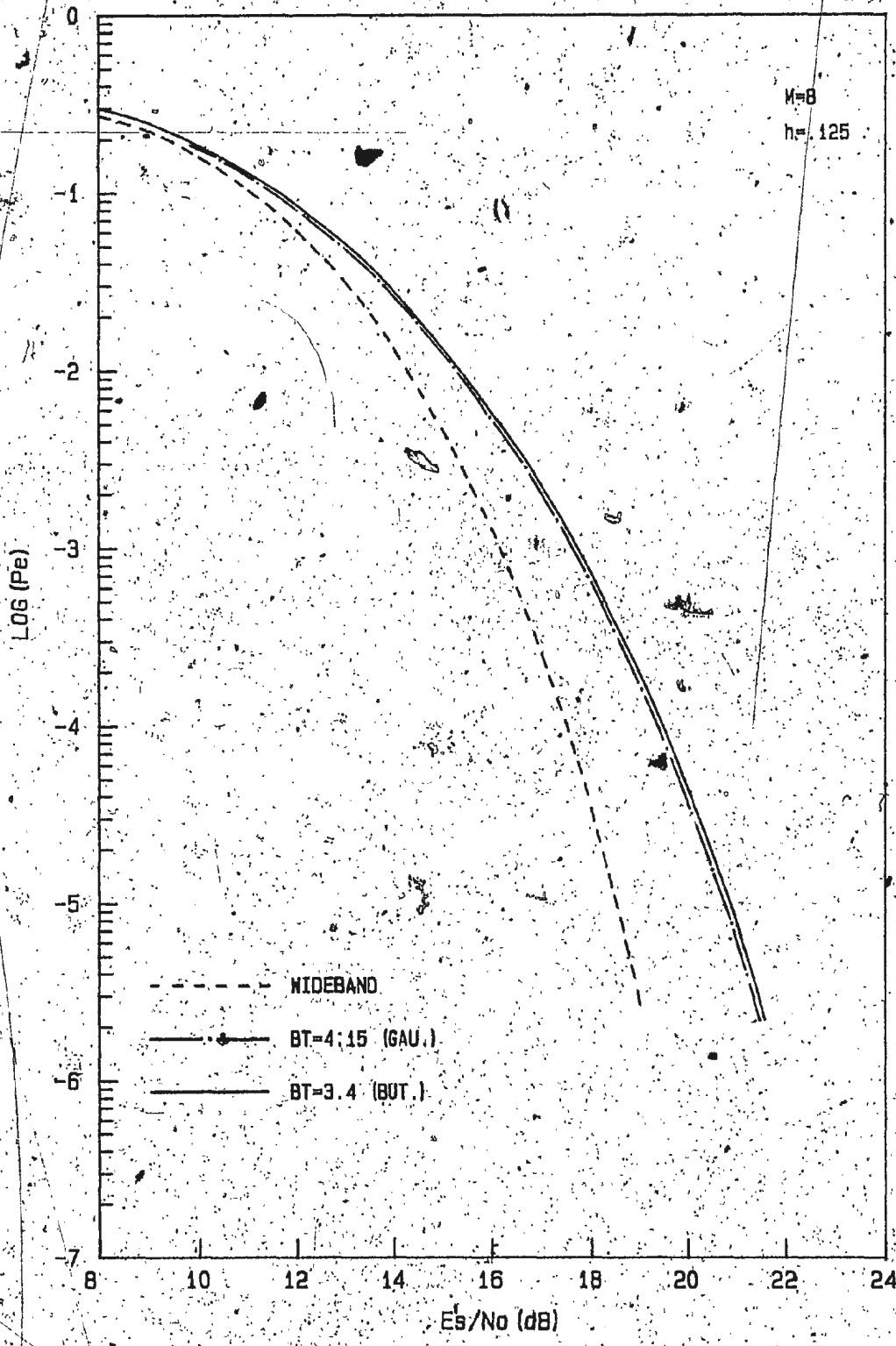

Fig. 3.12 b Symbol Error Probability of Octonary CPFSK with Modulation Index 0.125, for CD-DD Detection in Wideband and Bandlimited Channels

10^{-5}, obtained from Figs. (3.10) to (3.12).

These observations indicate that the use of the binary system always leads to better performance than higher order systems.

It can be further derived that ISI places lower limits on BT for M>2, below which the detection schemes become useless (This is similar to the limit on the symbol timing error discussed in the previous chapter). For LD detection and DC detection, BT has to satisfy the inequality, $\beta_{(M-1),-(M-1)} < \frac{\pi}{2M}$ and this follows from the fact that the maximum allowable error in the decision variable due to ISI is $\frac{\pi}{M}$. Clearly this is satisfied for M=2, but it places lower limits on BT for M>2. These limits for M=4 and 8 are tabulated in Table (3.2). It is important to note that these are approximate values determined using the sequence of repetitive ±(M-1) (i.e. ... + (M-1), -(M-1), + (M-1) ..), instead of the one which gives the maximum error in the phase difference; ... + (M-1), ... + (M-1), + (M-1), - (M-1), + (M-1), + (M-1) ... + (M-1) .... Similarly for the CD-DD detection scheme, BT has to satisfy, $\beta_{(M-1),-(M-1)} < \frac{\pi}{M}$ and it places a lower limit on BT for M>2. As in the case of LD detection and DC detection, this lower limit has been approximately evaluated considering the sequence;

Table (3.3).

Minimum BT Values for CD-DD Detection

	M=4	M=8
Gau.	0.6425	1.558
But.	0.6503	1.466

(... + (M-1), - (M-1), - (M-1), +(M-1), + (M-1), - (M-1), - (M-1), + (M-1) ...), instead of the sequence; (... + (M-1), ... + (M-1), -(M-1) ... - (M-1), ...), the one which gives the maximum phase error. The numerical values of these limits are tabulated in Table (3.3) for M=4 and 8 cases.

Since the assumption on the single symbol interference is required only for the calculation of P_{clicks} of the LD detection, the performance evaluation of the CD-DD detection is valid for much lower values of BT which satisfy only the adjacent ISI requirement.

Since the Butterworth filter has nonlinear phase response, it is important to note that the time shift between the filtered phase $\theta(t)$ and the received phase $\phi(t)$ has to be considered in the calculations. This shift varies slightly from pattern to pattern, but it is reasonable to consider the shift corresponding to the worst combination of repetitive pattern of $\pm(M-1)$ throughout the calculations.

The effect of noise correlation has not been taken into account in the analysis of the LD detection and DC detection. This is because the effect of noise correlation is insignificant for BT values greater than 1.0. Finally, the number of Fourier coefficients N' required to maintain a constant accuracy also varies from case to case, but a value of 20 is ample in any case.

3.7 Conclusions

In this chapter we have compared the performance of the three detection schemes over a bandlimited channel for $h = \frac{1}{M}$. The effect of intersymbol interference caused by adjacent symbols has been considered. A method for analyzing ISI which involves multipattern averaging using a few number of basic symbol patterns has been presented. Numerical results obtained with Gaussian and second order Butterworth filters indicate that the CD-DD scheme has better performance and higher tolerance to ISI than the LD detection and DC detection schemes whereas the latter two have almost identical performance and sensitivities to ISI. Finally, it has been shown that the ISI influence becomes stronger as M increases, which makes the performance of the binary CPFSK system better than that of multilevel CPFSK systems.

Table 3.1

E_b/N_0 values at a Bit Error Probability of 10^{-5} for Selected BT_b values

		M=2		M=4		M=8	
		BT_b	E_b/N_0	BT_b	E_b/N_0	BT_b	E_b/N_0
Gau.	LD & DC	1.0	13.75	1.5	19.67	2.0	26.81
	CD-DD	0.59	9.90	0.9	14.83	1.38	21.43
But.	LD & DC	1.0	14.16	1.25	18.14	1.667	26.38
	CD-DD	0.56	10.04	0.837	14.02	1.13	21.15

Table (3.2)

Minimum BT Values for LD Detection and DC Detection

	M=4	M=8
Gau.	1.331	3.122
But.	1.228	2.643

CHAPTER 4

LD DETECTION AND DC DETECTION OF CPFSK SIGNALS WITH ARBITRARY MODULATION INDEX

4.1 Introduction

In this chapter, we consider two special cases, namely Limiter Discriminator detection of M-ary CPFSK with arbitrary value of the modulation index and DC detection of binary CPFSK with arbitrary value of the modulation index. In the LD detection case, the objective is to determine the best value for the modulation index which yields minimum error probability under bandlimited conditions. In the DC detection case, the objective is to evaluate the performance of the DC detector which employs a delay line whose value is dependent on the modulation index of the binary CPFSK signals. As before, the bandlimiting effect of the IF filter is taken into account.

4.2 Optimum Modulation Index Eyaluation for LD Detection

4.2.1 General

In Chapters 2 and 3 we have restricted our analysis to CPFSK signals with modulation index $\frac{1}{M}$. Although CD-DD scheme and DC detection scheme are suitable for this

value of modulation index, LD detection can be used for any value of modulation index. In this section, we consider the performance of LD detection for $h > \frac{1}{M}$, in order to determine the values of h which yield minimum error probabilities. Similar studies have been performed previously on binary CPFSK signals [25,40,41] for bandlimited channels. In this chapter we carry out a detailed evaluation of optimum h values for binary, quaternary and octonary CPFSK signals for both wideband and bandlimited channels.

First, we consider the analysis for a wideband channel. The error probability expressions which have been derived in section 2.3.3 are employed after suitable modifications to accommodate any value of h. Secondly, we consider the analysis for a bandlimited channel. In this case, the expressions which have been derived in section 3.5.3 are used with suitable modifications. Finally, numerical results are presented for both wideband and bandlimited channels. Numerical results for bandlimited channels have been computed assuming a Gaussian filter and a second order Butterworth filter as IF filters.

In Chapter 3, the sampling instants for the Butterworth filter have been obtained by considering the worst case symbol pattern. In this section, we shall verify the sampling instants which are determined using the worst case symbol pattern are good approximations to the sampling

instants when the symbol patterns are different from the worst case pattern.

4.2.2 Wideband Channel

The error probability of the LD detection for an arbitrary value of the modulation index h, is obtained by modifying Eqn. (2.13) as,

$$P_e(M) = \frac{2(M-1)}{M} F_1(-\pi h) + \frac{Mh}{4} e^{-\rho}, \quad \rho >> 1 \qquad (4.1)$$

$$= P_{cont.} + P_{clicks} \qquad (4.2a)$$

where

$$P_{cont.} = \frac{2(M-1)}{M} F_1(-\pi h) \qquad (4.2b)$$

$$P_{clicks} = \frac{Mh}{4} e^{-\rho} \qquad (4.2c)$$

and

$$F_1(\alpha) = -\frac{Sgn(\alpha)}{2\pi} \int_0^{\frac{\pi}{2} - |\alpha|} e^{-\rho \frac{\sin^2 \alpha}{1 + \cos \alpha \cos \theta}} d\theta \qquad (4.2d)$$

It follows from Eqns. (4.2a), (4.2b) and (4.2c) that for a given value of ρ, $P_{cont.}$ decreases while P_{clicks} increases with increasing h. This implies that there exists an optimum value of h for which the average error probability is a minimum (see Fig. (4.1)). From Eqns. (4.2a), (4.2b) and (4.2c), we observe that $h_{opt.}$ must satisfy,

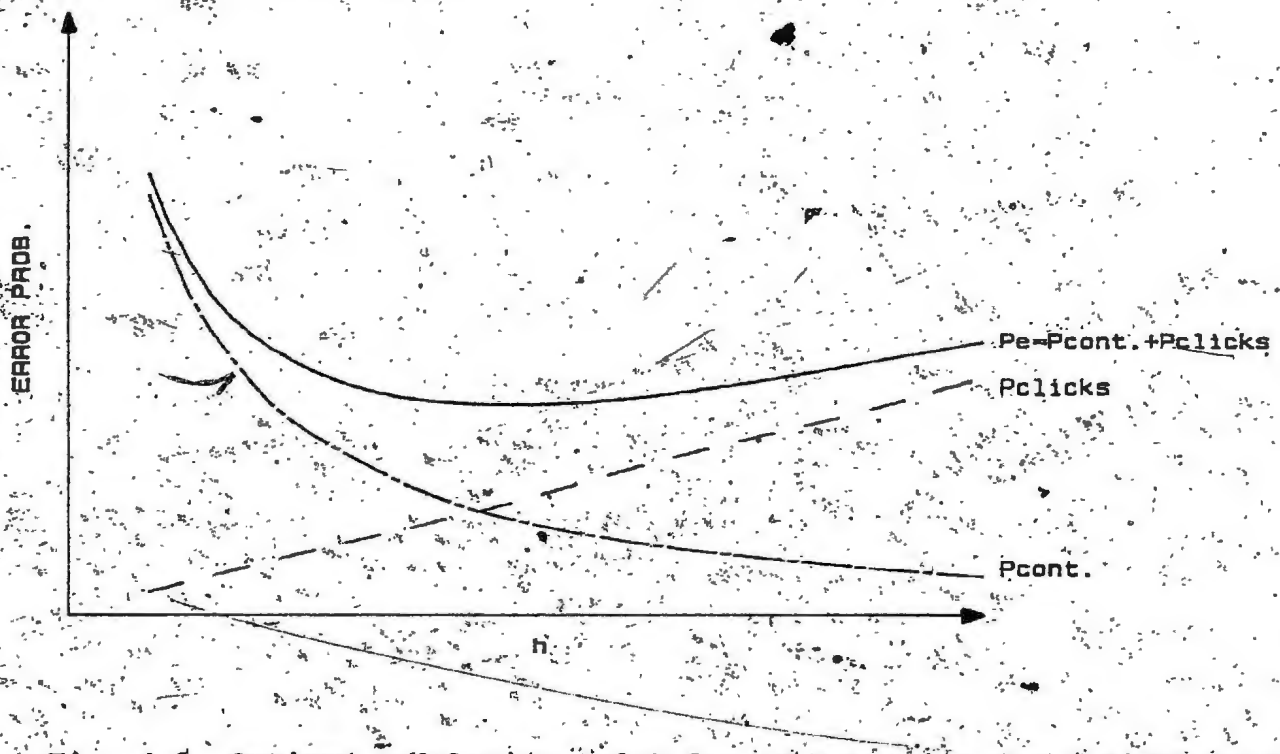

Fig. 4.1 Optimum Modulation Index for LD Detection for a Wideband Channel

$$\frac{\partial P_{cont.}}{\partial h} + \frac{\partial P_{clicks}}{\partial h} = 0 \qquad (4.3a)$$

i.e.

$$\frac{2(M-1)}{M} \frac{\partial}{\partial h} \{F_1(-\pi h)\}\Big|_{h=h_{opt.}} + \frac{M}{4} e^{-\rho} = 0 \qquad (4.3b)$$

Since $\frac{\partial}{\partial h} F_1(-\pi h)$ cannot be expressed in closed form, $h_{opt.}$ is evaluated numerically by plotting P_e against h. We note that since $h_{opt.}$ depends on SNR, it can be evaluated for pre-selected SNR values only.

It can be observed from Fig. (4.1) that the value of P_e increases slightly as h increases in the interval $1>h>h_{opt.}$. Moreover, as $P_{cont.}=0$ for h=1 (follows from the assumption of $p(\alpha)$ mod 2π made in section 2.3.3), the only contribution to P_e for h=1 is made by P_{clicks}.

i.e.

$$P_e\Big|_{h=1} = P_{clicks}\Big|_{h=1} = \frac{M}{4} e^{-\rho} \qquad (4.4)$$

Therefore, the value $\frac{M}{4} e^{-\rho}$ can be considered as an upper bound on the minimum error rate of the LD detector. It is always possible to reduce the error rate below $\frac{M}{4} e^{-\rho}$ by varying h.

4.2.3 Bandlimiting Channel

The analysis of the LD detection for $h = \frac{1}{M}$, which has been presented in section 3.5.3 can be generalized for

any modulation index h, by making the following modifications in Eqns. (3.9), (3.17b), (3.28b) and (3.28c) as,

$$\phi(t) = \begin{cases} \dfrac{\pi a_n h t}{T}, & 0 < t < T \\ \dfrac{\pi a_{n+1} h t}{T} + (a_n - a_{n+1})\pi h, & T < t < 2T \\ \phi(4T-t), & 2T < t < 4T \end{cases} \tag{4.5}$$

$$\rho(t) = \frac{E_s}{N_0} \frac{|H(\frac{a_n h}{2T})|^2}{T \int_{-\infty}^{\infty} |H(f)|^2 \, df} \tag{4.6a}$$

$$\geq \frac{E'_s}{N_0} |H(\frac{a_n h}{2T})|^2 \tag{4.6b}$$

$$P_{cont.} = 1 - \frac{2}{M^3}\Big\{ \sum_{i=1}^{(\frac{M}{2}-1)} \sum_{\ell=1}^{M} \sum_{t=1}^{M} Pr[-\pi h < -(\beta_{a_i,a_\ell} + \beta_{a_i,a_t}) + \alpha < \pi h] + \sum_{\ell=1}^{M} \sum_{t=1}^{M} Pr[-\pi h < -(\beta_{(M-1),a_\ell} + \beta_{(M-1),a_t}) + \alpha \leq \pi] \Big| \tag{4.7}$$

$$P_{clicks} = \frac{1}{\pi M^3} \sum_{i=1}^{\frac{M}{2}} \sum_{\ell=1}^{M} \sum_{t=1}^{M} \Big| \int_{T/2}^{T} \{ e^{-\rho_{a_i,a_\ell}(\tau)} \cdot \theta_{a_i,a_\ell}(\tau) + e^{-\rho_{a_i,a_t}(\tau)} \cdot \theta_{a_i,a_t}(\tau) \} d\tau \Big| \tag{4.8}$$

We again observe that there exists an optimum h which yields minimum error probability for a given SNR (E_s/N_0) and BT as in the case of a wideband channel (see Fig. (4.2)). In this case the variation of P_{clicks} with h is no longer linear. As before, $h_{opt.}$ has to satisfy Eqn. (4.3a) but a simplification similar to that of Eqn. (4.3b) is not possible. As in wideband channels, the $h_{opt.}$ values in bandlimited channels are obtained numerically by plotting P_e against h. The required P_e values are calculated as described in section 3.5.3 with the above modifications.

4.2.4 Numerical Results and Conclusions

As in Chapters 2 and 3, numerical results have been obtained for the cases M = 2, 4 and 8. Fig. (4.3) shows P_e vs. h variations for a wideband channel for selected SNR (E_s/N_0) values. These SNR values are selected so that the corresponding error probabilities lie in the range of 10^{-5} as this range is widely used in practice. Figs. (4.4) and (4.5) show these variations for the bandlimited case using a Gaussian and a second order Butterworth filter, for selected BT and SNR values. The error probability variations for selected cases are compared with those of the wideband case and are shown in Figs. (4.6) - (4.8). Comparing these variations with the corresponding variations for $h = \frac{1}{M}$ in Chapter 3 (see Figs. (3.9) - (3.11)), it can be clearly seen

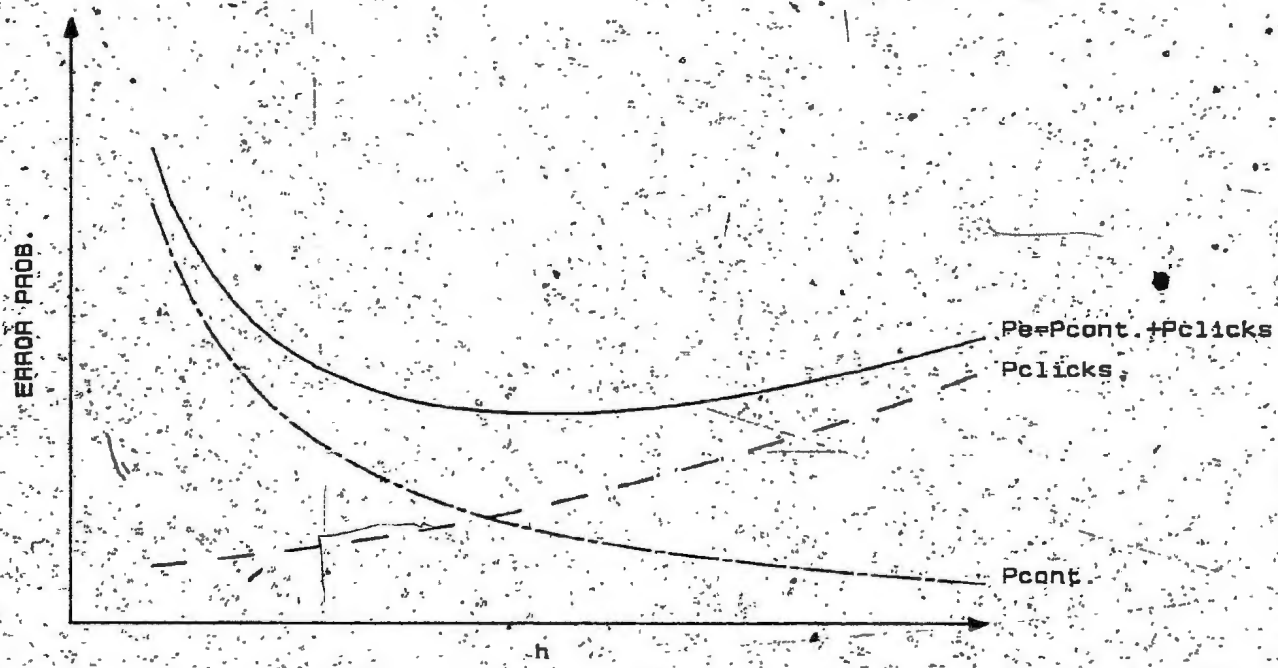

Fig. 4.2 Optimum Modulation Index for LD Detection for a Bandlimited Channel

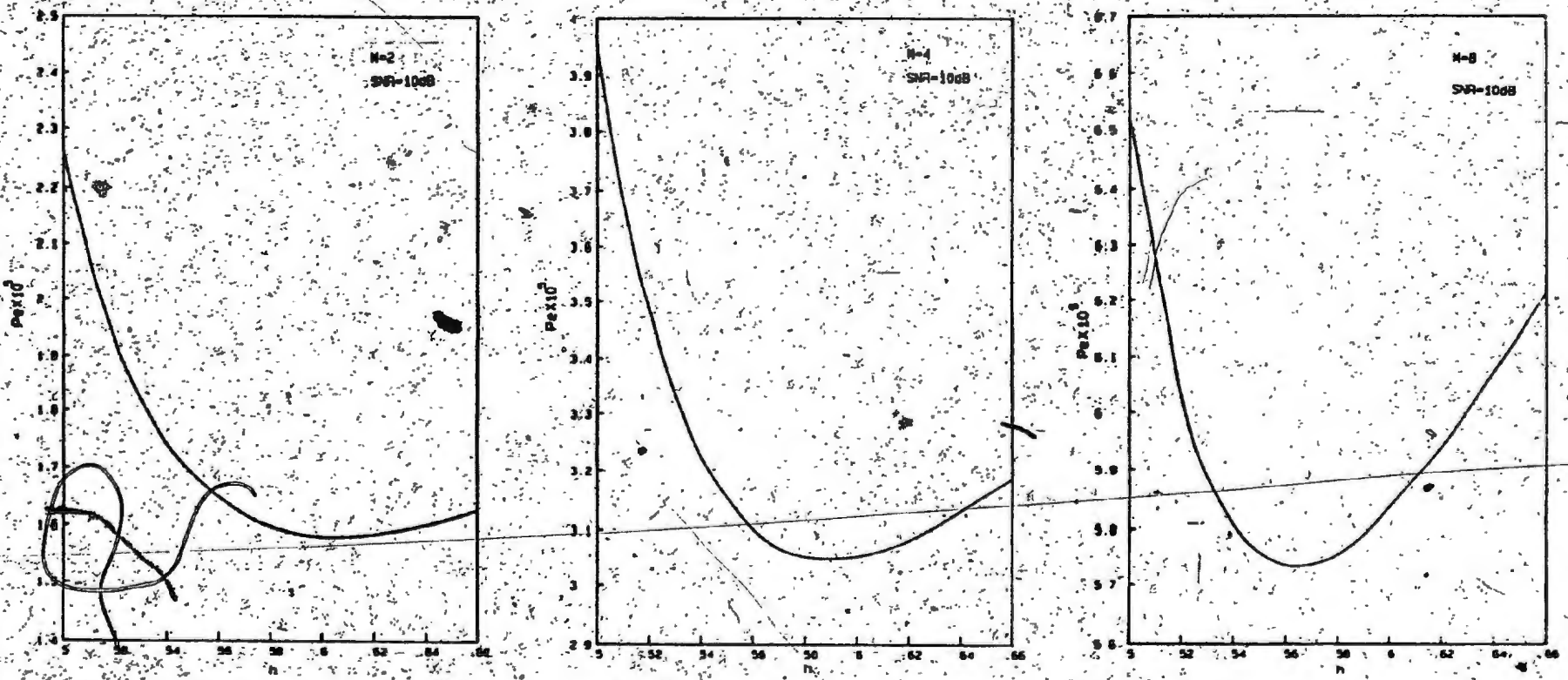

Fig. 4.3 Symbol Error Probability versus Modulation Index of M-ary CPFSK for LD Detection for a Wideband Channel (M=2,4 and 8)

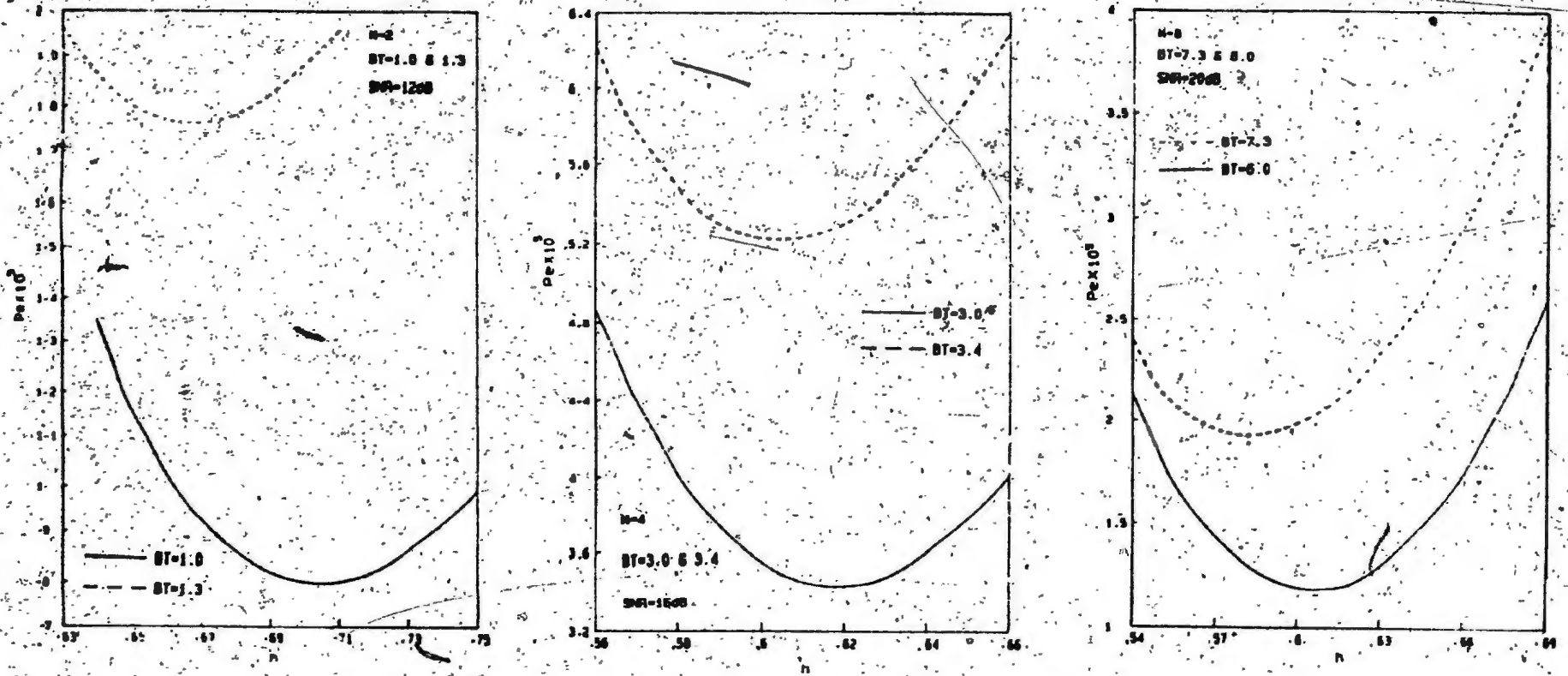

Fig. 4.4 Symbol Error Probability versus Modulation Index of M-ary CPFSK for LD Detection for a Gaussian Filter (M=2,4 and 8)

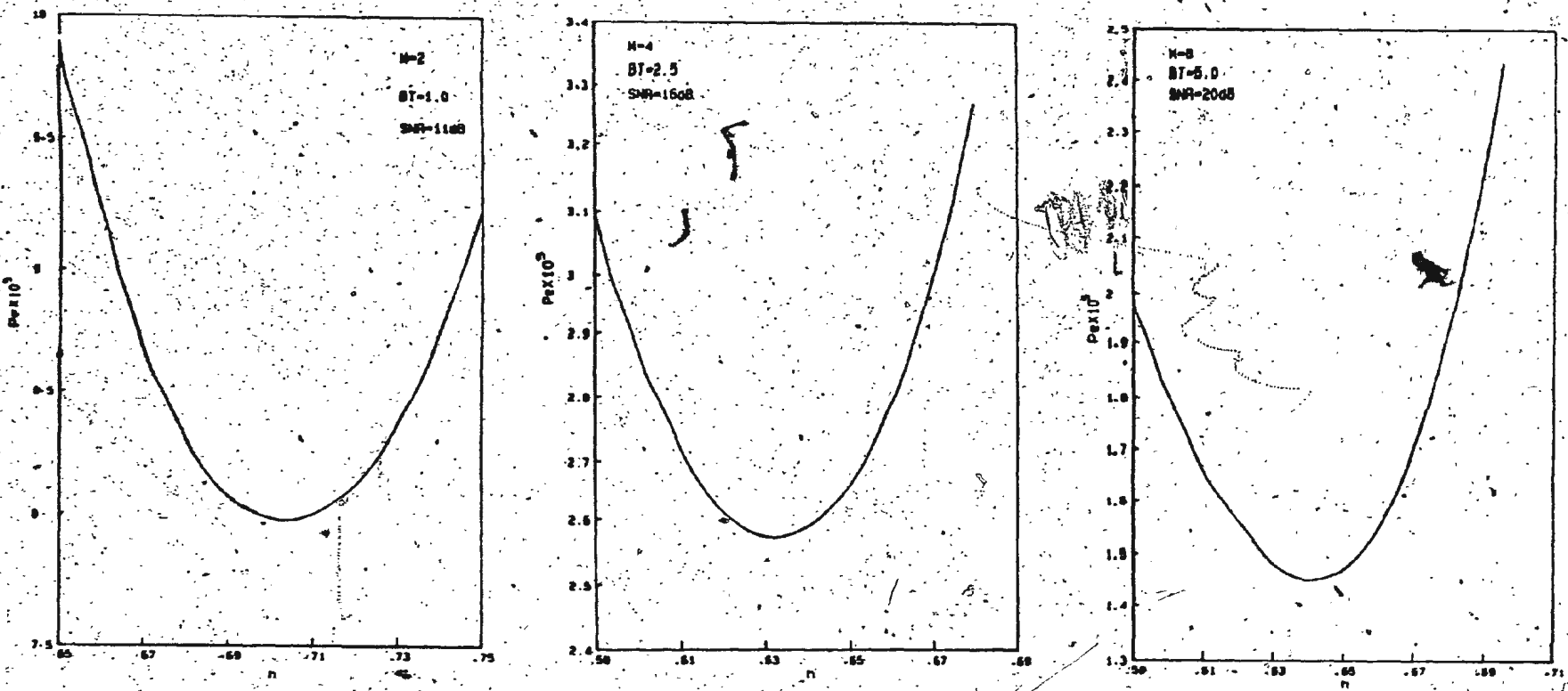

Fig. 4.5 Symbol Error Probability versus Modulation Index of M-ary CPFSK for LD Detection for a Second Order Butterworth Filter (M=2,4 and 8)

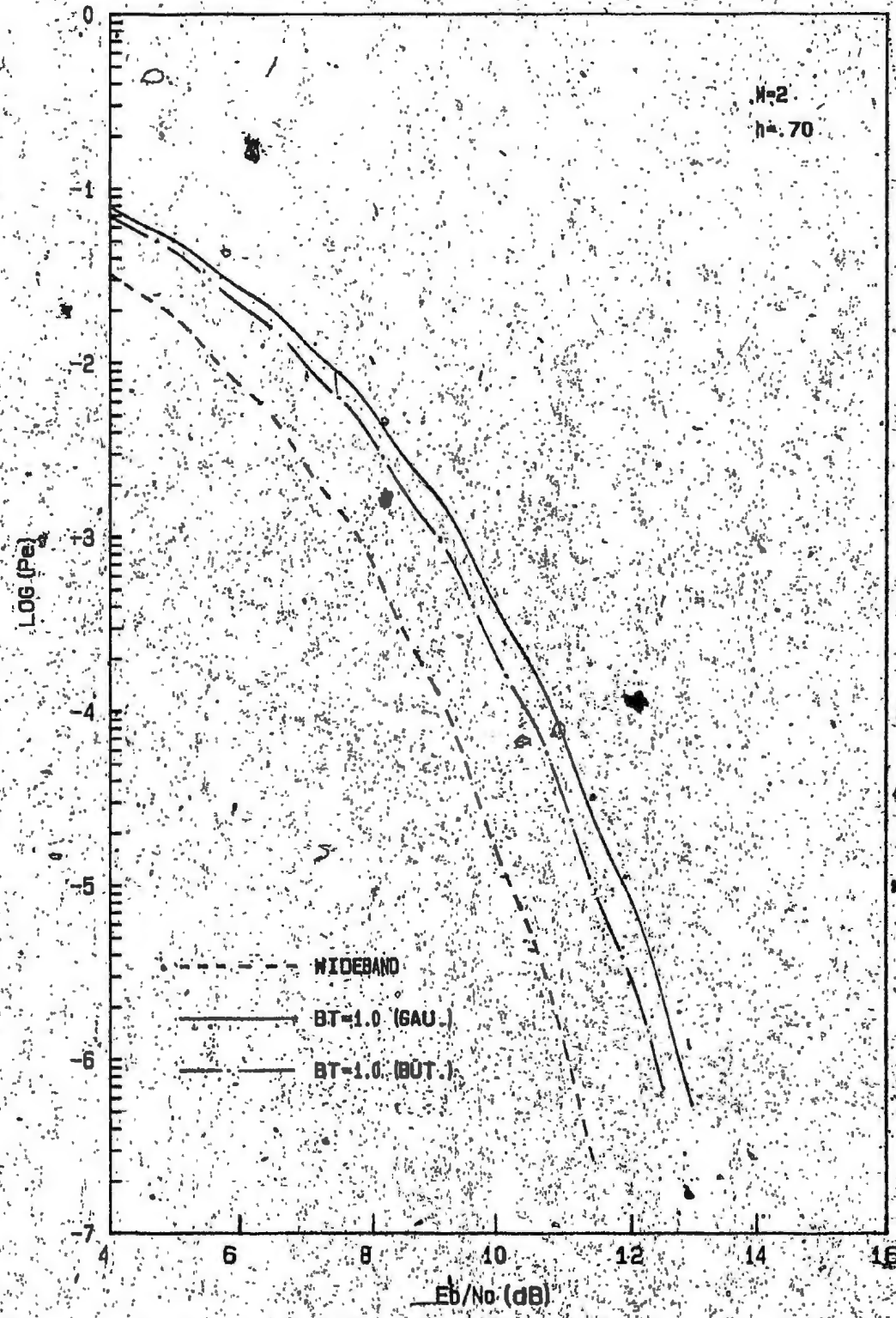

Fig. 4.6 Symbol Error Probability of Binary CPFSK with Modulation Index 0.7 for LD Detection in Wideband and Bandlimited Channels

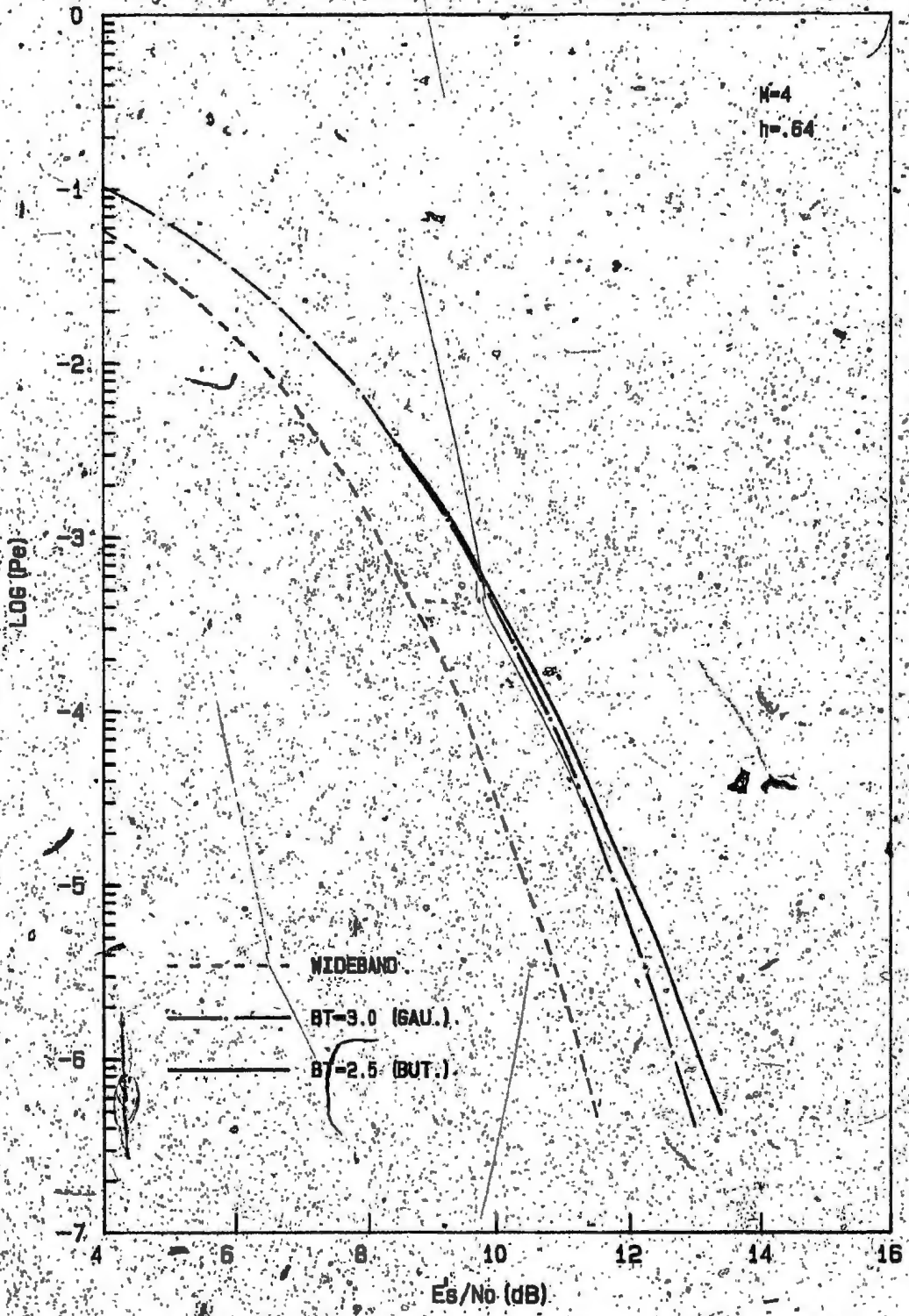

Fig. 4.7 Symbol Error Probability of Quaternary CPFSK with Modulation Index 0.64, for LD Detection in Wideband and Bandlimited Channels

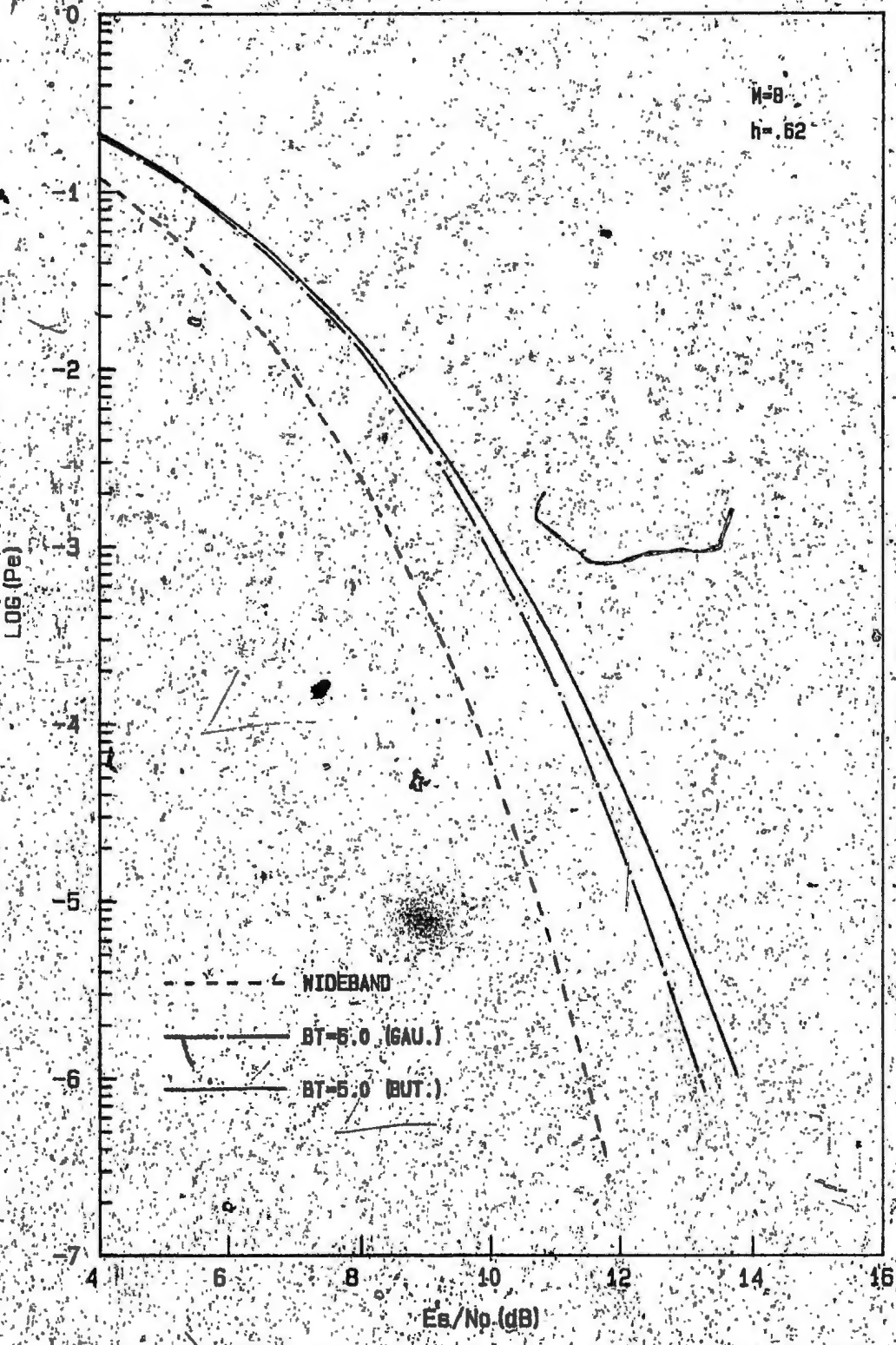

Fig. 4.8 Symbol Error Probability of Octonary CPFSK with Modulation Index 0.62, for LD Detection in Wideband and Bandlimited Channels

that the performance of LD detection can be improved significantly by increasing h above $\frac{1}{M}$ and also this improvement becomes more significant for higher values of M. However, it is to be noted that any increase of h results in a wider spectrum (see Fig. (1.6)). Thus one has to compromise between the performance (or signal power) and the bandwidth when selecting a suitable value for h in using LD detection.

In Chapter 3, the sampling instants for the Butterworth filter were found approximately using the worst combination of repetitive ±(M-1) symbols. The overall optimum sampling instants differ slightly from these and have to be evaluated numerically. Fig. (4.9) shows the error probability variations with D for two SNR values when BT=5.0 and h=0.62; where D is the ratio of the shift between the sampling instants and the symbol changes of the transmitted signal (see Fig. (3.1)) to the symbol interval; i.e. $D = \frac{\delta'}{T}$. We recall, the value of D determined using the worst combination is 0.0988 for the above case. It is observed from the numerical results, that the evaluation of sampling instants using the worst combination is a reasonable approximation to the sampling instants of all other combinations.

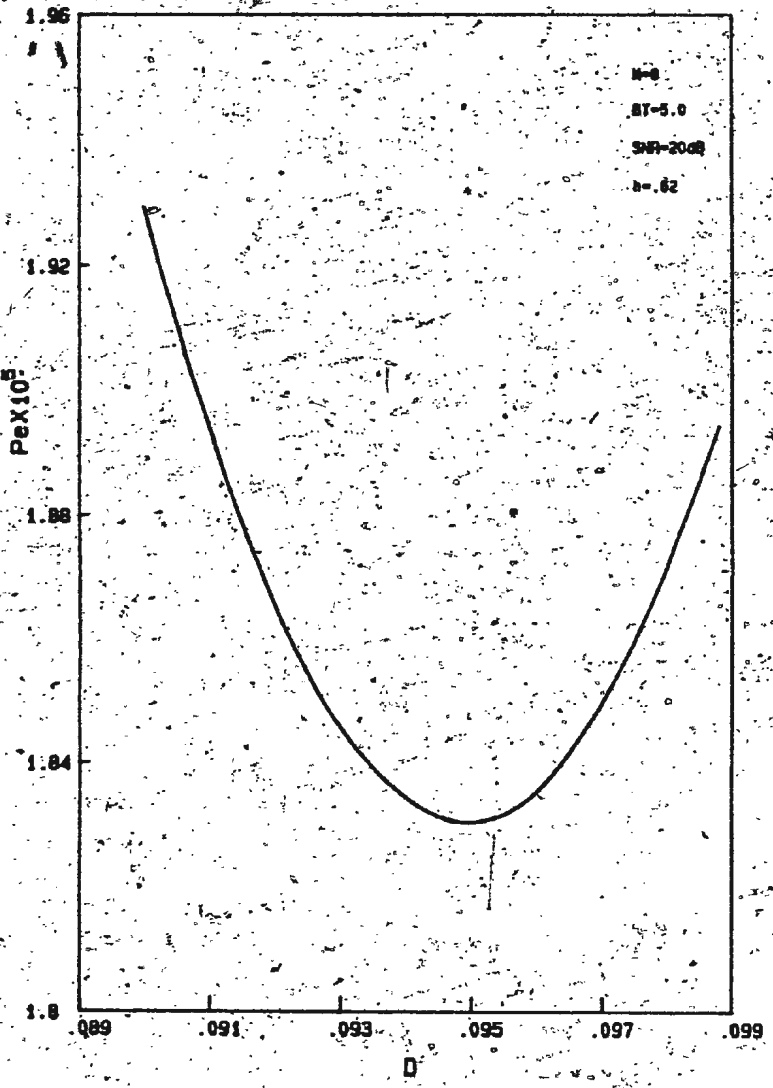

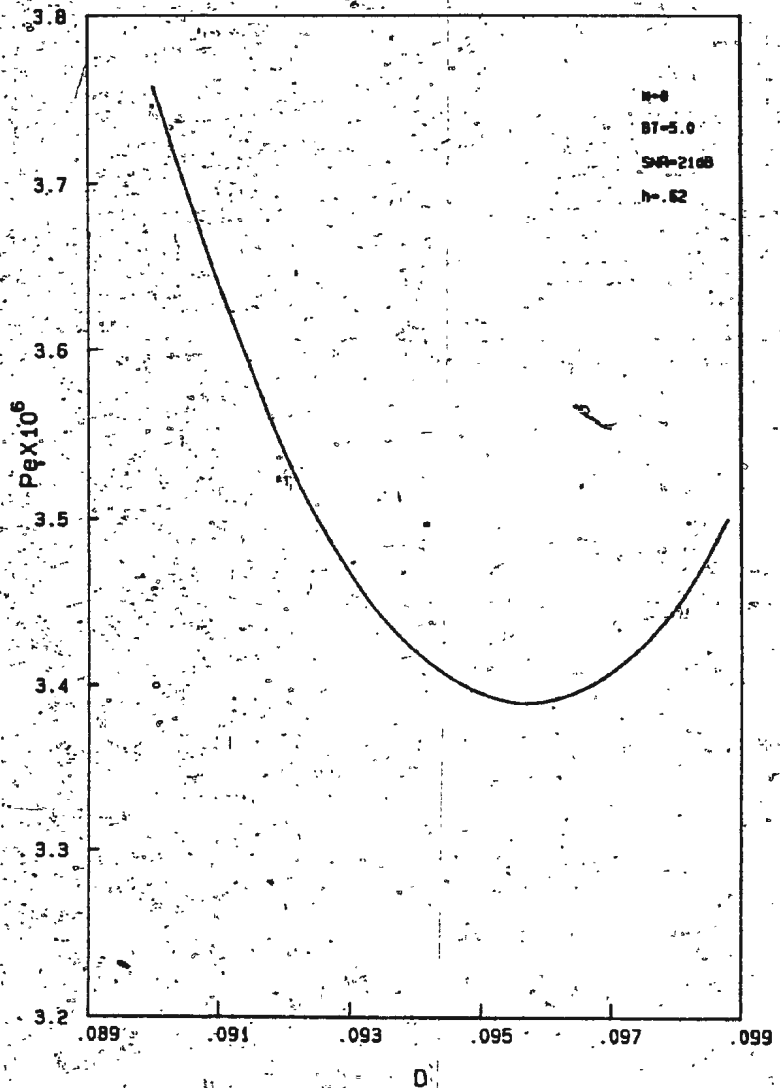

Fig. 4.9 Symbol Error Probability versus Sampling Instant of Octonary CPFSK with Modulation Index 0.62, for LD Detection for Second Order Butterworth Filter with BT=5.0

4.3 Performance Analysis of Variable Delay Differential Detection

4.3.1 General

In Chapters 2 and 3, we have considered the DC detection of M-ary CPFSK signals with modulation index $\frac{1}{M}$. The DC detection scheme considered so far has utilized a one symbol interval delay in order to derive the required phase difference. In ref. [14], it has been shown that for binary CPFSK, one-bit delay differential detection is optimum only for h=0.5 and for other values of h>0.5, the delay needs to be adjusted depending on the value of h in order to obtain optimum performance. The desired delay interval can be shown to be $\tau = \frac{T}{2h}$; where T is the bit duration. We refer to the differential detection which employs the above delay as the variable delay differential detection.

In ref. [38], the performance of the one-bit delay differential detector has been evaluated for the detection of binary CPFSK signals with modulation index h>0.5. These results indicate that one-bit delay differential detection yields poorer performance than LD detection except for h=0.5. In the following subsections, we compare the performance of variable delay differential detection with that of LD detection and one-bit delay differential detection in bandlimited channels. The methodology we employ in out

analysis is based on the results obtained by Pawula [25].

4.3.2 Variable Delay Differential Detection

Recalling from section 1.3, a binary CPFSK signal with modulation index h can be represented as,

$$x(t) = \sqrt{\frac{2E_b}{T}} \cos(\omega_c t + \phi(t)) \qquad (4.9)$$

where $\phi(t) = \frac{\pi h}{T} \int_{-\infty}^{t} d(\tau)\, d\tau$ in which $d(t)$ is the baseband binary data waveform. E_b and T denote the signal energy and bit duration respectively.

The phase difference $\Delta\phi$ that results from sampling x(t) at two instants in time within a given bit interval, say in the nth bit interval, can be expressed as,

$$\Delta\phi = \phi(t+\tau) - \phi(t) = \frac{\pi a_n h \tau}{T} \qquad (4.10)$$

Observing that sin $\Delta\phi$ is the decision variable, in ref. [14] it has been shown that the desired delay τ which yields optimum performance is $\tau = \frac{T}{2h}$. The variable delay differential detection which employs the above delay interval is shown in Fig. (4.10). It can be noticed that DC detection of CPFSK signals shown in Fig. (1.4), can be simplified as in Fig. (4.10) for binary CPFSK signals.

Recalling section 1.3.2, the decision variable of the variable delay differential detector can be written as,

$$\sin \Delta\Psi = \sin(\Delta\theta + \Delta\eta)$$

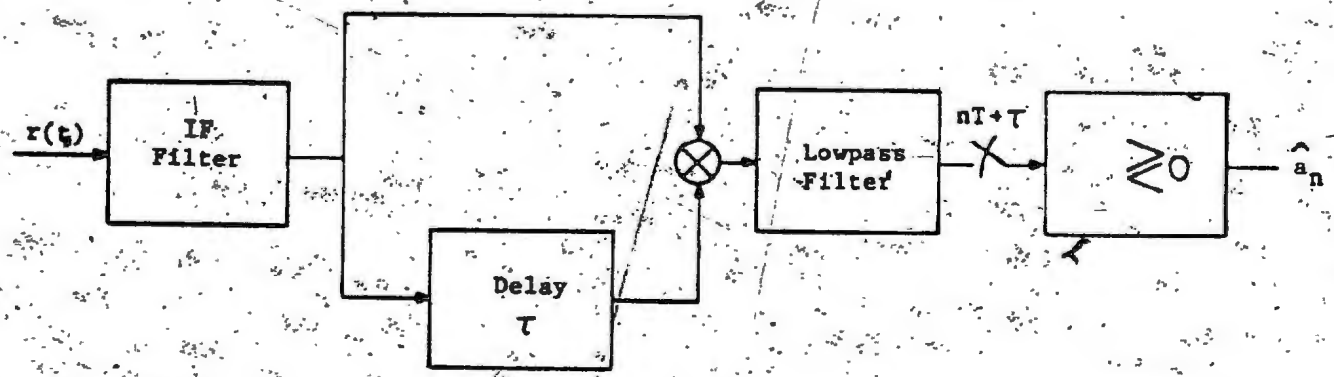

Fig. 4.10 Variable Delay Differential Detector

where

$$\Delta\theta = \theta(t_0) - \theta(t_0 - \tau)$$

and

$$\Delta\eta = \eta(t_0) - \eta(t_0 - \tau)$$

The detector makes its decision by testing the sign of sin $\Delta\Psi$ and decides in favour of '1' if sin $\Delta\Psi > 0$ and in favour of '-1' if sin $\Delta\Psi < 0$. The bit error probability of this receiver, assuming that '1' was sent, can be written as

$$P_e = 1 - Pr(0 < \Delta\Psi < \pi) \qquad (4.11)$$

As in Chapter 3, considering adjacent bit interferences, the error probability can be written as,

$$P_e = 1 - \frac{1}{4}[Pr(0<\Delta\Psi<\pi|_{111}) + Pr(0<\Delta\Psi<\pi|_{010}) + 2\ Pr(0<\Delta\Psi<\pi|_{011})] \qquad (4.12)$$

Each probability term in Eqn. (4.12) can be evaluated by employing the formula derived by Pawula et. al. [26] as,

$$Pr(0<\Delta\Psi<\pi) = F(\pi) - F(0) + 1$$

$$= \frac{1}{2}\left[1 + \sqrt{1 - \frac{\beta^2}{\alpha^2}}\ I_e\left(\frac{\beta}{\alpha}, \alpha\right)\right]$$

$$= 1 - \sqrt{\alpha^2 - \beta^2} \int_0^{\pi} \frac{e^{-(\alpha-\beta\cos\theta)}}{\alpha-\beta\cos\theta}\, d\theta$$

where

$$\alpha = \frac{u - wr\cos\Delta\theta}{1-r^2} \quad ; \quad \beta = \sqrt{\alpha^2 - \frac{w^2\sin^2\Delta\theta}{1-r^2}}$$

$$u = -\frac{1}{2}\,[\rho(t) + \rho(t-\tau)] \quad ; \quad v = \frac{1}{2}\,[\rho(t) - \rho(t-\tau)]$$

$$w = \sqrt{u^2 - v^2} \quad ; \quad r(\tau) = \frac{F^{-1}[|H(f)|^2]}{\int_{-\infty}^{\infty} |H(f)|^2\, df}$$

and $I_e(k,x)$ is the Rice function which is tabulated in [29] and [31].

The values of $\Delta\theta$, u and v are dependent on the bit patterns being conditioned and one needs these values for each of the conditioning bit pattern for computation of the error probability. These values of $\Delta\theta$, u and v can be derived from the results of ref. [25] as given below.

(a) 111 bit pattern

$$\Delta\theta = \frac{\pi}{2} \quad ; \quad u = R_d \quad ; \quad v=0$$

(b) 010 bit pattern,

$$\Delta\theta = 2\tan^{-1}\left[\frac{m \sin\left(\frac{\pi}{4h}\right)}{1 + n\cos\left(\frac{\pi}{2h} - \delta\right)}\right] \quad ; \; u = R_a \; ; \; v = 0$$

(c) 011 bit pattern

$$\Delta\theta = \frac{\pi}{4} + \tan^{-1}\left[\frac{m \sin\left(\frac{\pi}{4h}\right)}{1+n\cos\left(\frac{\pi}{2h} - \delta\right)}\right] \; ; \; u = \frac{R_a + R_d}{2} \; ; \; v = \frac{R_a - R_d}{2}$$

The variables m, n, δ, R_d and R_a for the three cases above

are given as,

$$m = \frac{2h^2\left|H\left(\frac{1}{2T}\right)\right|}{1-h^2}\cot\frac{\pi h}{2} \quad ; \quad n = \frac{2h^2\left|H\left(\frac{1}{T}\right)\right|}{4-h^2} \quad , \quad \delta = H\left(\frac{1}{T}\right) - 2\,H\left(\frac{1}{2T}\right)$$

$$R_d = \frac{E_b}{N_o}\left\{\frac{\left|H\left(\frac{h}{2T}\right)\right|^2}{T\int_{-\infty}^{\infty}|H(f)|^2 df}\right\},$$

$$R_a = \frac{E_b}{N_o}\left\{\frac{\sin\frac{\pi h}{2}}{\frac{\pi h}{2}}\right\}^2 \frac{\left[\left(m\sin\left(\frac{\pi}{4h}\right)\right)^2 + \left(1 + n\cos\left(\frac{\pi}{2h} - \delta\right)\right)^2\right]}{T\int_{-\infty}^{\infty}|H(f)|^2 df}$$

4.3.3 Numerical Results and Conclusions

In this subsection we compute the error probabilities for a Gaussian and a second order Butterworth filter. The lowpass transfer functions and the normalized auto-correlation functions of these filters are given as,

(a) Gaussian filter

$$H(f) = e^{-\pi f^2/2B^2}$$

$$r(\tau) = e^{-\pi(B\tau)^2}$$

(b) Second order Butterworth filter

$$H(f) = \frac{2}{1 + (1+j\sqrt{8}f/B)^2}$$

$$r(\tau) = e^{-\left(\frac{B\pi|\tau|}{\sqrt{2}}\right)}\left[\cos\left(\frac{B\pi\tau}{\sqrt{2}}\right) + \sin\left(\frac{B\pi|\tau|}{\sqrt{2}}\right)\right]$$

The error probabilities are computed for the Gaussian filter for the time bandwidth products BT = 1, 2 and 3 and for the modulation indices h = 0.7 and 1.0 and plotted in Figures (4.11) and (4.12) with those of LD detection [38] for comparison. We observe the variable delay differential detection and LD detection yield approximately the same performance. Although LD detection appears to be marginally better than differential detection, the difference is too small to be of any practical importance. The only noticeable deviation occurs for the case BT = 1 and h = 1 where LD detection is about 0.75 dB better than differential detection at high signal to noise ratios. In Fig. (4.13), the two detection schemes are compared for the Butterworth filter and we note again that they yield approximately the same performance. It appears that the filters having nonlinear phase response have the same effect on the two detection schemes.

In Fig. (4.14), the performance of one-bit delay differential detection [38] is compared with that of variable delay differential detection. We observe that variable delay differential detection improves the performance significantly for all values of h. The two detections become identical for h = 0.5, since the delay τ is T for this case.

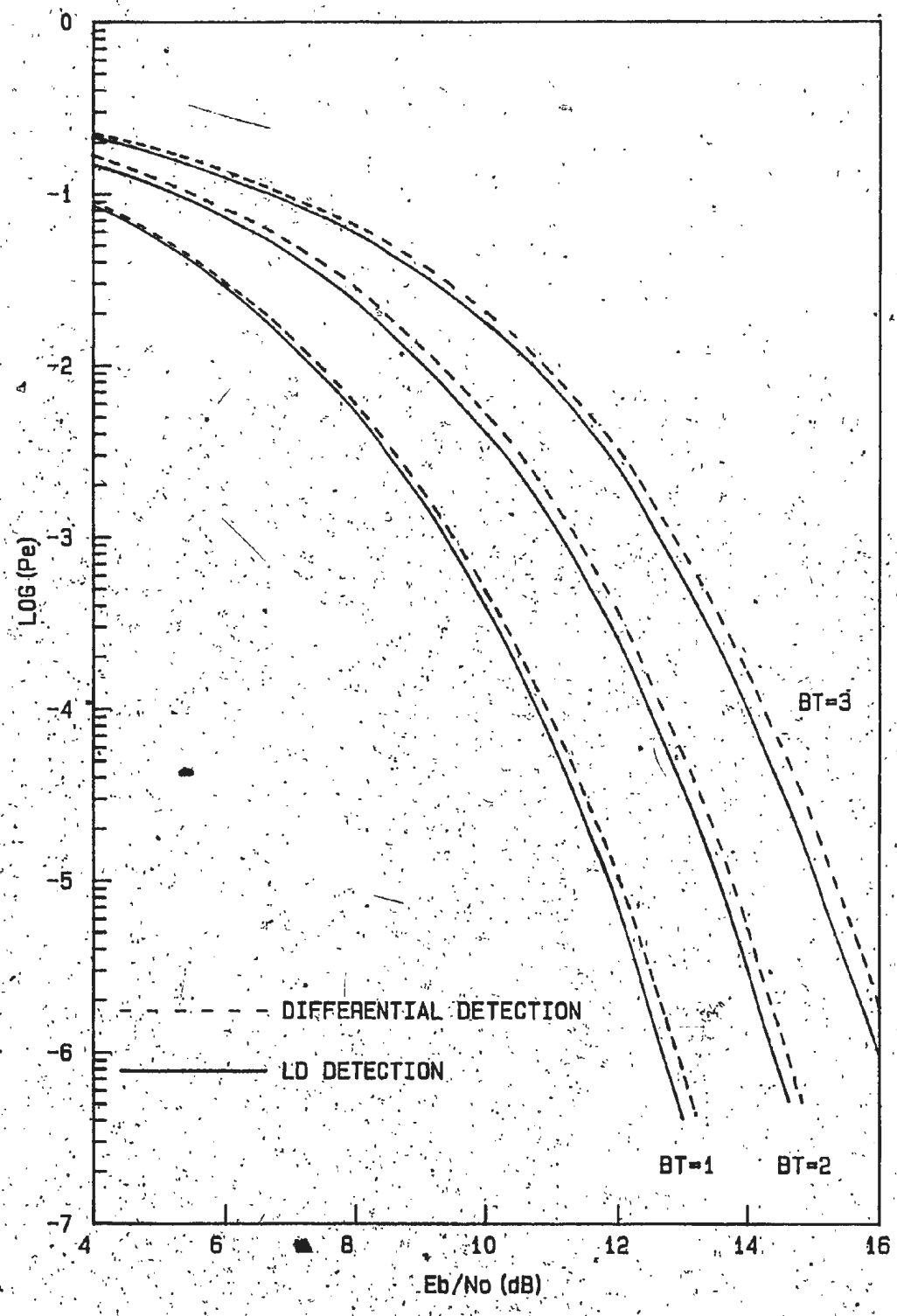

Fig. 4.11 Comparison of LD Detection and Differential Detection of Binary CPFSK with Modulation Index 0.7, for Gaussian Filter

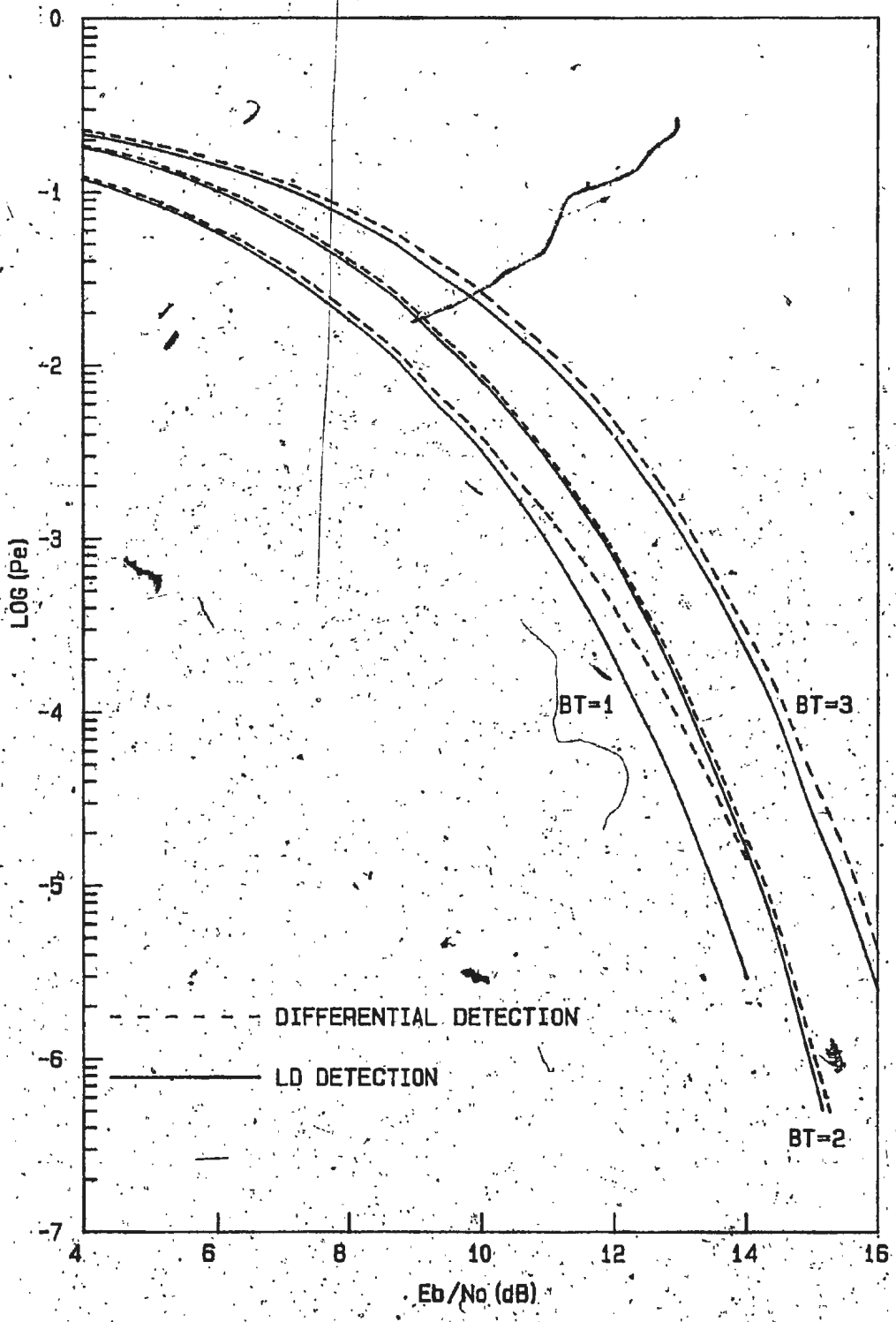

Fig. 4.12 Comparison of LD Detection and Differential Detection of Binary CPFSK with Modulation Index 1.0, for Gaussian Filter

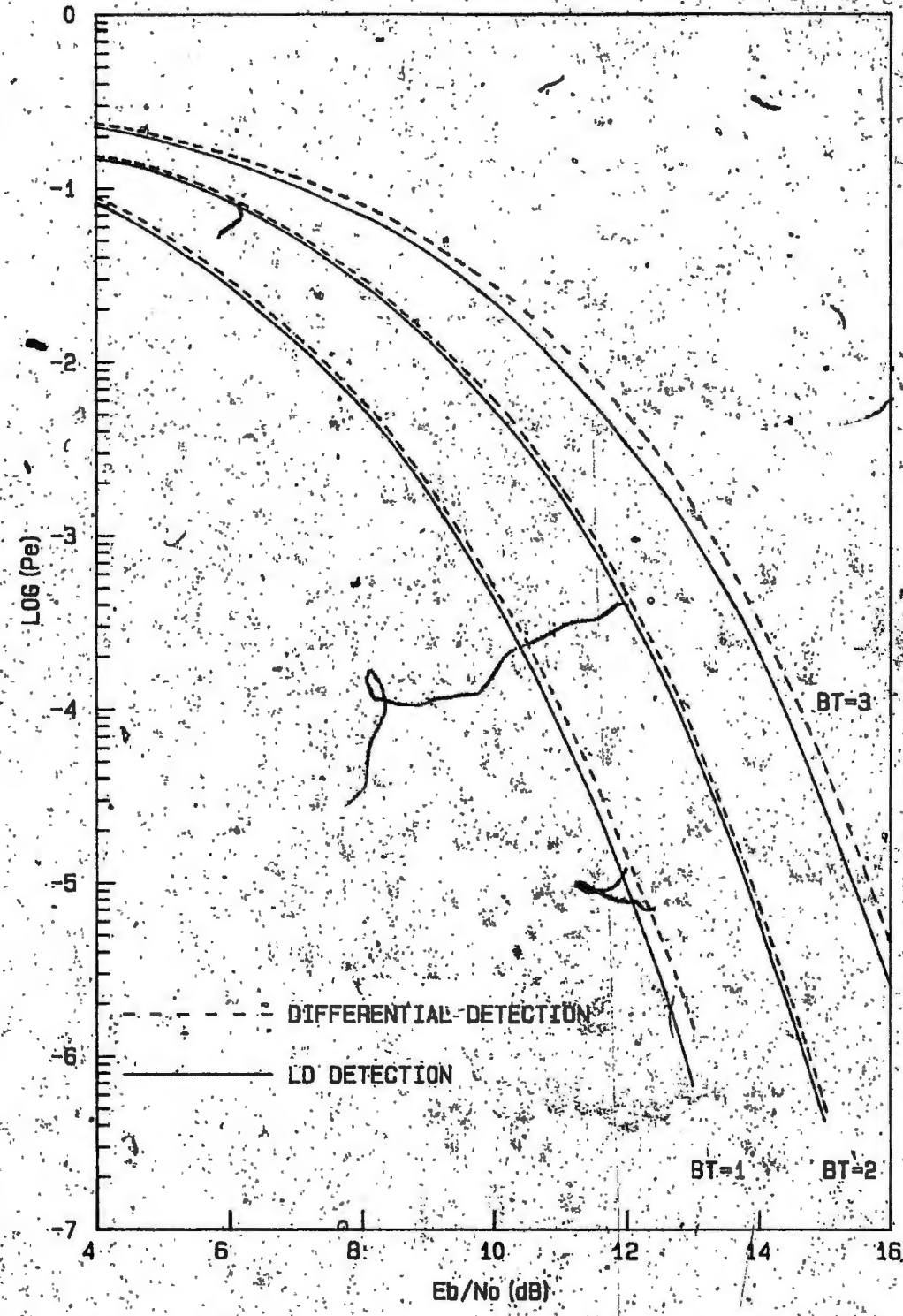

Fig. 4.13 Comparison of LD Detection and Differential Detection of Binary CPFSK with Modulation Index 0.7, for Second Order Butterworth Filter

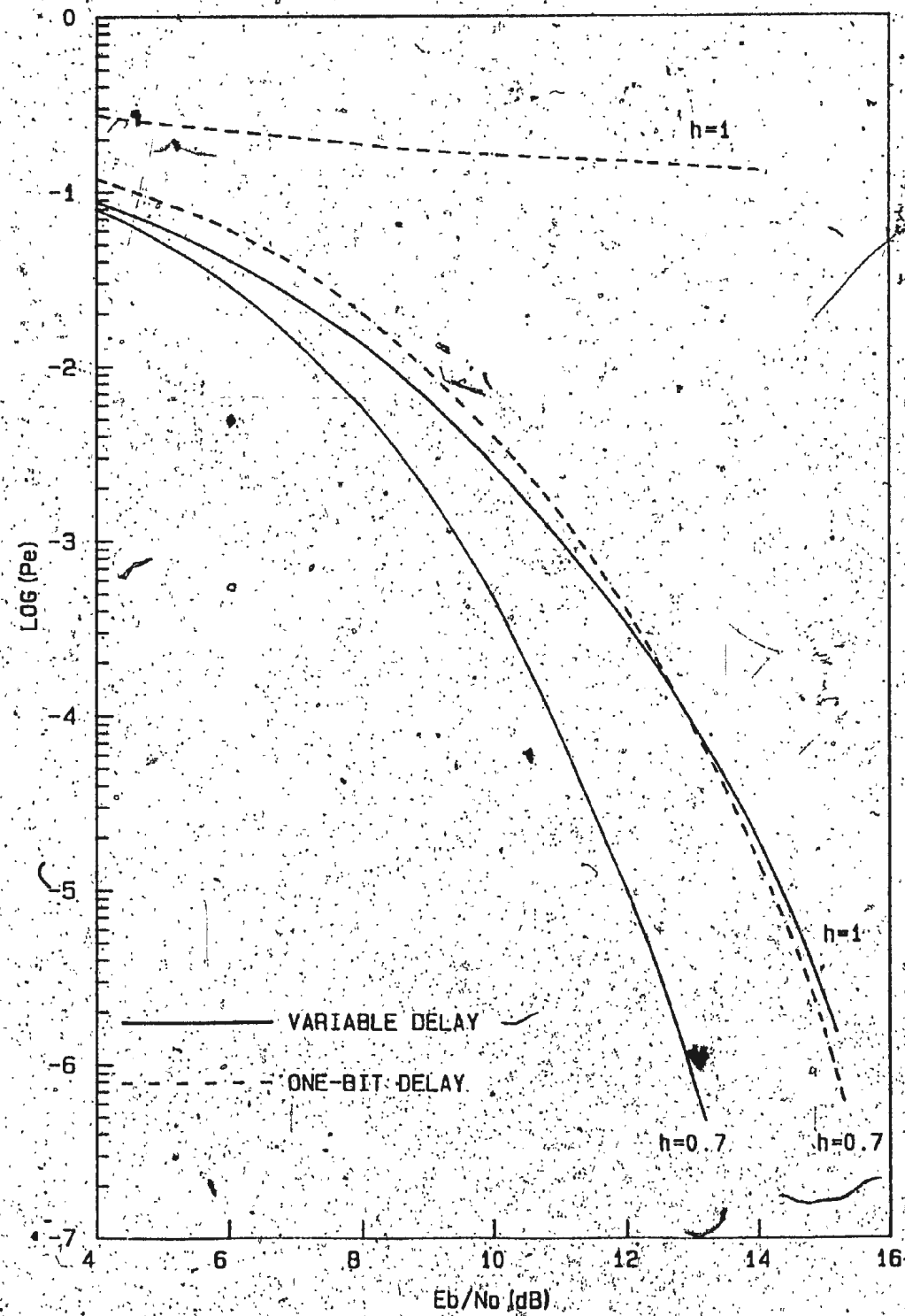

Fig. 4.14 Comparison of Variable Delay Differential Detection and One-Bit Delay Differential Detection of Binary CPFSK for Gaussian Filter with BT=1 (h=0.7 and 1.0)

CHAPTER 5

DIGITAL COMPUTER SIMULATION OF CPFSK SIGNALLING SYSTEMS

5.1 Introduction

In Chapters 3 and 4, we have analyzed the performance of the three detection schemes for bandlimited channels. In order to verify the results and the validity of the assumptions made in obtaining those results, a computer simulation is performed. Since the performance of binary CPFSK signals has been extensively studied and well documented in the literature, we restrict our simulation to quaternary CPFSK and octonary CPFSK. The purpose of this chapter is to present the computer simulation results.

The simulation involves the generation of periodic data sequences and Gaussian noise samples and then counting the number of errors at the receiver. In simulating the LD receiver, the effect of clicks is calculated numerically rather than actually simulating the phase noise process. This is because it is extremely difficult to simulate the continuous phase noise process. However, for both DD and CD-DD receivers, the error rate is evaluated using strict simulation as these receivers do not require the continuous phase noise in order to make a decision.

5.2 Simulation Model

In this section we consider the details of the digital computer simulation of the CPFSK system. Fig. (5.1) shows the simulation model being considered.

5.2.1 Transmitter

A sequence generator randomly selects symbols $(a_0, a_1, \ldots, a_{L-1})$ from the set $\{\pm 1, \pm 3 \ldots \pm(M-1)\}$, where L is the number of symbols in the sequence. The transmitted phase angle during the nth symbol interval, $nT<t<(n+1)T$, follows from the phase continuity requirement as,

$$\phi(t) = \begin{cases} \dfrac{\pi a_n h}{T} t + \pi h \sum_{\ell=0}^{(n-1)} a_\ell - n\pi a_n h & , \ 1 < n < (L-1) \\ \dfrac{\pi a_0 h}{T} t & , \ n = 0 \end{cases} \qquad (5.1)$$

and $\phi(0) = 0$

The transmitted phase angle given by Eqn. (5.1), is corrupted by the channel noise and is further distorted by IF filtering.

5.2.2 Filtering and Phase Noise

We employ the method used in Chapter 3 by considering Fourier Series expansions of $\sin \phi(t)$ and $\cos \phi(t)$ in order to obtain the filtered signal. Instead of

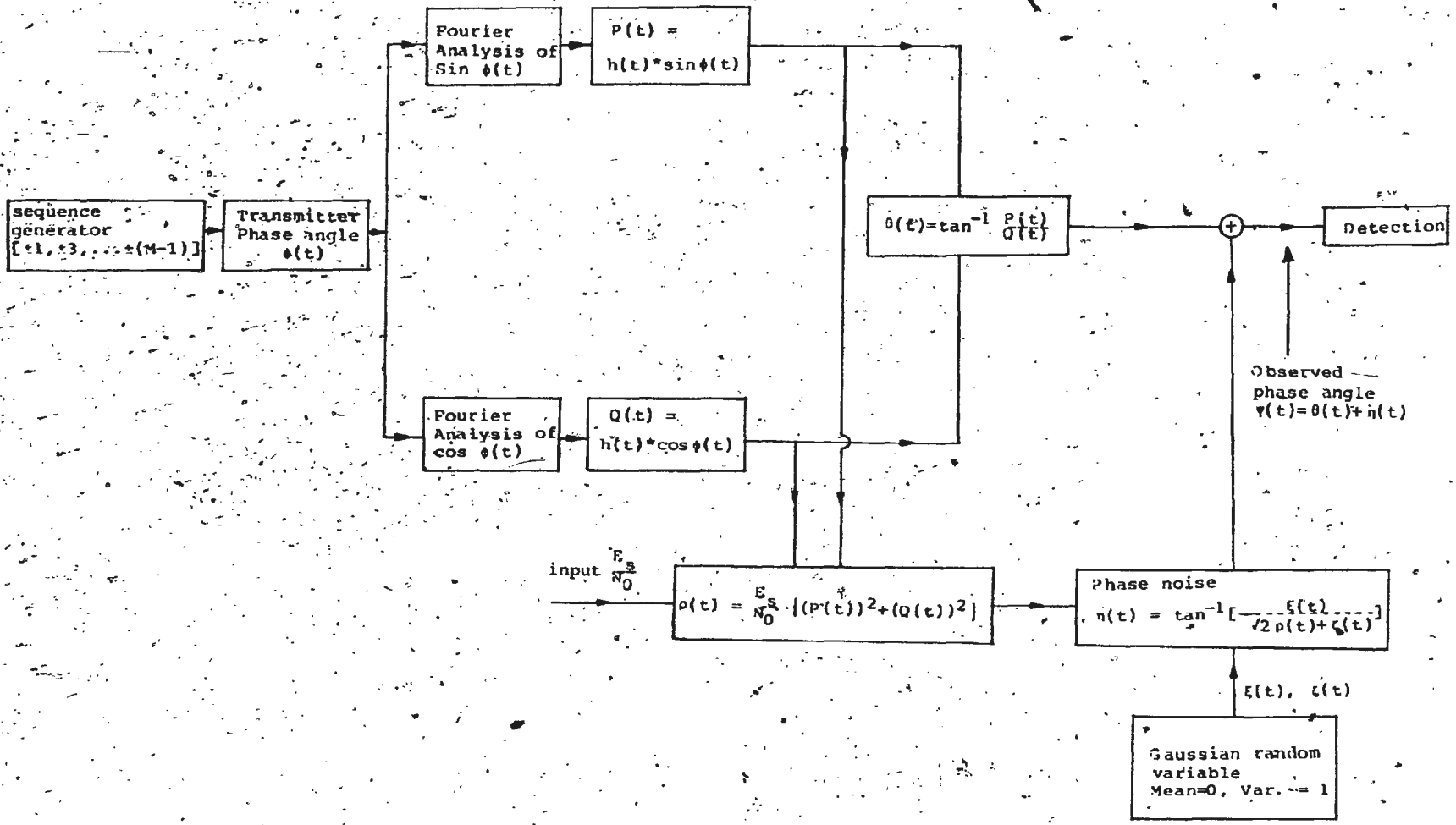

Fig. 5.1 Simulation Model

the two symbol ISI used in Chapter 3, L number of randomly selected symbols are used in the present analysis.

We recall the expression for the filtered signal from section (3.2) as,

$$r_0(t) = R(t)\cos(\omega_c t + \theta(t) + \eta(t)) \qquad (5.2)$$

where

$$\theta(t) = \tan^{-1}\frac{h(t) * \sin\phi(t)}{h(t) * \cos\phi(t)} \qquad (5.3)$$

$$\rho(t) = \frac{E_s}{N_0}\frac{a^2(t)}{T\int_{-\infty}^{\infty}|H(f)|^2 df} \qquad (5.4a)$$

$$= \frac{E_s'}{N_0}a^2(t) \qquad (5.4b)$$

$$a(t) = \left\{(h(t) * \sin\phi(t))^2 + (h(t) * \cos\phi(t))^2\right\}^{1/2} \qquad (5.5)$$

and

$$\eta(t) = \tan^{-1}\frac{n_s(t)}{\sqrt{\frac{2E_s}{T}}a(t) + n_c(t)}$$

$$= \tan^{-1}\frac{\xi(t)}{\sqrt{2\rho(t)} + \zeta(t)} \qquad (5.6)$$

$\xi(t)$ and $\zeta(t)$ are Gaussian random variables with zero mean and unit variance. The convolutions $h(t) * \sin\phi(t)$ and $h(t) * \cos\phi(t)$ are obtained by considering the Fourier series expansions of $\sin\phi(t)$ and $\cos\phi(t)$ as,

$$\sin \phi(t) = \frac{A_0}{2} + \sum_{p=1}^{N'} A_p \cos (2\pi p f_0 t) \qquad (5.7a)$$

and

$$\cos \phi(t) = \frac{B_0}{2} + \sum_{p=1}^{N'} B_p \cos (2\pi p f_0 t); \; f_0 = \frac{1}{2LT} \qquad (5.7b)$$

These expansions are derived by considering an even symmetric variation for $\phi(t)$ about t=LT as,

$$\phi(t) = \phi(2LT - t) \qquad (5.8)$$

The Fourier Coefficients, A_p's and B_p's are obtained as,

$$A_p = \frac{2}{LT} \int_0^{LT} \sin \phi(t) \cos (2\pi p f_0 t) \, dt \qquad (5.9a)$$

$$B_p = \frac{2}{LT} \int_0^{LT} \cos \phi(t) \cos (2\pi p f_0 t) \, dt \qquad (5.9b)$$

where p = 0,1 ... N' and N' is the number of harmonics required to express the filtered signal accurately. Combining Eqns. (5.3), (5.4a), (5.4b) and (5.7b) one obtains,

$$\theta(t) = \tan^{-1} \frac{P(t)}{Q(t)} \qquad (5.10)$$

and

$$\rho(t) = \frac{E_s}{N_0} \frac{\left[(P(t))^2 + (Q(t))^2\right]}{T \int_{-\infty}^{\infty} |H(f)|^2 \, df} \qquad (5.11)$$

where

$$P(t) = \frac{A_0}{2} + \sum_{n=1}^{N'} A_p \, |H(pf_0)| \, \cos(2\pi p f_0 t) \qquad (5.12a)$$

and

$$Q(t) = \frac{B_0}{2} + \sum_{p=1}^{N'} B_p \, |H(p\, f_0)| \, \cos(2\pi p f_0 t) \qquad (5.12b)$$

Eqns. (5.6), (5.9a), (5.9b), (5.10) and (5.11) are used to simulate the filtered phase and its noise component. The phase angle $\Psi(t) = \theta(t) + \eta(t)$ is then employed in the detection process.

5.3 Performance Evaluation

The phase angle $\Psi(t)$ is sampled at the signalling rate to obtain the set $\{\Psi(T), \Psi(2T) \ldots \Psi((L-1)T)\}$. The sample values of $\Psi(t)$ are used to detect the symbols and the errors are counted to estimate the error probabilities of CD-DD detection, DC detection and $P_{cont.}$ of LD detection. The contribution of the clicks to the error probability of LD detection, P_{clicks} is determined using Eqns. (5.10) and (5.11). The CD-DD detection and DC detection techniques are simulated for $h = \frac{1}{M}$ whereas LD detection is simulated for arbitrary value of h.

5.3.1 CD-DD Detection

Recalling from section 3.5.1, the simulation model for this detection can be represented as shown in Fig. (5.2). The simulated error probability is obtained using the error count as,

$$P_e = \frac{\text{number of errors counted}}{\text{number of symbols transmitted}} \qquad (5.13)$$

5.3.2 DC Detection

The model for this detection scheme is shown in Fig. (5.3). The error probability is calculated using Eqn. (5.13).

5.3.3 LD Detection

Recalling from section 3.5.3, the error probability of the LD detection for arbitrary value of h can be written as,

$$P_e = P_{cont.} + P_{clicks} \qquad (5.14)$$

where

$$P_{cont.} = \begin{cases} 1-Pr[-\pi h < \{\Psi((n+1)T)-\Psi(nT)\}-\pi a_n h < \pi h] & , \quad |a_n| \neq (M-1) \\ 1-Pr[-\pi h < \{\Psi((n+1)T)-\Psi(nT)\}-\pi a_n h < \infty] & , \quad a_n = (M-1) \\ 1-Pr[-\infty < \{\Psi((n+1)T)-\Psi(nT)\}-\pi a_n h < \pi h] & , \quad a_n = -(M-1) \end{cases} \qquad (5.15)$$

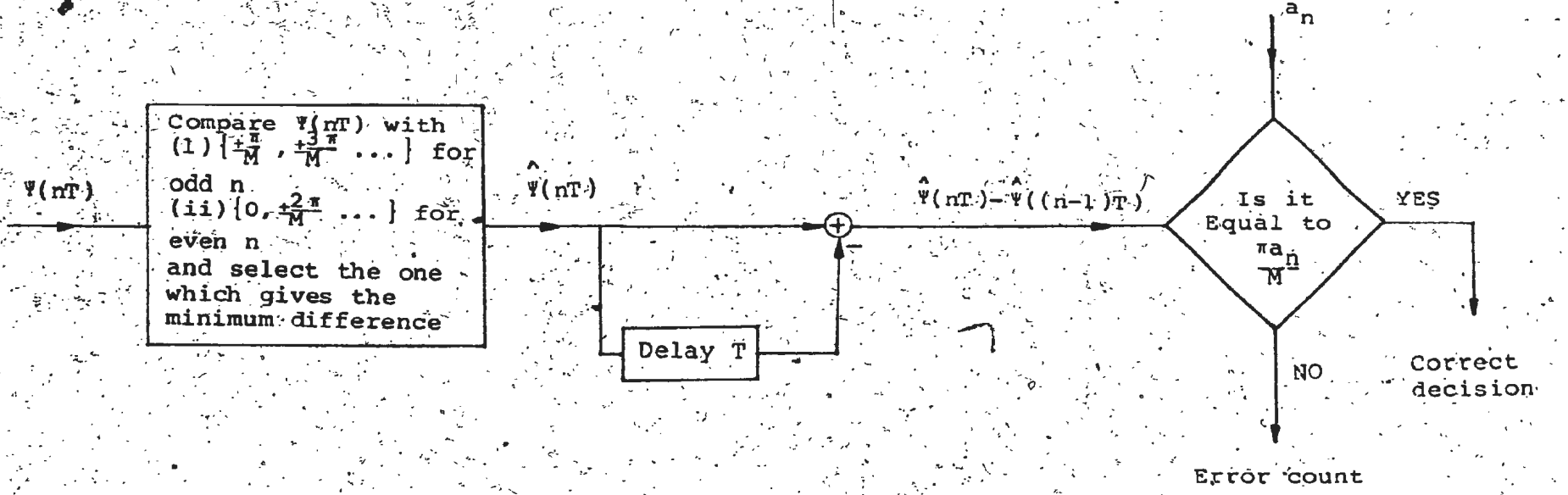

Fig. 5.2 Simulation of CD-DD Detection

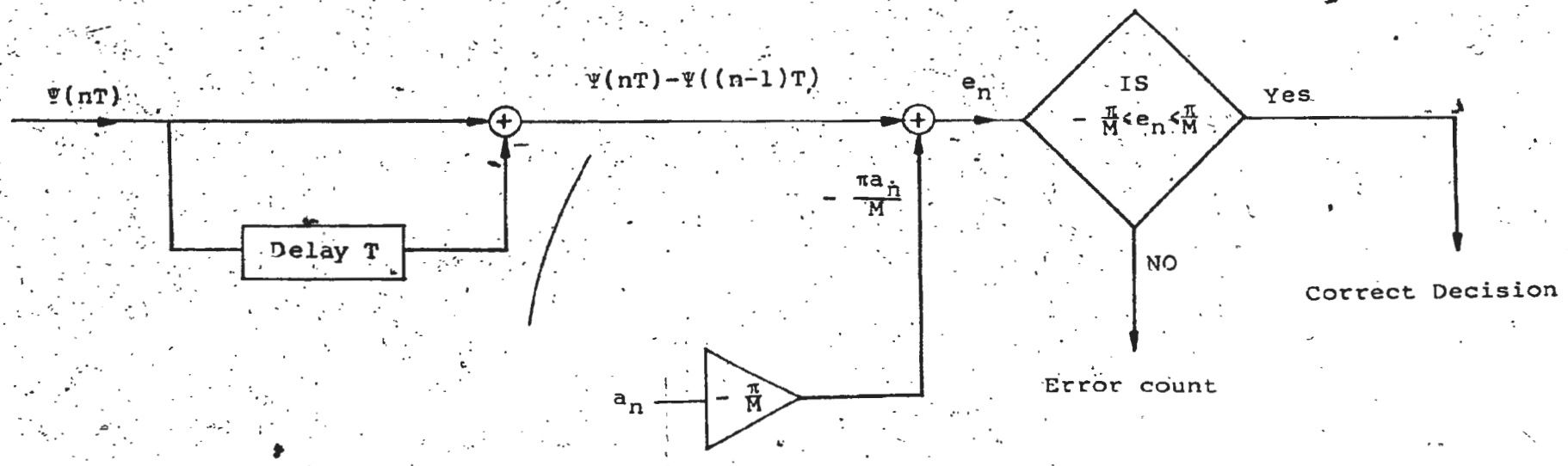

Fig. 5.3 Simulation of DC Detection

and

$$P_{clicks} = \frac{1}{2\pi} \left| \int_{nT}^{(n+1)T} e^{-\rho(\tau)} \dot{\theta}(\tau)\, d\tau \right| \qquad (5.16)$$

$P_{cont.}$ is simulated as in DC detection with slight modifications and is shown in Fig. (5.4).

P_{clicks} is obtained by numerically evaluating the integral given by Eqn. (5.16) and then averaging over the symbols. Hence the simulated value for P_{clicks} is written as,

$$P_{clicks} = \frac{1}{2\pi L} \sum_{n=0}^{L} \left| \int_{nT}^{(n+1)T} e^{-\rho(\tau)} \dot{\theta}(\tau)\, d\tau \right| \qquad (5.17)$$

5.4 Numerical Results and Discussion

In this section we present the results obtained by simulation for the error probabilities for the three detection techniques. These results are obtained for a Gaussian IF filter for the BT and h values given in Table (5.1).

Table (5.1)

BT and h Values for the Simulation

	M=4		M=8	
	BT	h	BT	h
LD	3.0	0.64 & 0.25	6.0	0.62 & 0.125
DC	3.0	0.25	6.0	0.125
CD-DD	1.8	0.25	4.15	0.125

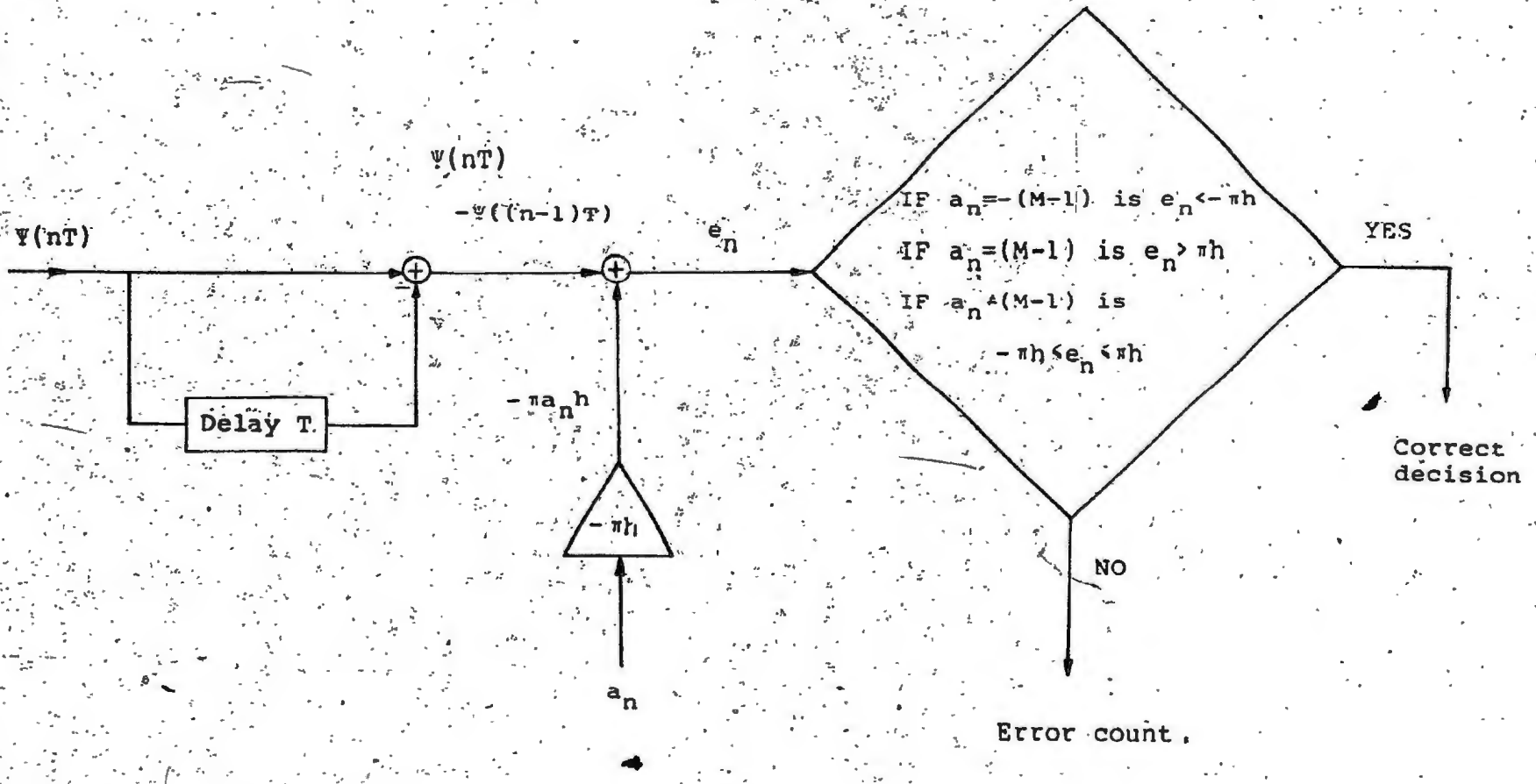

Fig. 5.4 Simulation of $P_{cont.}$ for LD Detection

The simulation is carried out using 96 randomly selected symbols generated in 8 sets, each of which consisting of 12 symbols. Hence the number of symbols used in every set L, has been taken as 12. In every set the number of harmonics N', has been chosen as 96 to maintain sufficient accuracy. Finally, the error count has been considered as 20 throughout the simulation. With this error count we maintain over 90% confidence in our simulation error probabilities, to be within 35% of the actual error probabilities.

The simulated error probabilities are plotted in Figs. (5.5) - (5.8) for various E_s'/N_0 values with the theoretical results obtained in Chapters 3 and 4. It is clearly seen that the theoretical results are in good agreement with the simulated results.

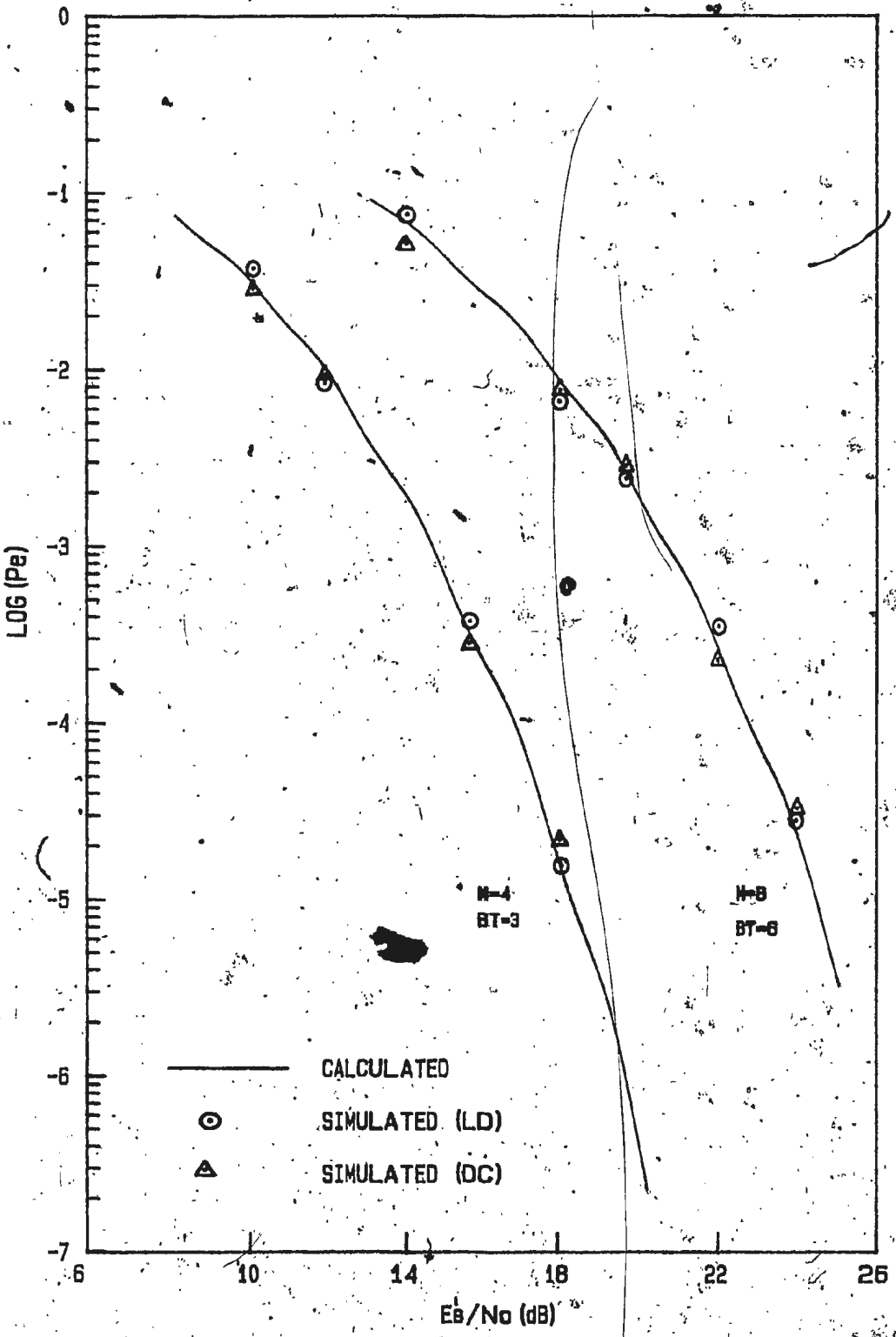

Fig. 5.5 Theoretical and Simulated Symbol Error Probabilities of LD Detection and DC Detection, for M-ary CPFSK with Modulation Index $\frac{1}{M}$, for Gaussian Filter (M=4 with BT=3.0 and M=8 with BT=6.0)

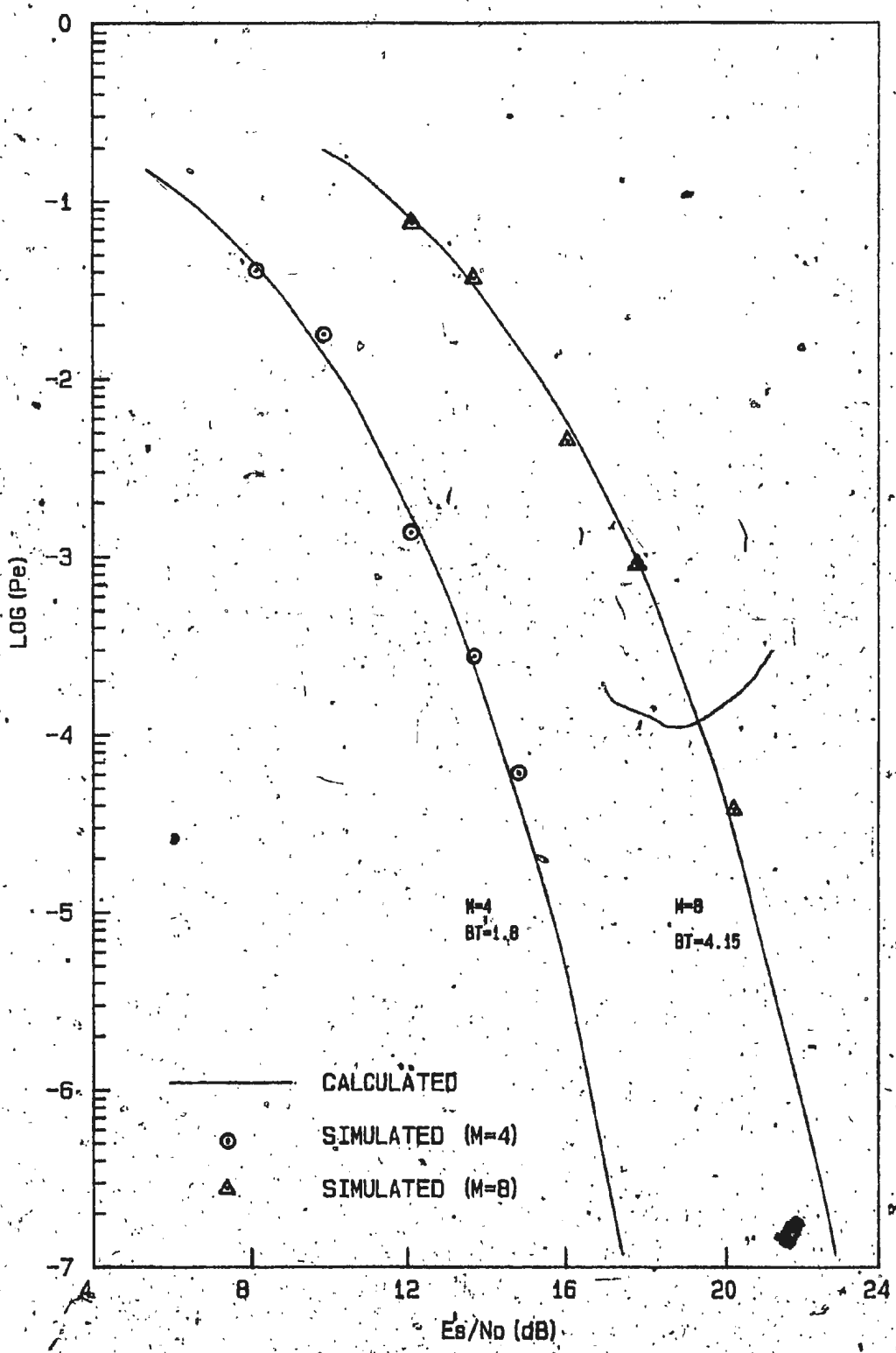

Fig. 5.6 Theoretical and Simulated Symbol Error Probabilities of CD-DD Detection, for M-ary CPFSK with Modulation Index $\frac{1}{M}$, for Gaussian Filter
(M=4 with BT=1.8 and M=8 with BT=4.15)

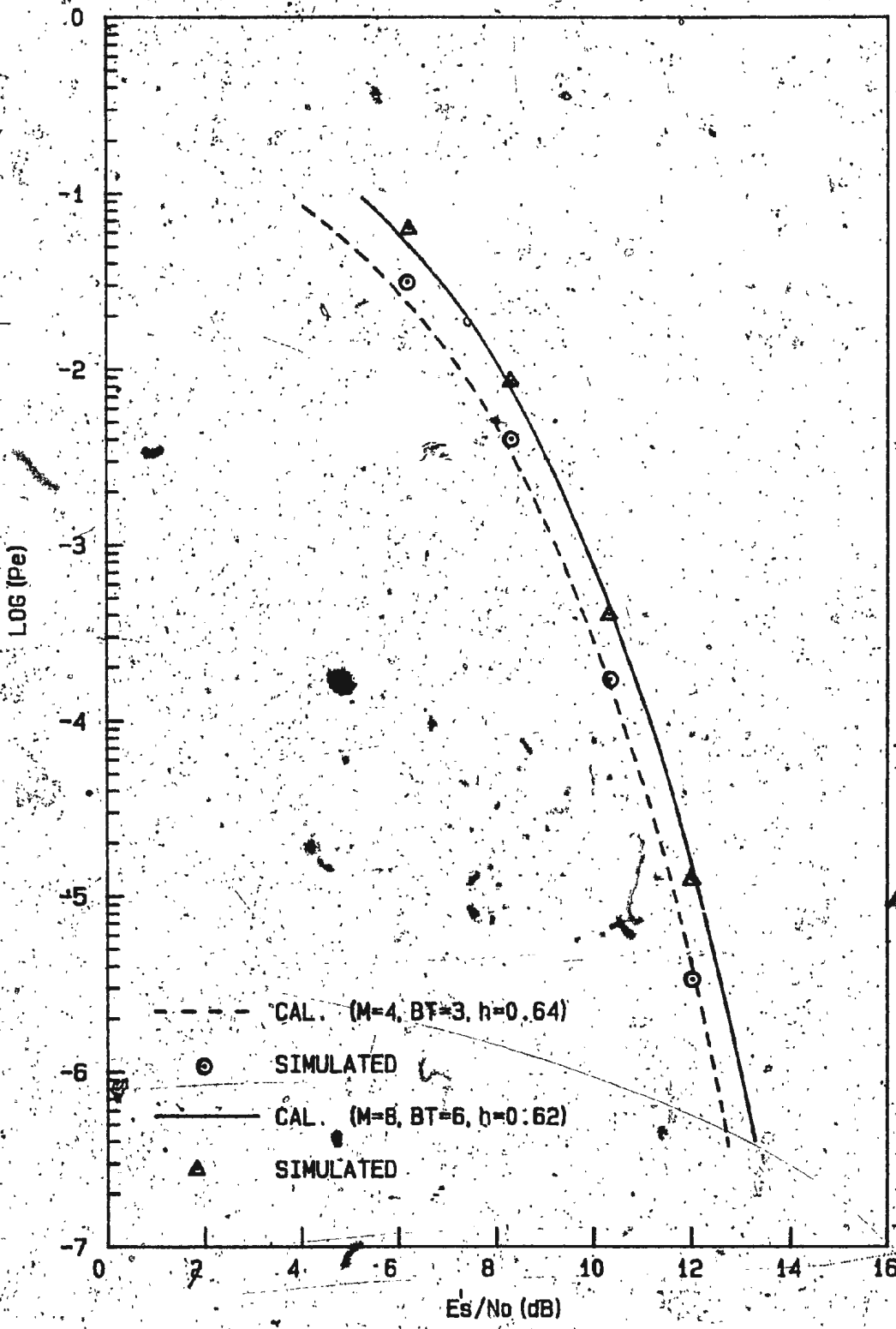

Fig. 5.7 Theoretical and Simulated $P_{cont.}$ Probabilities of LD Detection, for M-ary CPFSK, for Gaussian Filter (M=4 with BT=3.0 and M=8 with BT=6.0)

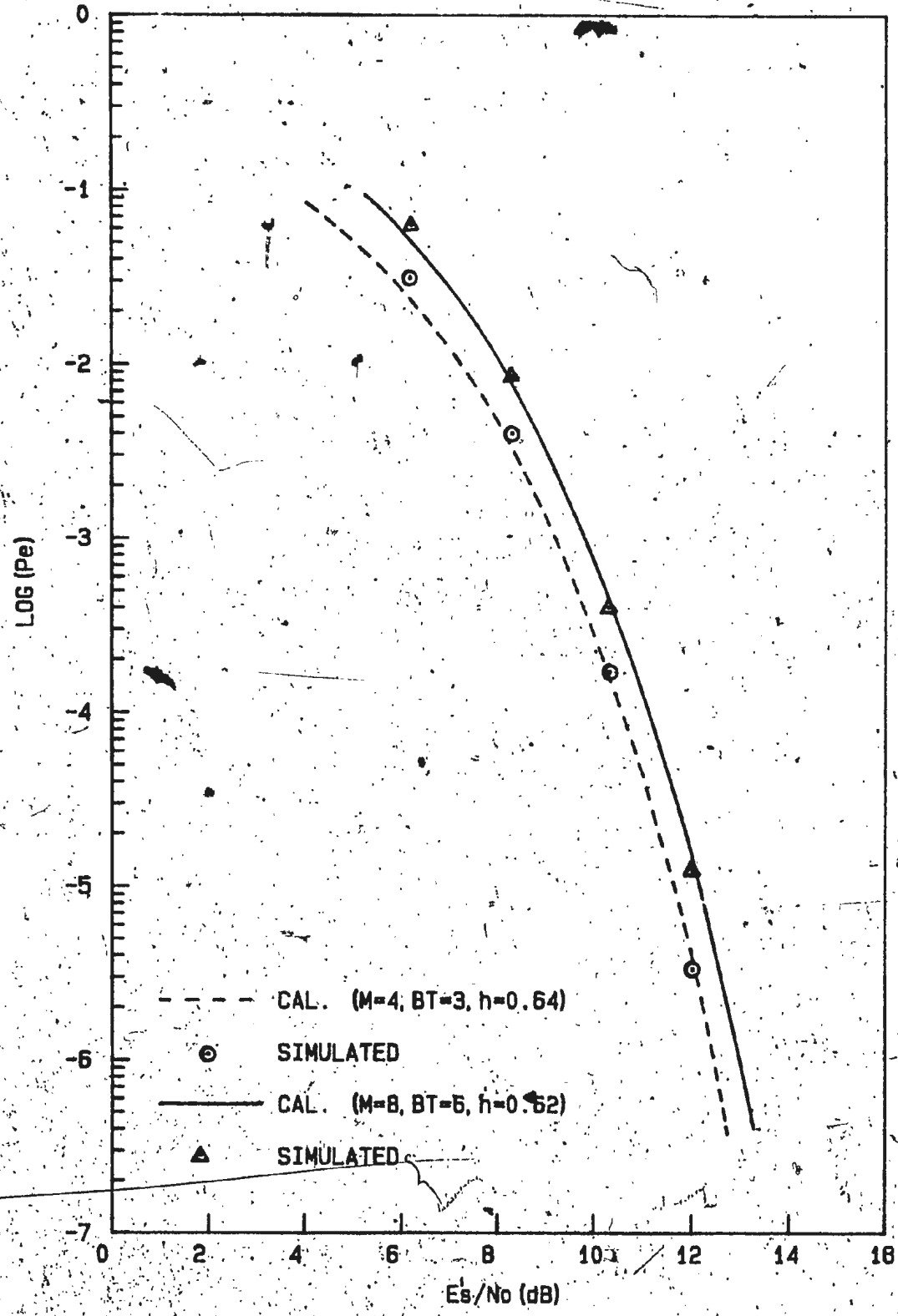

Fig. 5.8 Theoretical and Simulated p_{clicks} Probabilities of LD Detection, for M-ary CPFSK, for Gaussian Filter (M=4 with BT=3.0 and M=8 with BT=6.0)

CHAPTER 6

CONCLUSIONS

6.1 Discussion

In this thesis we have analyzed the performance of Differentially Coherent (DC) detection, Coherent Detection-Differential Decoding (CD-DD) detection and conventional Limiter Discriminator (LD) detection of M-ary Continuous Phase Frequency Shift Keyed (CPFSK) signals.

The properties of CPFSK signals and the operation of the three detection schemes have been discussed in Chapter 1. In Chapter 2, the performance of the three detection schemes have been analyzed for a wideband channel [42]. The modulation index was assumed to be $\frac{1}{M}$. The effect of symbol timing errors has also been considered. It has been concluded that the CD-DD scheme has better performance than the DC detection and LD detection schemes. This observation has been made even in presence of symbol timing errors. It has also been observed that DC detection and LD detection techniques yield almost identical performance. Finally, it has been observed that baseband symbol pulse shaping could be used to reduce the timing error effect in all three detection schemes.

In Chapter 3, the comparison of the detection schemes has been carried out for a bandlimited channel for $h = \frac{1}{M}$, considering only adjacent intersymbol interferences. A technique has been developed for taking into account the effect of ISI. Numerical results have been obtained for a Gaussian and a second order Butterworth filter. It has been concluded that the CD-DD scheme has better performance than the LD detection and DC detection whereas the latter two have almost identical performance.

In Chapter 4, two special cases have been considered, namely, the performance evaluation of LD detection for arbitrary value of h and the performance evaluation of DC detection of binary CPFSK signals using a delay line whose delay interval is dependent on the modulation index. In the LD detection case, it has been shown that the performance of the LD detection can be improved by increasing h above $\frac{1}{M}$. The optimum value of h which yields the minimum error probability has been obtained. In the second case, the performance of the DC detection of binary CPFSK signals which employs a delay line, whose delay interval is dependent on the modulation index h [14], has been analyzed for a bandlimited channel. It has been concluded that [43] in contrast to the one-bit delay differential detection [38], variable delay differential detection yields performance comparable to LD detection.

Finally, in Chapter 5, a digital computer simulation has been carried out to verify the analytical results obtained in Chapters 3 and 4 for quaternary CPFSK and octonary CPFSK signals. The simulation results are in close agreement with the analytical results. Therefore, we conclude that our analytical results and the assumptions made in deriving those analytical results are reasonably valid.

6.2 Possible Extensions

It has been observed that ISI in a bandlimited channel causes severe performance degradation specially for multilevel signalling systems. It would therefore be very useful to find a technique to combat the effect of ISI and also to devise new detection techniques which are more robust to ISI than those we have analyzed in this thesis.

In order to reduce ISI, one could possibly employ baseband pulse shaping; we have observed in this thesis that baseband pulse shaping can reduce the effect of timing errors. Another observation we have made is that the effect of ISI is minimal at middle of the symbol intervals. This property could perhaps be used to derive a new detection scheme which uses the samples taken at the mid points of the signalling intervals rather than at symbol transition instants.

From our analysis it was observed that CD-DD detection performs considerably better than LD detection and DC detection. However, the successful implementation of the CD-DD receiver depends on the practicability of generating a coherent carrier at the receiver, which we have not considered in this thesis. Therefore, it is useful to investigate an efficient carrier recovery technique for M-ary CPFSK signals.

BIBILIOGRAPHY AND LIST OF REFERENCES

1. Amoroso, F.: Pulse and Spectrum Manipulation in the Minimum Frequency Shift Keying (MSK) Format. IEEE Trans. on Communications, Vol. COM -24, March 1976, pp. 381-384.

2. Anderson, R. R. et. al. : Differential Detection of Binary FM.BSTJ, Vol. 44, 1965,pp. 111-170.

3. Anderson R. R. and Salz, J.: Spectra of Digital FM. BSTJ, Vol. 44, July/Aug. 1965, pp. 1165-1189.

4. Aulin, T. and Sundberg, C.E.W.: Continuous Phase Modulation - Part I: Full Response Signalling. IEEE Trans. on Communications, Vol. COM-29, 1981, pp. 196-209.

5. Aulin, T. and Sundberg, C. E. W.: Calculating Digital FM Spectra by Means of Autocorrelation. IEEE Trans. on Communications, Vol. COM-30, 1982, pp. 1828-1841.

6. Baker, T. T.: Asymptotic Behaviour of Digital FM Spectra. IEEE Trans. on Communications, Vol. COM-22, Oct. 1974, pp. 1585-1594.

7. Bennett, W. R. and Rice, S. O.: Spectral Density and Autocorrelation Functions Associated with Binary Frequency Shift Keying. BSTJ, Vol. 42, Sept. 1963, pp. 2355-2385.

8. Bennett, W. R. and Salz, J.: Binary Data Transmission By FM over a Real Channel. BSTJ, Vol. 42, Sept. 1963, pp. 2387-2426.

9. Cartier, D. E.: Limiter-Discriminator Detection Performance of Manchester and NRZ coded FSK. IEEE Trans. on Aerospace and Electronic Systems, Vol. AES-13, Jan. 1977, pp. 62-70.

10. Chen, C.: Note on Discriminator of PCM/FM.IEEE Trans. on Aerospace and Electronic Systems, Vol AES-4, May 1968, pp. 478-479.

11. Chen, C.: Discriminator Detection of Wideband PCM/FM. IEEE Trans. on Aerospace and Electronic Systems, Vol. AES-5, Jan. 1969, pp. 126-127.

12. deBuda, R.: Coherent Demodulation of Frequency Shift Keying with Low Deviation Ratio. IEEE Trans. on Communications, Vol. COM-20, June 1972, pp. 429-435.

13. Ekanayake, N.: M-ary Continuous Phase Frequency Shift Keying with Modulation Index $\frac{1}{M}$. IEE Proceedings, Part F, Communications, Radar and Signal Processing, Vol. 131, April 1984, pp. 173-178.

14. Ekanayake, N.: On Differential Detection of Binary FM. IEEE Trans. on Communications, Vol. COM-32, April 1984, pp. 469-470.

15. Forney, G. D, Jr.: The Viterbi Algorithm. Proc. IEEE, Vol. 61, pp. 268-278, March 1973.

16. Gronemeyer, S. A and McBride, A. L.: MSK and Offset QPSK Modulation. IEEE Trans. on Communications, Vol. COM-24, August 1976, pp. 809-820.

17. Klapper, J.: Demodulator Threshold Performance and Error Rates in Angle-Modulated Digital Signals. RCA Review, June 1966, pp. 226-244.

18. Lindsey, W. C. and Simon, M. K.: Telecommunication Systems Engineering, Prentice-Hall: Englewood Cliffs, N.J., 1973.

19. Luckey, R. W. et. al.: Principles of Data Communications, New York: McGraw-Hill, 1968.

20. Masamura, T. et. al.: Differential Detection of MSK with Nonredundant Error Correction. IEEE Trans. on Communications, Vol. COM-27, 1978, pp. 912-918.

21. Mathwick, H. R, et. al.: The Effect of Tandem Band and Amplitude Limiting of the E_b/N_0 Performance of Minimum (Frequency) Shift Keying (MSK). IEEE Trans. on Communications, Vol. COM-22, Oct. 1974, pp. 1525-1540.

22. Mazo, J. E. and Salz, J.: Theory of Error Rates for Digital FM. BSTJ, Vol. 45, Nov. 1966, pp. 1511-1535.

23. Meyerhoff, A. A. and Mazer, W. M.: Optimum Binary FM Reception using Discriminator Detection and IF Shaping. RCA Review, Vol. 22, Dec. 1961, pp. 698-728.

24. Osborne, W. P. and Luntz, M. B.: Coherent and Noncoherent Detection of CPFSK. IEEE Trans. on Communications, Vol. COM-22, Aug. 1974, pp. 1023-1036.

25. Pawula, R. F.: On the Theory of Error Rates for Narrowband Digital FM. IEEE Trans. on Communications, Vol. COM-29, Nov. 1981, pp. 1634-1643.

26. Pawula, R. F. et al.: Distribution of the Phase Angle Between Two Vectors Perturbed by Gaussian Noise. IEEE Trans. on Communications, Vol. COM-30, Aug. 1982, pp. 1828-1841.

27. Pelchat, M. G.: The Autocorrelation and Power Spectrum of PCM/FM with Random Binary Modulating Waveforms. IEEE Trans. on Space Electronics and Telemetry, March 1964, pp. 39-44.

28. Pelchat, M. G. et. al.: Coherent Demodulation of Continuous Phase Binary FSK Signals. Int. Telemetering Conf. Conv. Rec. (Washington, DC), 1971, pp. 181-190.

29. Rice, S. O.: Statistical Properties of a Sine Wave Plus Random Noise. BSTJ, Vol. 27, Jan. 1948, pp. 109-157.

30. Rice, S. O.: Noise in FM Receivers Time Series Analysis, M. Rosenblatt, Ed., Willey: New York, 1963, pp. 395-422.

31. Roberts, J. H.: Angle Modulation, Peregrinus: England, 1977.

32. Salz, J.: Performance of Multilevel Narrowband FM Digital Communication Systems. IEEE Trans. on Communications, Vol. COM-13, 1964, pp. 420-424.

33. Schilling, D. L. et. al.: Error Rates for Digital Signals Demodulated by an FM Discriminator. IEEE Trans. on Communications, Vol. COM-15, Aug. 1967, pp. 507-517.

34. Schonoff, T. A.: Symbol Error Probabilities for M-ary CPFSK: Coherent and Noncoherent Detection. IEEE Trans. on Communications, Vol. Com-24, June 1976, pp. 644-652.

35. Shaft, P. D.: Error Rate of PCM-FM Using Discriminator Detection. IEEE Trans. on Space Electronics and Telemetry, Dec. 1963, pp. 131-137.

36. Shimbo, O.: General Formula for Power Spectra of Digital FM Signals. Proc. IEEE, Vol. 113, Nov. 1965, pp. 1783-1789.

37. Simon, M. K.: A Generalization of Minimum Shift Keying (MSK) Type Signalling Based Upon Input Data Symbol Pulse Shaping. IEEE Trans. on Communications, Vol. COM-24, Aug. 1976, pp. 845-856.

38. Simon, M. K. and Wang, C. C.: Differential Versus Limiter-Discriminator Detection of Narrowband FM. IEEE Trans. on Communications, Vol. COM-31, Nov. 1983, pp. 1227-1234.

39. Tham, Q. C. and Lin, F. C.: Optimal and Suboptimal Performance of a PCM/FM Communication System. IEEE Trans. on Aerospace and Electronic Systems, Vol. AES-11, July 1975, pp. 575-581.

40. Tjhung, T. T.: Theory and Performance of Binary FM Systems in a Restricted Band. Res. Rept. 69-2, Dept. of EE, Queen's Univ., Kingston, Ont. Canada, 1969. Available as NTIS Document N69-36696.

41. Tjhung, T. T. and Wittke, P. H.: Carrier Transmission of Binary Data in a Restricted Band. IEEE Trans. on Communications, Vol. COM-18, Aug. 1970, pp. 295-304.

42. Fonseka, K. J. P. and Ekanayake, N.: Comparison of Three Detection Techniques for M-ary CPFSK with Modulation Index $\frac{1}{M}$. Proceedings of IEEE Global Telecom. Conference, 1984, pp. 22.6.1 - 22.6.7.

43. Fonseka, K. J. P. and Ekanayake, N.: Differential Detection of Narrowband Binary FM. To apper in IEEE Trans. on Communications, Vol. COM-33, July 1985.

APPENDIX A

CUMULATIVE PROBABILITY DENSITY FUNCTIONS OF PHASE ANGLE DIFFERENCE AND ABSOLUTE PHASE ANGLE FOR EQUAL SIGNAL CONDITIONS

Recalling that

$$\eta(t) = \tan^{-1}\left[\frac{n_s(t)}{A + n_c(t)}\right] \tag{A.1}$$

and

$$\alpha = \eta(t_2) - \eta(t_1)$$

the following results are obtained from ref. [26],

$$\Pr(\alpha_1 < \alpha < \alpha_2) = \begin{cases} F_1(\alpha_2) - F_1(\alpha_1) + 1 & , \quad \alpha_1 \leq 0 \leq \alpha_2 \\ F_1(\alpha_2) - F_1(\alpha_1) & , \quad \alpha_1 > 0 \text{ or } \alpha_2 < 0 \end{cases} \tag{A.2}$$

where $F_1(\alpha)$, the cumulative p.d.f. of the noise in phase angle difference α, is given as,

$$F_1(\alpha) = -\frac{\mathrm{Sgn}(\alpha)}{4\pi} \int_{-\pi/2}^{\pi/2} \frac{e^{-\rho(1-\cos\alpha\cos t)}}{1 - \cos\alpha\cos t}\, dt \tag{A.3}$$

Using the transformation $(1-d\cos\theta)(1+d\cos t) = 1 - d^2$, Eqn. (A.3) can also be expressed as,

$$F_1(\alpha) = -\frac{\mathrm{Sgn}(\alpha)}{2\pi} \int_0^{\frac{\pi}{2} - |\alpha|} e^{-\rho \frac{\sin^2 \alpha}{1+\cos \alpha \cos \theta}} d\theta \qquad (A.4)$$

For the Coherent Detection - Differential Decoding case, the following expression for the cumulative p.d.f. of the absolute phase noise $\eta(t)$ can be similarly used:

$$F_2(\eta) = -\frac{\mathrm{Sgn}(\eta)}{2\pi} \int_0^{\frac{\pi}{2} - |\eta|} e^{-\rho \sin^2 \eta \sec^2 \theta} d\theta \qquad (A.5)$$

APPENDIX B

EVALUATION OF FOURIER COEFFICIENTS

We recall Eqn. (3.9);

$$\phi(t) = \begin{cases} \frac{\pi a_n h t}{T} & , \quad 0 < t < T \\ \frac{\pi a_{n+1} h t}{T} + (a_n - a_{n+1})\pi h & , \quad T < t < 2T \end{cases} \tag{B.1}$$

The pth Fourier coefficient of $\sin \phi(t)$ can be written as,

$$A_p = \frac{1}{T}\left[\int_0^T \sin\left(\frac{\pi a_n h t}{T}\right)\cos\left(\frac{\pi p}{2T} t\right)dt + \int_T^{2T} \sin\left\{\frac{\pi a_{n+1} h t}{T} + \pi h(a_n - a_{n+1})\right\} \cos\left(\frac{\pi p}{2T} t\right) dt\right]$$

i.e.
$$A_p = \left[\frac{1 - \cos\left(\pi a_n h + \frac{p\pi}{2}\right)}{2\pi a_n h + p\pi} + \frac{1 - \cos\left(\pi a_n h - \frac{p\pi}{2}\right)}{2\pi a_n h - p\pi}\right]$$

$$-\left[\frac{\cos\{(2\pi a_{n+1} h + p\pi) + \pi h(a_n - a_{n+1})\}}{2\pi a_{n+1} h + p\pi} + \frac{\cos\{(2\pi a_{n+1} h - p\pi) + \pi h(a_n - a_{n+1})\}}{(2\pi a_{n+1} h - p\pi)}\right]$$

$$+\left[\frac{\cos\{\pi a_{n+1} h + \frac{p\pi}{2}) + \pi h(a_n - a_{n+1})\}}{2\pi a_{n+1} h + p\pi} + \frac{\cos\{(\pi a_{n+1} h - \frac{p\pi}{2}) + \pi h(a_n - a_{n+1})\}}{2\pi a_{n+1} h - p\pi}\right] \tag{B.2}$$

Similarly, the pth Fourier coefficient of $\cos \phi(t)$ can be written as,

$$B_p = \frac{1}{T}\left[\int_0^T \cos\left(\frac{\pi a_n h t}{T}\right)\cos\left(\frac{\pi p t}{2T}\right)\,dt + \int_T^{2T} \cos\left\{\frac{\pi a_{n+1} h t}{T} + \pi h(a_n - a_{n+1})\right\} \cos\left(\frac{\pi p t}{2T}\right) dt\right].$$

i.e.,

$$B_p = \left[\frac{\sin(\pi a_n h + \frac{p\pi}{2})}{2\pi a_n h + p\pi} + \frac{\sin(\pi a_n h - \frac{p\pi}{2})}{2\pi a_n h - p\pi}\right]$$

$$+\left[\frac{\sin\{(2\pi a_{n+1} h + p\pi) + \pi h(a_n - a_{n+1})\}}{2\pi a_{n+1} h + p\pi} + \frac{\sin\{(2\pi a_{n+1} h - p\pi) + \pi h(a_n - a_{n+1})\}}{2\pi a_{n+1} h - p\pi}\right]$$

$$-\left[\frac{\sin\{(\pi a_{n+1} h + \frac{p\pi}{2}) + \pi h(a_n - a_{n+1})\}}{2\pi a_{n+1} h + p\pi} + \frac{\sin\{(\pi a_{n+1} h - \frac{p\pi}{2}) + \pi h(a_n - a_{n+1})\}}{2\pi a_{n+1} h - p\pi}\right] \qquad (B.3)$$

($h = \frac{1}{M}$ case has been used for the numerical calculations.)

APPENDIX C

CUMULATIVE PROBABILITY DENSITY FUNCTIONS OF PHASE ANGLE DIFFERENCE AND ABSOLUTE PHASE ANGLE FOR UNEQUAL SIGNAL CONDITIONS AND NO NOISE CORRELATION

Recalling that

$$\alpha = \eta(t_2) - \eta(t_1)$$

the following results are obtained from ref. [26] neglecting the noise correlation as,

$$\Pr(\alpha_1 < \alpha < \alpha_2) = \begin{cases} F_1(\alpha_2) - F_1(\alpha_1) + 1 & , \quad \alpha_1 < 0 < \alpha_2 \\ F_1(\alpha_2) - F_1(\alpha_1) & , \quad \alpha_1 > 0 \text{ or } \alpha_2 < 0 \end{cases} \tag{C.1}$$

where

$$F_1(\alpha) = -\frac{w \sin \alpha}{4\pi} \int_{-\pi/2}^{\pi/2} \frac{e^{-[u - v\sin t - w\cos \alpha \cos t]}}{u - v\sin t - w\cos \alpha \cos t} \, dt \tag{C.2}$$

and

$$u = \frac{\rho(t_1) + \rho(t_2)}{2} \; ; \; v = \frac{\rho(t_2) - \rho(t_1)}{2} \; : \; w = \sqrt{\rho(t_1)\,\rho(t_2)}$$

can be used for the LD detection and DC detection. For the CD-DD case, the following expression given in ref. [26] can be used.